Designing a high-throughput screen for small molecule modulators of the molecular motor KIF1A

by

Dominik Gabrych

B.Sc., Simon Fraser University, 2016

Thesis Submitted in Partial Fulfillment of the

Requirements for the Degree of

Master of Science

in the

Department of Molecular Biology and Biochemistry

Faculty of Science

Declaration of Committee

Name: **Dominik Gabrych**

Degree: **Master of Science**

Thesis title: **Designing a high-throughput screen for small molecule modulators of the molecular motor KIF1A**

Committee: **Chair:**   Sharon Gorski
Professor, Molecular Biology and Biochemistry

Michael Silverman
Supervisor
Professor, Biological Sciences

David Vocadlo
Committee Member
Professor, Molecular Biology and Biochemistry

Michel Leroux
Committee Member
Professor, Molecular Biology and Biochemistry

Mani Larijani
Examiner
Associate Professor, Molecular Biology and Biochemistry

Abstract

The neuron-specific kinesin, KIF1A, is involved in the transport of cargos critical for neuronal function such as synaptic vesicle precursors and dense-core vesicles. Notably, mutations in KIF1A are implicated in the pathogenesis of neurological disorders such as hereditary spastic paraplegia. Therapies that specifically target KIF1A do not currently exist. I developed a high-throughput, phenotypic screen for small molecule modulators of KIF1A. I used two-color fluorescent imaging to identify a cell-based, phenotypic assay that allows for characterization of the inactive, autoinhibited form of KIF1A and the active form of KIF1A. When expressed in COS-7 and SK-N-SH cells, wild-type KIF1A-GFP is diffusely distributed and does not co-localize with the microtubule marker EB3-mKate2. The hyperactive mutant V8M KIF1A-GFP does co-localize with microtubules and distributes peripherally. These findings support the feasibility of a functional assay to distinguish between the active and inactive forms of KIF1A in a high-throughput screening format.

Keywords: KIF1A; Neuronal Transport; Neurodegenerative Disorders; Assay Development; High-throughput screen; Drug discovery

Acknowledgements

I would like to thank my senior supervisor, Dr. Michael Silverman for giving me the opportunity to work in his laboratory as a Master's student. Throughout my time in his laboratory, he showed an abnormal amount of patience and offered boundless guidance as I waded through the trials and tribulations of science. I hope the stress that I caused him will be alleviated once the college football season starts. This acknowledgement would not be complete without the seasoned help and humour of our lab mate and manager Andrew. My work would not be as complete if not for the wisdom he imparted in the lab, and life in general. Lastly, I would like to extend my gratitude to my supervisory committee, Dr. David Vocadlo and Dr. Michel Leroux, for their invaluable advice and timely feedback throughout this project.

Table of Contents

List of Tables

List of Figures

List of Acronyms

ARL-8	Arf-like small GTPase
BDNF	Brain-Derived Neurotropic Factor
CaM	Calmodulin
CaMKII	Calmodulin Kinase II
CC	Coiled-Coil
CMV	Cytomegalovirus
CV	Coefficient of Variation
DCV	Dense-Core Vesicle
EB3	End-Binding Protein 3
EF1α	Eukaryotic Translation Elongation Factor 1α
ELIPA	Enzyme Linked Inorganic Phosphate Assay
FracAtD	Fraction at Distance
HSAN2C	Hereditary Sensory and Autonomic Neuropathy Type 2C
HSP	Hereditary Spastic Paraplegia
KAND	KIF1A-Associated Neurological Disorder
KIF	Kinesin Superfamily Proteins
KLC2	Kinesin Light Chain 2
LoG	Laplacian of Gaussian
MD	Motor Domain
NC	Neck Coil
NL	Neck Linker
NPY	Neuropeptide-Y
PEHO	Progressive Encephalopathy with Edema, Hypsarrhythmia and Optic Atrophy
PH	Pleckstrin Homology
SPG	Spastic Gait Gene
SVP	Synaptic Vesicle Precursor
WT	Wild-Type

Chapter 1.   Introduction

Neurons are highly polarized cells comprised of morphologically, biochemically, and functionally distinct extensions of the cell body: the axon and dendrites. Establishing and maintaining these unique domains depends on the bidirectional transport of cargos within these microtubule-based structures. Active transport utilizes motor proteins, namely the kinesin superfamily (KIFs) for anterograde transport, and cytoplasmic dynein for retrograde transport. When any aspect of this process is dysregulated the resulting "transportopathy" contributes to neurological disorders, such as Huntington's, Alzheimer's, and Parkinson's disease (Millecamps & Julien, 2013). Hereditary spastic paraplegias (HSPs) are also a family of such transport-related diseases with over 80 spastic gait genes (SPG), specifically characterized by lower extremity spasticity. HSPs may present in both pure and complicated forms where the former is primarily limited to progressive lower-extremity spastic weakness and the latter also includes symptoms such as ataxias and cognitive impairments (Blackstone, 2018). Inheritance patterns can be autosomal dominant, autosomal recessive, X-linked, or of mitochondrial (maternal) inheritance (Hedera, 2018). Dominant *de novo* mutations have also been described (Hedera, 2018). Multiple genes in the trafficking pathway related to microtubule function and organelle biogenesis are representative disease loci, such as Spastin (SPG4) and adaptor protein-4 (AP-4; SPG47), respectively (Hazan et al., 1999; Marras et al., 2016). Notably, kinesins are also causal in HSP, specifically mutations in Kinesin-I/KIF5A

(SPG10) and two kinesin-3 family members; KIF1A (SPG30) and KIF1C (SPG58; Blackstone, 2018).

HSP-related kinesin mutations have primarily been documented by clinical symptoms and gross pathology combined with medical imaging such as MRI (Lee et al., 2015; Roda et al., 2017). Furthermore, many thorough studies have previously detailed the inheritance patterns and gene mutations in KIF5 (Liu et al., 2014) and kinesin-3 family members (Oteyza et al., 2014; Lee et al., 2015). The structure and function of these kinesins have also been reviewed at length by Hirokawa et al., 2009, and Siddiqui & Straube, 2017, in addition to how HSP mutations impair motor function (Ebbing et al., 2008; Kawaguchi, 2013; Oteyza et al., 2014; Lee et al., 2015; Niwa et al., 2016; Cheon et al., 2017). These mutations lead to the loss of motor motility or the inability to pause at sites of capture such as at synapses. Unfortunately, due to the homology of the affected domains, motor domain-specific therapeutics are difficult to develop. Another avenue exists to understand the downstream effects of motor impairment by proxy of the motors' cargo function. No histopathological and little cell biological data assessing perturbations in cargo localization allowing one to infer how mutations in kinesin-3 contribute to HSPs exist. As such, discovery and development of targeted therapeutics and tool compounds is difficult, and to date no therapeutics that target transport kinesins exist.

High-throughput screening provides a platform for large-scale assaying of novel and pre-existing compounds on known pathological phenomena using robotics, platform-specific software, and optimized and validated assays. However, for reliable data regarding effects of the compounds and biologics on pathological events present in transport motor-based neurological disorders, robust functional assays must be developed. Fortunately, functional assays exist that probe a variety of domains and their actions for transport-based kinesins including ATPase activity, microtubule binding, and translocation along microtubules. As such, high-throughput screening may serve as a viable platform for discovering novel compounds and biologics that may alleviate the deleterious physiological phenomena seen in transport-based neurological disorders.

In this chapter, I will begin by providing a comprehensive overview of neuronal transport including the components critical for its proper function and how regulation via external factors affect transport. I follow this portion by talking specifically about the neuronal-enriched kinesin-3 family member, KIF1A, which has a variety of critical roles

2

in proper neuronal development, maintenance, and viability. KIF1A's structure, function and regulation will be discussed along with its role in KIF1A-associated neurological disorders (KAND), specifically HSP. Furthermore, I will discuss known functional assays that probe a variety of critical parameters in the functioning of transport motors and overview the current literature regarding high-throughput screening and kinesin motors. Lastly, I will introduce an outline of my research objectives which revolved around the design and validation of a high-throughput screen for small molecule modulators of the neuron-enriched kinesin-3 family member, KIF1A.

1.1. Overview of Neuronal Transport

Microtubule-based intracellular transport is required by all eukaryotic cells for proper spatiotemporal delivery of organelles, mRNA and soluble proteins. Intracellular transport is particularly critical for neurons due to their extreme morphological dimensions, polarity, and need for efficient communication between the cell body and distal processes (Bentley & Banker, 2016). Cytosolic and cytoskeletal proteins, such as neurofilaments, tubulin, and tau are moved from the cell body by slow transport, ranging from 0.2 to 2.5 mm per day (Roy, 2014). Slow transport is an essential aspect to neuronal function, and defects in this process contribute to an array of pathologies including Charcot-Marie-Tooth, amyotrophic lateral sclerosis, and Parkinson's disease (Yuan et al., 2017). This form of transport is mechanistically distinct utilizing primarily kinesin-1 family members and not kinesin-3 (Hirokawa & Tanaka, 2015). By contrast, membranous organelles are moved to the axon terminals by fast transport, which can exceed 400 mm per day (Hirokawa & Tanaka, 2015). Because the axon is largely devoid of biosynthetic machinery, it relies on anterograde axonal transport to supply axon terminals with cargos such as synaptic vesicle precursors (SVP), dense core vesicles (DCV), and other Golgi-derived proteins and lipids. Retrograde transport from distal portions of the neuron is of equal importance to prevent accumulation of toxic aggregates by clearing recycled or misfolded proteins (Hinckelman et al., 2013; Millecamps and Julien, 2013), as well as supporting synapse-cell body communication by signaling endosomes ferrying trophic signals (Olenick et al., 2019). This bidirectional intracellular transport is driven by kinesin and cytoplasmic dynein motor proteins that use

ATP hydrolysis to provide the energy to transport cargos anterogradely towards the synapse or retrogradely towards the cell body, respectively (Figure 1.1).
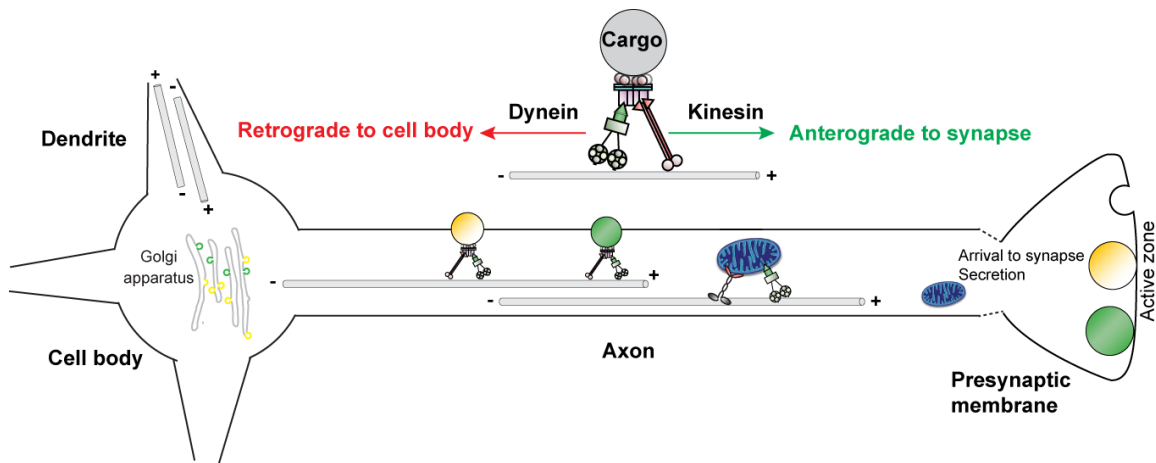
Figure 1.1. Schematic of bidirectional, intraneuronal transport.
The bidirectional transport of cellular cargos via motor proteins is important for the development, maintenance, and viability of neurons. The kinesins drive anterograde transport of cargos such as SVPs and DCVs from the soma to the axon, while dynein drives retrograde transport of cargos such as mitochondria from the axon and the dendrites towards the soma.

The kinesins are a superfamily of microtubule-based motors consisting of 15 families, totalling 45 KIF-encoding genes (Figure 1.2A; Hirokawa et al., 2009). The domain structure remains relatively consistent in each kinesin, generally consisting of a motor domain and a coiled-coil domain (Endow et al., 2010). Gene-specific domains are present such as the pleckstrin homology domains of the kinesin-3 motors KIF1A and KIF1Bβ, the PX domain of KIF16B, or the CAP-Glycine domain of KIF13B (Steinmetz and Akhamanova., 2008; Xue et al., 2010). Furthermore, the kinesins can be subdivided into three categories based on the terminus at which their motor domain is located and thus their directionality of transport along microtubules (Figure 1.2B; Hirokawa et al., 2009). The N-kinesins, which include my protein of interest, KIF1A, have their motor domain located at their amino terminus and thus translocate towards the plus-end of microtubules. Conversely, C-kinesins, such as the mitotic motor KIFC3, contain their motor domain at their carboxy terminus and move towards the minus end of microtubules. Interestingly, the third category of kinesin, the M-kinesins such as KIF2A, contain their motor domain neither at the amino nor carboxy terminus and function in the depolymerization of microtubules.
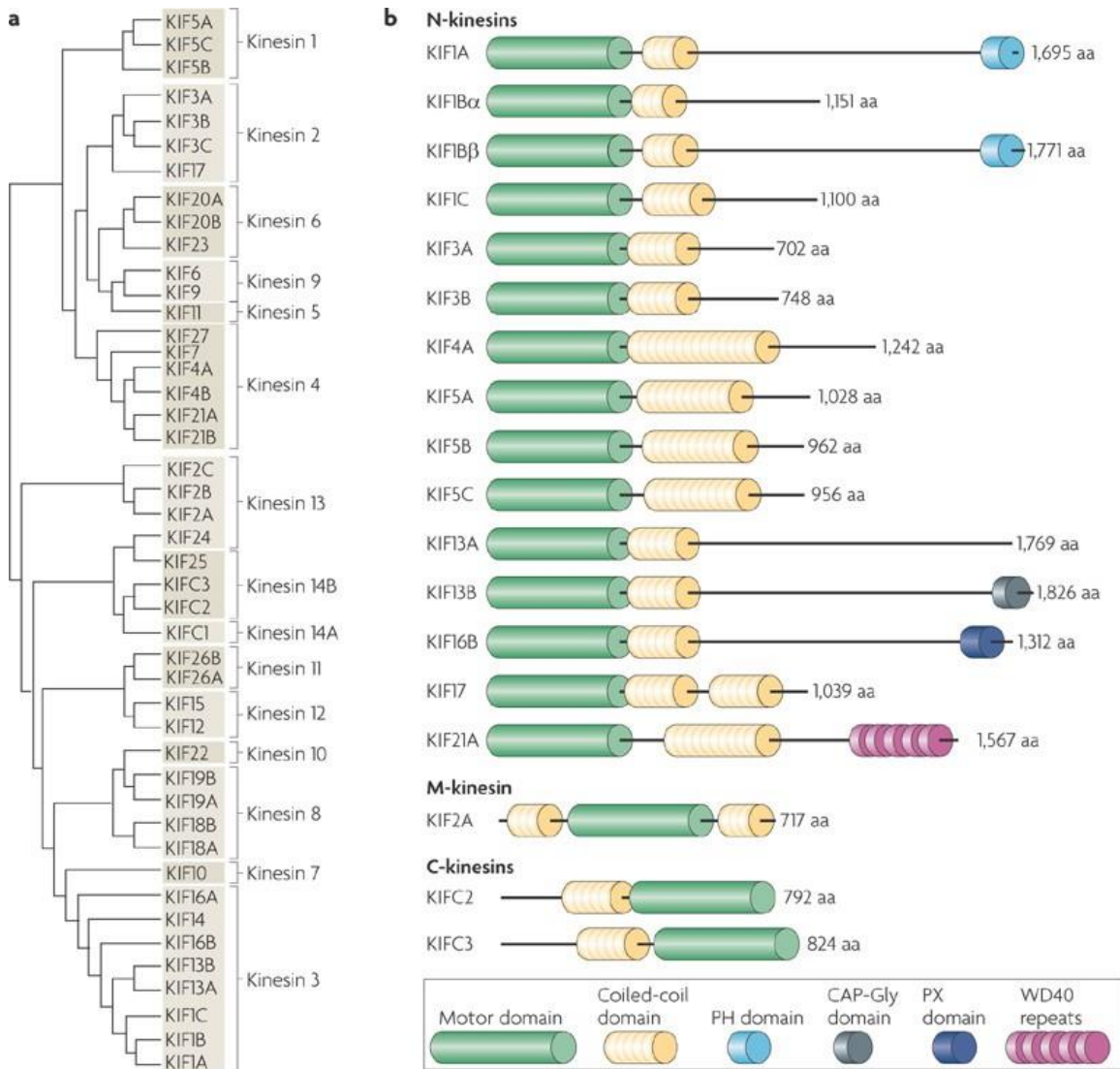
Figure 1.2. The kinesin superfamily of proteins.
A) A phylogenetic tree of the 15 kinesin families including all 45 KIF-encoding genes. B) A schematic representation of the N-, M-, and C-kinesins and their respective domains. N-kinesins are defined by their motor domain at the amino-terminus. The M-kinesin are defined by their motor domain at neither terminus. The C-kinesins are defined by their motor domain at the carboxy-terminus. (Hirokawa et al., 2009).

Although motor domains and certain coiled-coil domains remain highly conserved across kinesin families, the number of coiled-coil domains and kinesin-specific domains, as mentioned previously, differ giving rise to differences in motor properties and specificity of cargos. In terms of motor properties, ATPase efficiency (as defined as step per second), motor regulation via activation, and regulation of motor activity by kinases, GTPases, and phosphatases differ between kinesins, even those belonging to the same family (Hirokawa et al., 2009; Verhey and Hammond., 2009; Siddiqui and Straube.,

2017; Gan et al., 2020). The ATPase domain, for example, is highly conserved between all kinesins with little variation in sequence, however, ATPase step-rate, a measure of how many steps a kinesin can take per cycle of hydrolysis, between kinesins can vary (Song et al., 2001; Bergnes et al., 2005). Furthermore, even though KIF1C and KIF1A belong to the same family and are both autoinhibited *in vitro* and *in vivo*, the distinct structure and number of their coiled-coil domains results in differences in how autoinhibition and release of that autoinhibition occurs (Soppina et al., 2014; Siddiqui et al., 2019). Notably, even with differing domains, there is overlap between functionality and specificity of cargo binding. For example, the neuron-enriched KIF1A, KIF1C, and the conventional kinesin-1 are able to transport dense-core vesicle cargo which contains molecules such as brain-derived neurotrophic factor (BDNF) and neuropeptide-Y (NPY) critical for neuronal function, previously thought to be a sole cargo of KIF1A (Gauthier et al., 2004; Lim et al., 2017; Stuchi et al., 2018). This overlap in function has interesting implications in neuronal disorders where cargo transport is interrupted, such as in HSP, as the redundancy of this cargo transport may reduce the severity of effects that may have been caused by complete ablation of proper delivery of the cargo. Cargo overlap is not limited to just neuron-specific factors but may also include critical cellular organelles such as mitochondria and lysosomes (Figure 1.3; Pilling et al., 2006; Farias et al., 2017). Furthermore, membranes and lipid droplets are transported by kinesins (Pollock et al., 1999; Shubeita et al., 2008). It is important to note that kinesins are not limited to transport and include functions in microtubule depolymerization and various mitotic events which shows just how critical this family of motor proteins is to proper cellular functioning (Hirokawa et al., 2009). Therefore, it is no surprise that dysfunction of kinesins are implicated and causal in a variety of disorders such as ciliopathies, cancer, and neurological disorders such as Huntington's, Alzheimer's and HSP.

Dynein on the other hand, is the retrograde transport counterpart to the transport kinesins. Dynein is composed of two heavy chains, two light chains, two intermediate light chains, and two light intermediate chains. Importantly, dynein's mobility on microtubule tracks is heavily regulated by dynactin, a multi-subunit protein complex (Reck-Peterson et al., 2018). The dynein-dynactin complex traffics a variety of cargos including organelles such as mitochondria and lysosomes, macromolecules, and various vesicular cargos (Figure 1.3; Reck-Peterson et al., 2018). Interestingly, dynein and kinesins work in a coordinated fashion to orchestrate the movement of a variety of

vesicular and non-vesicular cargos (Gennerich and Vale, 2009). KIF1A, for example, is regulated by dynein through the p150 subunit of the dynactin complex (Chen et al., 2019). Furthermore, bidirectional transport BDNF, a critical neuronal cargo trafficked by KIF1A, KIF1C and kinesin-1, is disrupted when dynactin's interaction with carboxypeptidase-E, a possible cargo adaptor for KIF1A, is altered (Park et al., 2008). Moreover, bidirectional transport by KIF1A and the dynein/dynactin complex is integral in the circulation of DCV-based cargos in *Drosophila* needed for proper synaptic distribution of DCV contents (Moughamian and Holzbaur., 2012; Wong et al., 2012). To underscore the importance of this motor complex in neurons, mutations in the *DYNC1H1* gene encoding dynein heavy chain are causal in motor neuropathies such as Charcot-Marie-Tooth (CMT) disease and dominant spinal muscular atrophy with lower extremity predominance (SMA-LED) that show closely related symptomology to KAND disorders (Eschbach et al., 2013; Hoang et al., 2017).

Notably, axonal and dendritic transport tends to be conflated in the literature. Although mechanistically related, there are key features that distinguish the axon from dendrites that affect transport. For example, dendrites contain microtubules of mixed polarity, whereas the axon contain microtubules of plus-end out orientation (Figure 1.3). Additionally, post-translational modifications on tubulin monomers have region-specific effects on kinesins. Several recent reviews delineate distinguishing features between axonal and dendritic transport (Maeder et al., 2014; Nirschl et al., 2017; Kelliher et al., 2019).

Although seemingly straightforward, the regulation of transport is extremely complex. For example, the Golgi apparatus is the primary site responsible for the maturation of membrane-bound and secreted proteins, and their subsequent segregation into specific organelles based on sorting signals (Bentley & Banker, 2016). Once transport vesicles are formed, they bind to motors typically utilizing a motor-cargo adaptor that can include small GTPases, scaffolding proteins, or the cargo itself (Figure 1.3). This step of motor-cargo recruitment is complex as there are dozens of post-Golgi cargos and as many transport motors. Although motors are capable of "multi-tasking", in that one motor is capable of binding several different cargos, specific motors bind only a subset of cargos (Maday et al., 2014). Furthermore, many neuronal cargos eventually display a polarized distribution, for example, presynaptic proteins are delivered to the axon, and postsynaptic receptors, such as glutamate receptors are trafficked to

dendrites (Figure 1.3; Bentley & Banker, 2016). Thus, neurons tightly regulate this delivery either by indirect transport mechanisms where cargo may travel into both the axon and dendrite, yet fuses and is retained in the correct membrane, which is typical of the axon. By contrast, dendritic proteins are dependent upon directed transport where motors either recognize dendritic microtubules or are excluded from the axon by a filter located in the axonal initial segment (Gumy & Hoogenraad, 2018). Finally, neuronal cargos may be generated at other locations within the cell. For example, autophagosomes are formed in the distal axon and undergo a series of fluctuating transport dynamics from bidirectional in the distal axon towards a bias of retrograde, dynein-based transport towards the cell body (Stavoe & Holzbaur. 2019). Mitochondria, which are distributed throughout the neuron undergoing fusion, fission, and remodeling, also travel bidirectionally in both axons and dendrites (Figure 1.3; Saxton & Hollenbeck, 2012). Taken together, HSP-related kinesin mutations, and those found in other disease states, will reduce the efficacy of active transport and perturb cargo delivery, ultimately leading to neuronal dysfunction.
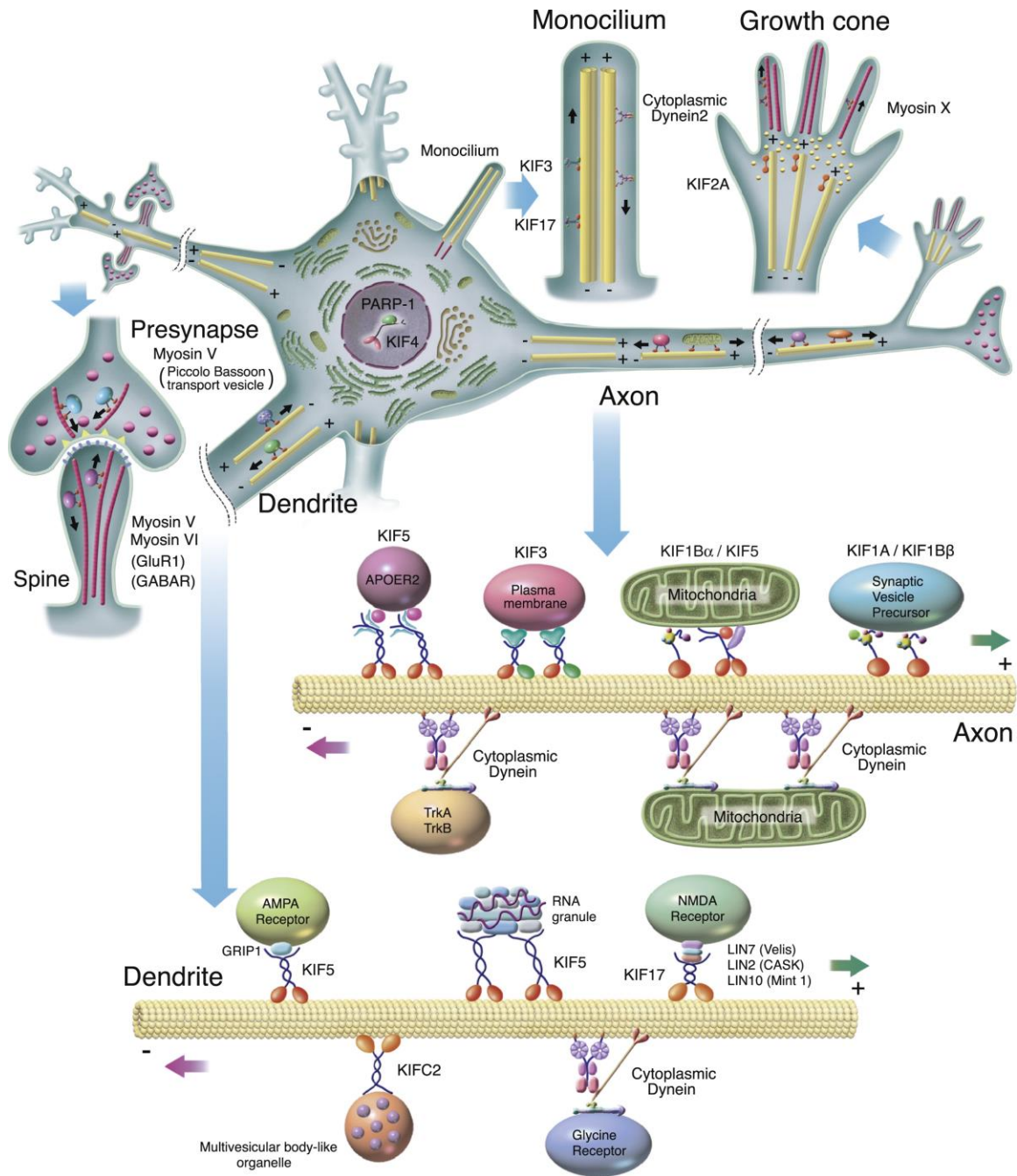
Figure 1.3. Intracellular transport of cargos in neurons.
A variety of motor proteins drive the transport of heterogeneous cargos intraneuronally. Kinesins, such as KIF1A and kinesin-1, drive anterograde transport of cargos including organelles, RNA granules, and SVPs. Cytoplasmic dynein drives retrograde transport of cargos such as AMPA and Glycine receptor containing vesicle populations. Differential distribution of cargos is driven and determined by different adaptors, motor proteins, and differential orientations of microtubule populations between axons and dendrites. (Hirokawa et al., 2010).

1.2. KIF1A Structure and Function

KIF1A carries a number of critical cargos, including synaptic vesicle precursors, dense core vesicles, and BACE-containing vesicles all of which will be explored in greater depth in the following section (Figure 1.4A). KIF1A is generally similar in overall domain structure to the well-studied conventional kinesin (KIF5), but with important distinctions. KIF1A, a neuron-enriched motor, belongs to the Walker-type ATPase family: ATPase's defined by a conserved phosphate-binding loop (P-loop) containing Walker A and Walker B motifs (Hirokawa et al., 2009). The entire kinesin-3 family motor domain sequence is highly conserved with KIF1A being no exception. The motor domain (MD) is composed of both a catalytic core in which the N-terminal half acts as the ATP catalytic center with the P-loop forming the nucleotide-binding pocket, while the C-terminal half acts as the MT-binding surface (Hirokawa et al., 2009). The MD is connected via a flexible neck linker (NL) to a neck coil domain (NC), which is followed by the coiled-coil 1 (CC1), forkhead-associated (FHA), coiled-coil 2 (CC2) and coiled-coil 3 (CC3) domains, respectively. There is also a pleckstrin homology (PH) region which acts as a C-terminal lipid-binding domain (Figure 1.4A). Furthermore, KIF1A contains an insert of positively-charged lysine residues in loop 12, an area between the NC and CC1 domain, known as the K-loop, which is also conserved across the kinesin-3 family (Hirokawa et al., 2009). This region allows for enhanced binding to the C-terminal region of tubulin known as the E-hook (glutamine rich). As a result, KIF1A undergoes super-processive movement making it especially efficient for long-range axonal transport (Soppina et al., 2014).
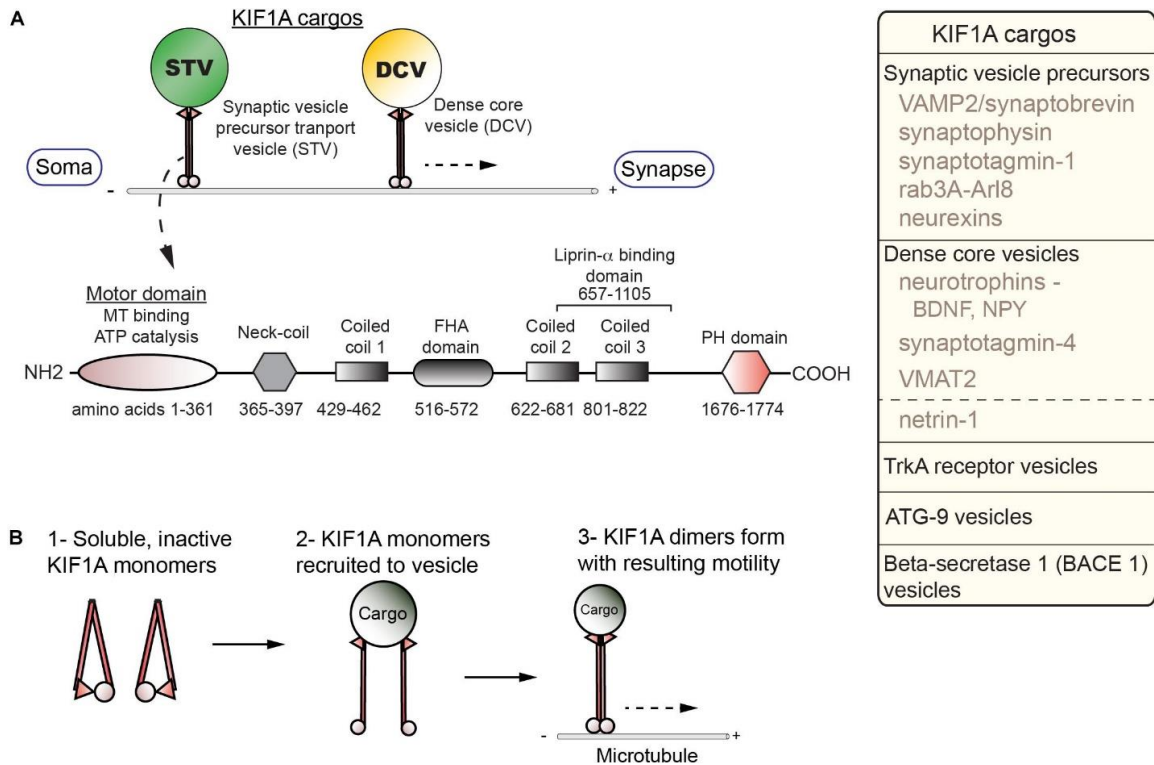
Figure 1.4. Cargoes, structure, and regulation of KIF1A.
A) KIF1A is a homodimer that traffics a number of cargos (box; right) from the soma to distal portions of axon including synapses. Below, a schematic indicates the domains identified in KIF1A (Gabrych et al., 2019). B) Diagram of activation steps of KIF1A. KIF1A exists as a soluble, inactive monomer which upon cargo binding results in a dimerization and activation of the motor. (Gabrych et al., 2019).

Regulation of KIF1A is complex and not fully understood. Competing models have posited that KIF1A is a motile monomer (Okada et al., 1995), an autoinhibited dimer (Hammond et al., 2009; S. Niwa, Pers. Comm.), or monomers that dimerize on the cargo membrane (Tomoshige et al., 2002; Soppina et al., 2014). The current model demonstrates activation of KIF1A is dependent on a monomer to dimer transition at the cargo surface (Figure 1.4B; Soppina & Verhey., 2014). This process involves relief of autoinhibition, a regulatory mechanism seen in other KIFs. The formation of the dimer at the cargo surface depends on an interaction between the NC and CC1 domains. To form a dimer, an intramolecular interaction between the NC and CC1 domains must be relieved (Figure 1.5A; Soppina & Verhey, 2014). In the case of synaptic vesicle precursors, relief of autoinhibition involves interactions with the GTPase ARL-8 and CC domains of UNC-104/KIF1A (Niwa et al., 2016). The dimer forms via an intermolecular reaction between the NC domains of the monomers and allows for motility. The catalytic core, a region containing several pathogenic mutations in KIF1A, is regulated by switch

II, a part of the C-terminal MT-binding surface (Hirokawa et al., 2009). This works in concert with the NL, with the complex acting as an actuator to produce mechanical work. Switch I, a segment between the P-loop and switch II, links, and therefore regulates, the switch II-NL complex via the nucleotide state of the binding pocket (Figure 1.5B; Hirokawa et al., 2009).

A   B
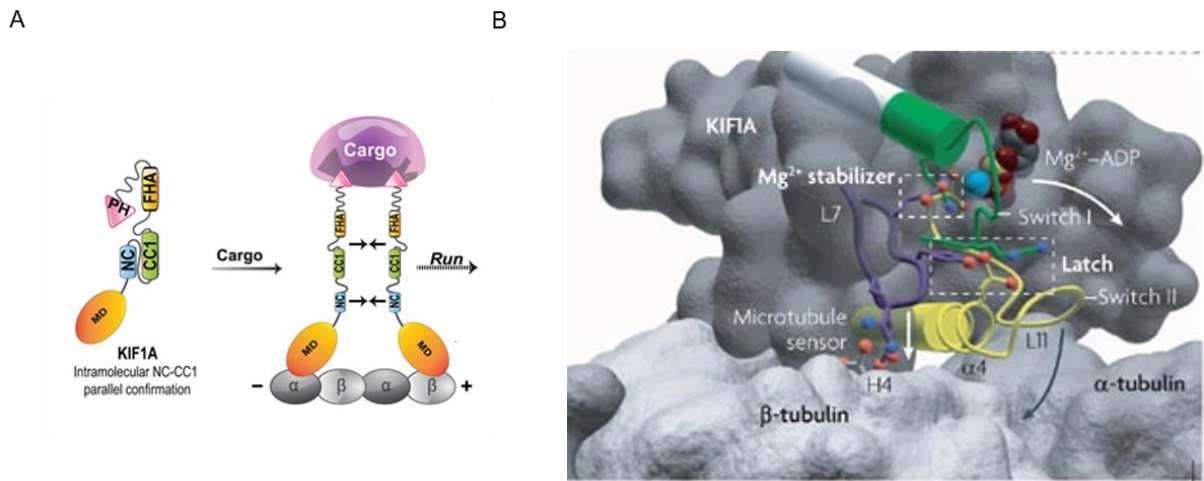
Figure 1.A. KIF1A structure and regulation.
A) A schematic representing the domains involved in the autoinhibitory regulation of KIF1A. The NC and CC1 interact to form an autoinhibited monomer. Upon binding of cargo autoinhibition is relieved and interactions between the NC and CC1 domains of monomers allow for formation of a processive dimer that can bind to microtubules and begin transport. (Soppina et al., 2014). B) A representative image KIF1A motor domain's catalytic core. Switch II acts in concert with the neck linker (green and white rod) to produce mechanical work. Switch I links the P-loop and switch II regulating the Switch II-neck linker complex through the nucleotide state of the binding pocket (red and grey; Hirokawa et al., 2009). NC, neck-coil; CC,coil-coil; FHA, Forkhead association; PH, Pleckstrin homology.

Cargo binding is an essential aspect to motor-driven transport and has been reviewed extensively (Karcher et al., 2002; Vale, 2003; Ross et al., 2008; Bentley & Banker, 2016; Hayashi et al., 2019). Knowledge on KIF1A cargo binding and how it relates to motor function is still not well characterized, but certain mechanisms have been elucidated. One of the first mechanisms identified for KIF1A cargo interactions entails the C-terminal PH domain binding to phosphatidylinositol-4,5-bisphosphate $(PI(4,5)P_2)$ on synaptic vesicles in C. elegans neurons (Klopfenstein et al., 2004). However, protein-protein interactions lend specificity to cargo recognition and regulation. For example, the GTPase Rab3a regulates the binding of synaptic vesicle precursors (SVP) to KIF1A in a DENN/ MADD dependent mechanism (Niwa et al., 2008). DENN/MADD acts as a Rab3-effector, allowing for transport of SVPs down the axon. A

shift in the nucleotide state of Rab3 releases SVPs at the synapse. For DCVs, a few mechanisms have been described that may account for their trafficking. One such mechanism involves carboxypeptidase E (CPE), a transmembrane protein needed for neuropeptide processing, where it also acts as a cargo adaptor (Park et al., 2008; Ji et al., 2017). The cytoplasmic tail of CPE binds the dynein activator dynactin. Dynactin also recruits KIF1A, thereby creating a mechanism to potentially regulate the bidirectional transport of DCVs. Another mechanism implicated liprin-α as a possible KIF1A adaptor (Shin et al., 2003), however recent findings indicate that liprin-α, in addition to TANC2, act to capture KIF1A at specific sites (Stucchi et al., 2018). Instead, the PH domain, in concert with calmodulin (CaM), dictates binding and movement of DCVs in response to increases in Ca^{2+} concentrations through direct binding to the KIF1A stalk domain (Stucchi et al., 2018). Taken together, mutations that affect any one of the various cargo-binding and regulatory domains may lead to dysregulation of KIF1A-mediated cargo delivery.

KIF1A ferries a diverse set of cargos from the neuronal soma to distal locations located within the axon (Figure 1.4A). The proteins that KIF1A transports are involved in a host of processes that are critical for neuronal development, maintenance, and viability. Such processes include synapse formation and maintenance, autophagy, glial support of myelination, APP processing, neurite outgrowth and pathfinding, ion channel regulation, and more. Dysregulation of this transport may lead to a host of neurological disorders and potential pathways have been discussed at length (Gabrych et al., 2019). Generally, KIF1A cargos can be classified into three groups based on how they are packaged and delivered; SVP-mediated cargo, DCV-mediated cargo, and unconventional cargos that are not known to be packaged in DCV or SVP vesicles.

The first cargo identified for KIF1A was the synaptic vesicle precursors (SVP), a Golgi-derived organelle containing essential proteins required to build synapses and regulate synaptic vesicle release. KIF1A/UNC-104 misdelivery of SVPs alters the size and density of synapses in model organisms such as *C. elegans* and mice (Yonekawa et al., 1998; Niwa et al., 2016). SVPs are required in every neuron in the body, thus, KIF1A mutants may have broad effects on HSP patients. KIF1A traffics SVPs involved in various aspects of vesicle fusion and release, in particular, synaptotagmin-1 (syt-1), VAMP2, and synaptophysin (Okada et al, 1995; Yonekawa et al, 1998; Sgro et al, 2013). These proteins are expressed in all cells undergoing synaptic vesicle exocytosis,

therefore, any form of disruption may cause widespread synaptic dysfunction. Notably, when synaptophysin, an integral membrane protein localized to synaptic vesicles, is knocked out, mice closely mimic KAND disorders as epilepsy, hypotonia, and X-linked intellectual disability (Harper et al, 2017). The neurexins, which are single-pass transmembrane proteins acting as cell-adhesion molecules that are derived from three genes (*Nrxn 1-3),* are another set of KIF1A-trafficked cargos. They are mainly concentrated at presynaptic sites and broadly function in neurite outgrowth, synaptogenesis, and synaptic maturation (Dean et al, 2006; Gjorlund et al, 2012; Krueger et al, 2012; Gokce & Sudhof, 2013). Furthermore, mutations in neurexins are linked to several neurodevelopmental and psychiatric disorders such as autism, epilepsy, and mental retardation, mimicking what is seen in KAND (Kasem et al, 2018).

The second cargo identified for KIF1A/UNC-104 in *C.elegans* was the dense-core vesicle (DCV) (Zahn et al., 2004). This finding was subsequently confirmed in *Drosophila*, and rodent models (Barkus et al., 2008; Lo et al., 2011; Kondo et al., 2012). DCVs are Golgi-derived vesicles typified by the presence of granin family members, such as chromogranin A and B. DCVs contain a host of proteins necessary for proper neuronal development, function, and viability. Examples of cargos include neurotrophic peptides such as BDNF and NPY, both essential for a multitude of neuronal functions (Dieni et al., 2012; Russo, 2017). An additional cargo of note is pro-opiomelanocortin (POMC), a precursor polypeptide which can be cleaved into a host of physiological important peptides including a-MSH, ACTH, and endorphins (Cawley et al., 2016). Lastly, DCVs contain a host of other cargos including, proteases, protease inhibitors, and membrane proteins such as tissue plasminogen activator (tPA), neuroserpin, and vesicular monoamine transporter 2 (VMAT2), respectively (Nirenberg et al., 1995; Lochner et al., 1998; Ishigami et al., 2007). Despite the potential heterogeneity of DCVs across different neuron types, they share KIF1A transport mechanisms. As such, dysfunctional KIF1A-mediated DCV transport may lead to pathogenesis in neurons. To highlight the importance of these DCV cargos it is critical to state that abrogation of neurotrophins such as BDNF and NPY can result in severe motor impairment or death in mouse models (Ernfors et al., 1994; Duarte-Never et al., 2015). Furthermore, mislocalization of DCV cargos such as the secreted peptide, nerve growth factor (NGF) may result in differing effects within neurons such as apoptosis-induced axonal and somal degeneration or axonal pruning (Geden and Deshmukh., 2016; Geden et al.,

2019). Neurotrophin-3 (NT-3), another DCV cargo and secreted peptide, is critical for corticospinal tract axon collaterization in the developing nervous system, a nervous system tract consistently affected in KAND underpinning the importance of KIF1A-mediated cargo delivery (Schnell et al., 1994).

Unconventional KIF1A cargos that do not appear to be packaged in DCVs or SVPs also exist and play important roles in neuronal development, function, and survival. Tropomyosin receptor kinase A (TrkA), a receptor with a high affinity for NGF, binds NGF, and the TrkA-NGF complex is internalized and trafficked retrogradely to stimulate a PI3K-dependent signalling cascade that promotes neuronal survival (Marlin & Li, 2015; Tanaka et al., 2016). The high degree of TrkA expression within the dorsal root ganglion (DRG) primary afferent nociceptor sensory neurons may underlie the pathology seen in the KIF1A-dependent disorder HSAN II (Verge et al, 1992). Using KIF1A-haploinsufficient mouse models, Tanaka et al. demonstrated that mice not only developed sensory neuropathy with an attenuated pain response similar to that seen in HSAN II patients, but using live imaging studies in DRG sensory neurons that TrkA trafficking to distal axons and sensory neuron survival was significantly reduced (Tanaka et al, 2016). The loss of sensory neuron survival is consistent with KIF1A-knockout mouse models, which also display decreased sensory neuronal survival (Yonekawa et al, 1998). Additionally, a study found that in *C.elegans* KIF1A/Unc-104 transports ATG-9, an autophagy-related protein, to neurite tips and was critical for cytoskeletal organization and synaptic architecture (Stavoe et al., 2016). In vertebrates, ATG-9A deficient neurons show reduced neurite outgrowth, and in ATG-9A knockout mice signs of neurodegeneration are seen, including spongiosis of nerve fibers in both axonal terminals and axons (Yamaguchi et al., 2018). Notably, KIF1A also traffics ß-Secretase (BACE1), an aspartyl protease that regulates critical processes including neuronal growth, function, repair, and myelination by processing a number of essential proteins (Hung & Coleman, 2016; Yan, 2017). One notable substrate of BACE1 is the amyloid precursor protein (APP), where BACE1 cleavage leads to formation of amyloid beta (Aß), a by-product notable in the pathogenesis of Alzheimer's disease (Puzzo et al., 2008). BACE1 also cleaves the cell adhesion molecule Neuregulin-1 (NRG1) (Willem, 2016). NRG1 is critical in regulating PNS myelination, development of Schwann cells, and development of muscle spindles, processes affected in KAND (Fleck et al., 2012).

Clearly, KIF1A transports critical cargos that are implicated in pathological events seen in a host of neurological disorders.

1.3. KIF1A in Neurological Disorders

KIF1A mutants are causal in a group of neurological disorders under the umbrella term, KIF1A-associated neurological disorders (KAND). These consist currently of hereditary spastic paraplegia (SPG30 in the case of KIF1A; HSP), hereditary sensory autonomic neuropathy type 2C (HSAN 2C), and progressive encephalopathy with edema, hypsarrhythmia, and optic atrophy (PEHO syndrome; Gabrych et al., 2019). HSP is specifically characterized by lower extremity spasticity, however, it can occur in both pure and complicated forms (Blackstone, 2018). The pure form is limited to progressive lower-extremity spastic weakness, while the complicated form may include symptoms ranging from optic nerve impairment, to ataxias, to an array of cognitive impairments (Blackstone, 2018). Inheritance patterns can include autosomal dominant, autosomal recessive, X-linked, or mitochondrial inheritance (Hedera, 2018). Dominant *de novo* mutations may arise, however, these are rare as compared to inherited disease (Hedera, 2018). HSAN 2C is a less commonly seen disorder in KIF1A mutants that results in progressive loss of sensation in the hands and feet, with symptomology beginning at the fingers and toes seen as inflammation (Kurth et al., 2010). Loss of sensation may include pain, temperature and positional disturbances. Notably, sensory loss is due to a progressive degeneration of the sensory nerves, particularly myelinated fibers, with little to no loss in unmyelinated fibers (Hilz, 2002). Importantly, although degeneration of sensory nerves is seen, the disorder itself is not progressive. There is also autonomic involvement which manifests as severe feeding problems and apnea. PEHO syndrome, in addition to the pathos indicated in its name, presents in early life as infantile spasms, seizures, and may progress to severe intellectual deficits, and developmental pathologies such as tapered fingers and facial dysmorphisms. PEHO is an autosomal recessive and dominant disorder that presents as a progressive neurodegenerative disorder (Chitre et al., 2018). Similar to SPG30 and HSAN2C, developmental pathologies are seen which lends credence to the fact that these disorders are not strictly degenerative but may have an underlying dysfunctional developmental component. KIF1A mutants may affect a wide array of neuronal subtypes ranging from cortical neurons, to upper motor neurons, as well as sensory neurons

(Parodi et al., 2017). How different mutations affect different neuronal subtypes specifically is currently unknown. Even more notably, the same mutations may affect individuals differently leading to a discrepancy in symptomology between individuals. As with many other neurodegenerative disorders, HSP and HSAN 2C is neither treatable nor curable with current therapies. Rather, treatments center on relieving symptomology, such as the use of intrathecal Baclofen, and botulinum toxin injections to reduce spasticity, along with physical therapy for general motility and maintenance of strength (Fink, 2013; Bellofatto et al., 2019). To target the underlying pathophysiology in kinesin-3 motor-mediated HSP and HSAN2C, therapeutics would have to be mutation specific, as mutants exhibit loss-of-function or hyperactivity as is explained extensively in the following section.

1.4. KIF1A Disease Causing Mutations

SPG-30 causing KIF1A mutations are found in the motor, regulatory, and cargo binding regions (Figure 1.6). As such, specific mutations may differentially affect KIF1A function depending on the domain. For example, E253K affects ATPase activity within the motor domain, while the Q632* deletion mutant removes the CC2, CC3, and PH domains critical for regulation and cargo binding (Nieh et al., 2015; van de Warrenburg et al., 2016). The consequent changes in KIF1A function are ultimately mislocalization of cellular cargos via distinct mechanisms, including failure to properly regulate KIF1A motility and to bind to cargo. The extent and severity of SPG-30 symptomology is dictated by the patient's genotype and the resulting changes in KIF1A amino acid residues.
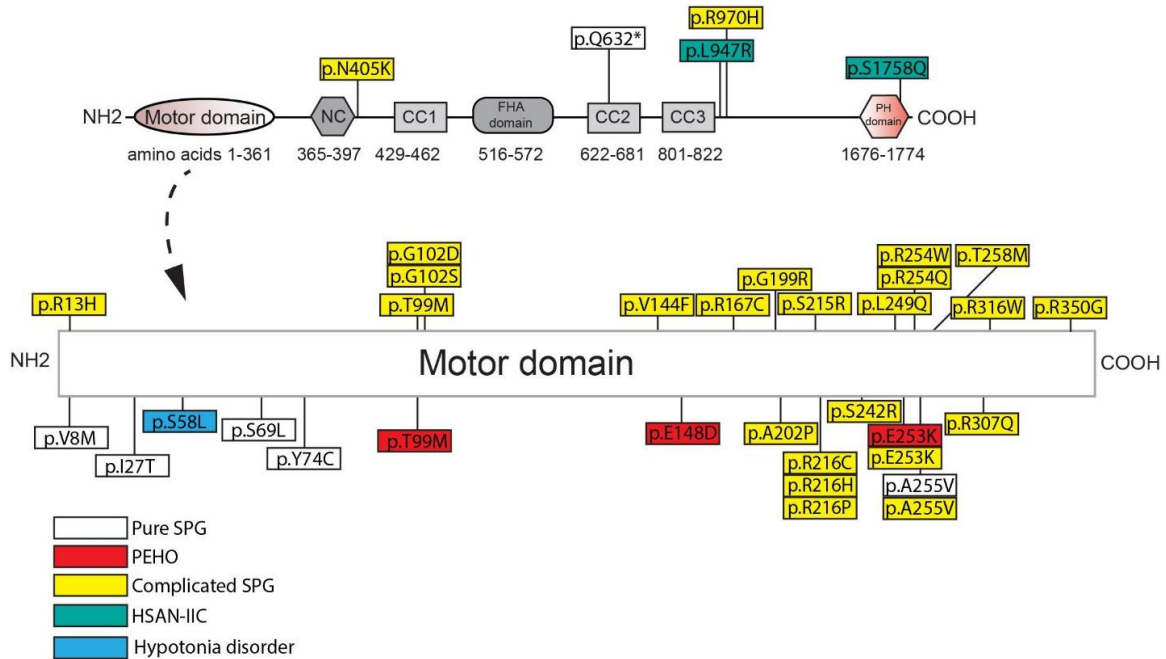
Figure 1.5. Amino acid changes in KIF1A in HSP and related disorders in humans.
A schematic of amino acid changes in KAND based on their structural location in KIF1A. Most mutations currently known are situated in the motor domain of KIF1A with only a few in regulatory and cargo binding regions of the motor (Gabrych et al., 2019). NC, neck-coil; CC, coil-coil; FHA, Forkhead association; PH, Pleckstrin homology.

Loss-of-function mutations in the motor domain of KIF1A constitute the vast majority of SPG-30 cases. They affect a variety of structural domains such as those critical for ATP hydrolysis, generation of mechanical force (Switch I and II), and microtubule binding (loop L8). Some examples include mutations that reside in Switch I (R216C) and Switch II (E253K), as well as mutants that destabilize loop L8 (R316W) (Lee et al., 2015; Nieh et al., 2015). The vast majority of KIF1A mutants have not been analyzed for function, but a subset results in impaired motility and/or an altered distribution compared to wild type, where the motor accumulates proximally. For example, the Switch II mutant E253K, and the ATP-binding cassette mutant T99M, have drastically reduced motility and are unable to reach the distal portions of the axon (Nieh et al., 2015; Cheon et al., 2017). This suggests that the inability to traffic cargos into the axon may underlie downstream pathogenesis in SPG-30. Surprisingly, gain-of-function mutations in KIF1A are also seen in SPG-30. Using single molecule assays, Chiba et al., recently demonstrated, that three KIF1A mutants causal in SPG-30 (V8M, R350G, A255V) had higher landing rates on MT's, along with a greater velocity than WT KIF1A in two of the three mutations (A255V had similar velocity to WT) (Chiba et al., 2019).

Notably in two of the mutants (V8M, A255V), SVPs accumulated at the axonal tips of *C.elegans* ALM neurons, suggesting that excessive cargo accumulation may be pathogenic.

Moreover, an interplay between a variety of factors influence the pathogenicity of the mutation including the functional domain, the amino acid properties, and heritability patterns. Conserved amino acid changes, such as the A255V mutant, tend to result in less severe effects on motor motility, which is reflected in reduced severity of symptomology (Nieh et al., 2015; Cheon et al., 2017). Mutants in which the residue properties are drastically changed, such as that in the E253K mutant, show much more severe motor motility changes, leading to complicated SPG-30 (Nieh et al., 2015; Cheon et al., 2017). Some SPG-30 loci have multiple different amino acid changes, for example, R216 mutations can be either a histidine, proline, or cysteine leading to differing clinical symptoms (Lee et al., 2015; Nieh et al., 2015; Travaglini et al., 2018). However, it is important to note that without histopathological samples, the link between changes in motor properties and symptomology is tenuous. Furthermore, prediction of the presentation of the disease based on the mutation is difficult. This is exemplified by the A255V mutant, as it causes both the pure and complicated forms of SPG-30 where a patient's genetic background will affect how the mutations manifest physiologically (Erlich et al., 2011; Klebe et al., 2012). Lastly, it is important to note that mutations implicated in complicated SPG-30, such as T99M and E253K, are causal in PEHO syndrome suggesting a similar etiology between the disorders (Lee et al., 2015; Nieh et al., 2015; Samanta & Gokden, 2019). Furthermore, a mutation exclusive to PEHO syndrome, E148D, presents with symptomology akin to complicated SPG-30, further suggesting that the etiology of these KIF1A-related disorders may be similar (Ohba et al., 2015).

Mutations that implicate regulatory and cargo binding regions of KIF1A are both causal in pure and complicated forms of SPG-30 and HSAN-IIC. Presently, no studies exist that assay the motility, regulatory, or cargo binding capabilities of these KIF1A mutants. However, mutations in the KIF1A PH domain lead to reduced cargo binding in *C. elegans*' neurons (Klopfenstein et al., 2004). Thus, disease loci that likely truncate the cargo binding domains of KIF1A, such as the pure SPG-30 Q632* mutant, might result in in a complete absence of cargo binding and delivery (van de Warrenburg et al., 2016). Despite such changes to KIF1A in SPG-30, patients can live for decades with this

disorder implying there is some redundancy in KIF1A function. One example may be that DCVs can be transported in tandem or by alternate motors such as KIF1C and KIF5 (Gauthier et al., 2004; Lim et al., 2017; Stuchi et al., 2018). The fidelity of cargo delivery may be altered when the complement of neuronal kinesins are shifted.

1.5. Functional Assays for Transport Kinesins

Biological assays that probe a host of parameters that constitute the functioning of a kinesin are integral for understanding transport motors and their roles in proper biological functioning and disease. In kinesins, the parameters that underlie its behavior as a transport motor fall under a few general categories; enzymatic function of the motor domain which underlie processivity, kinesin autoinhibitory regulation, and general transport parameters such as velocity, run length and pause duration. Fortunately, biophysical, biochemical, and cell biological assays that probe these functional parameters have been well-developed and used widely.

ATPase assays exist that examine functional parameters of the kinesin motor ATPase domain such as ATP hydrolysis rates, efficiency of an ATPase in driving a motor, and ability to bind microtubules as a function of ATP concentration. Typically, these assays are absorbance-based and rely on the catalyzed reaction between inorganic phosphate (a by-product of ATP hydrolysis) and another molecule, such as MESG (2-amino-6-mercapto-7-methylpurine ribonucleoside) in the case of an ELIPA (enzyme-linked inorganic phosphate assay), to cause a detectable absorbance shift relative to the amount of inorganic phosphate produced (Figure 1.7A; Webb., 1992). Conversely, assays exist that allow for assaying of ADP produced from ATP hydrolysis by converting ADP into a luminescent signal through an enzymatically coupled kinase and luciferase-based reaction (Figure 1.7B; Zegzouti et al., 2010). Many of these assays, such as the ELIPA mentioned previously and ADP-Glo assays exist commercially from companies such as Cytoskeleton Inc. and Promega and therefore are easily accessible and have been utilized in many experimental contexts, including high-throughput screens (Kadakkuzha et al., 2014). In a disease context, these assays constitute a robust method for detecting changes in ATPase domain activity when mutations are introduced in the motor domain of transport kinesins such as KIF1A. For example, the T99M SPG30-causing mutant is found within the ATP-binding cassette of KIF1A would benefit from this type of assay as it has been shown to have decreased

motility compared to wild-type KIF1A, but the cause is not yet known (Nieh et al., 2015; Cheon et al., 2017). *In silico* studies show that the T99M mutant affects ATP binding and ultimately an *in vitro* ATPase assay may show a reduction in ATPase efficiency experimentally (Nieh et al., 2015).
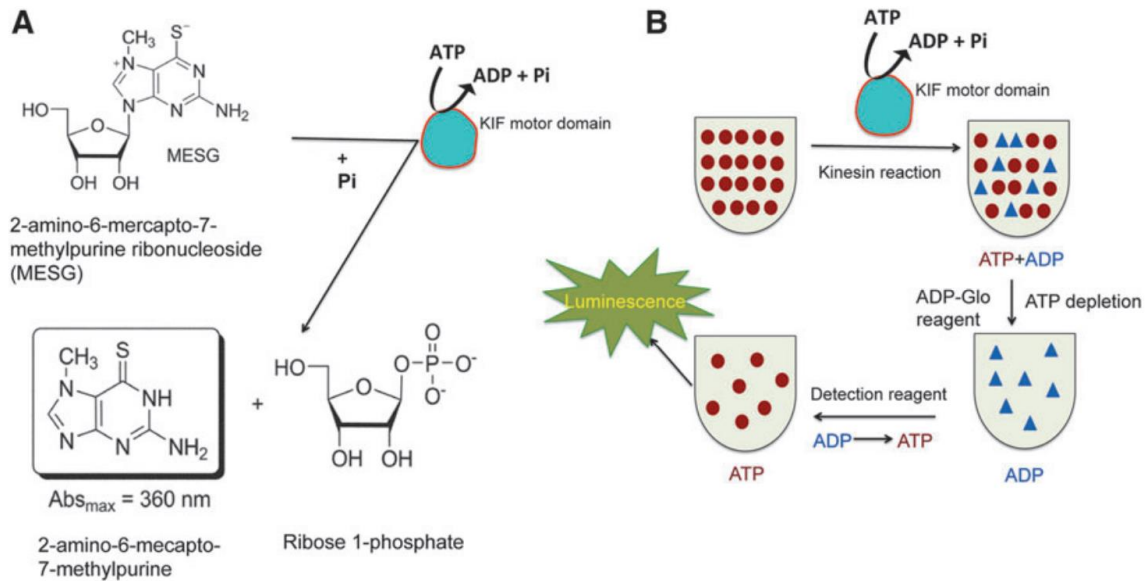
Figure 1.6. Schematic representation of common ATPase assays.
A) A schematic representation of an ELIPA ATPase assay. MESG is catalytically converted to 2-amino-6-mercapto-7-methyl purine in the presence of inorganic phosphate, a byproduct of ATP hydrolysis, causing a detectable absorbance shift from 330 to 360 nm. (Kadakkuzha et al., 2014) B) A schematic representation of an ADP-based ATPase assay. ADP produced as a byproduct of ATP hydrolysis is converted to a luminescent signal through an enzymatically-coupled kinase and luciferase-based reaction. ATP is depleted using a specific reagent (ADP-Glo™) following hydrolysis and a luciferase-based detection reagent is used to detect newly synthesized ATP. (Kadakkuzha et al., 2014).

Assays that probe the autoinhibitory regulation of transport kinesins are invaluable in assessing activation and inhibition of motors as a whole. Motors such as KIF1A, KIF1C, and kinesin-1 are found *in vitro* and *in vivo* in either an autoinhibited monomeric or dimeric form (Hammond et al., 2009; Siddiqui et al., 2019). This is seen in cells as a diffuse, soluble phenotype. Conversely, upon binding of a cargo or regulation by certain factors such as GTPases or kinases such as CaMKII, autoinhibition is relieved and the motor is bound to the microtubule. In cells, this is seen as a microtubule-bound, tubular phenotype, with typical peripheral accumulation of the motor due to its ability to translocate along microtubules (Figure 1.8; Hammond et al., 2009; Niwa et al., 2016). In fact, due to the robust nature of this assay in determining whether the motor itself is activated or not, I utilized this assay in the high-throughput screen I developed and

optimized as my thesis project. The degree of microtubule-binding and peripheral accumulation can be related to the extent of motor activation and has been used extensively in studies that probe autoinhibitory regulation in transport kinesins (Cai et al., 2007; Hammond et al., 2009; Niwa et al., 2016).
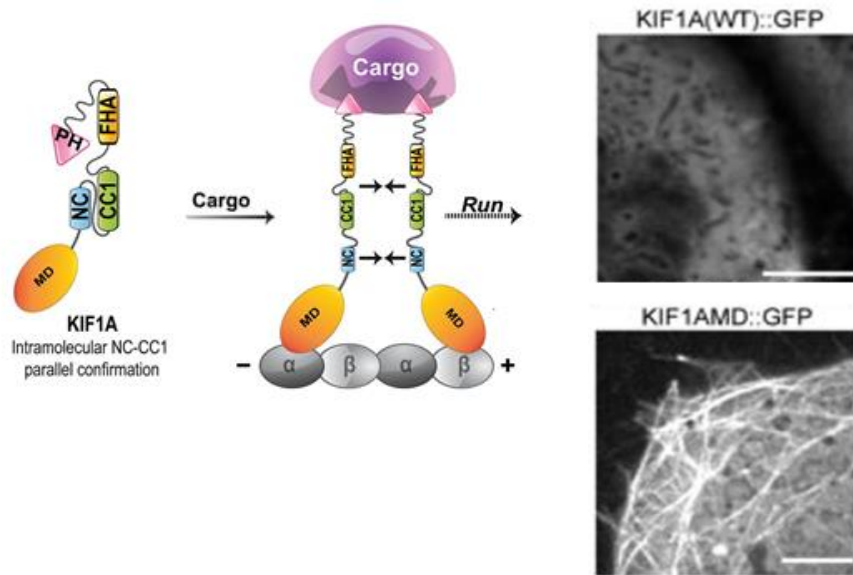
Figure 1.7. Microtubule-binding assay.
Microtubule-binding assays utilize the inherent autoinhibition and relief of autoinhibition of kinesins such as KIF1A and KIF1C to assess activation of the motor through microtubule binding. Motors that are autoinhibited such as the wild-type KIF1A, present as a soluble, diffuse signal *in vitro.* Upon relief of autoinhibition, motors such as the truncated motor domain of KIF1A, bind to microtubules and result in a tubular phenotype. (Soppina et al., 2014; Niwa et al., 2016).

The most common assays seen for probing kinesin activity, particularly in a neuronal context, are transport assays that utilize particle tracking and kymograph analysis, which allow for determination of parameters such the velocity of the motor, on/off rate, pause duration, and run length. These studies are incredibly useful in tracking cargo trafficking via molecular motors over variable distances over a predetermined period of time. Furthermore, these assays are integral for understanding the aforementioned parameters of the motor in an environmentally specific context. For example, using a microtubule-gliding assay, an assay in which the motor is affixed onto a glass surface and ATP and microtubules are supplied, one can assess motor velocity, on/off rate, pause duration, and run length in an environment completely devoid of external factors such as kinases, phosphatases, GTPases, chemical signals, and more (Figure 1.9; Lopes et al., 2019; VanDelinder et al., 2019; Kaneko et al., 2020).

Furthermore, one can alter the properties of the microtubules, such as supplying the motor with acetylated or tyrosinated microtubules, post-translational modifications known to affect a variety of motor parameters. Ultimately, this type of transport assay gives one complete control of the motor's environment. Conversely, using fluorescently-tagged motors and potential or known cargos, one can assess transport parameters in cells where the environment is more akin to that *in vivo* (Stucchi et al., 2018; Gan et al., 2020). One can assess how transport is affected under pathological conditions, such as by introducing Aβ to simulate Alzheimer's disease conditions, mutant α-synuclein to simulate Parkinson's disease conditions, or even introduce a mutant motor such as the SPG30 KIF1A mutants to see how the mutant motor functions in a cellular environment (Saha et al., 2004; Ramser et al., 2013; Chiba et al., 2019). Ultimately, this is a powerful way to study motors in a physiological context, albeit being more complex to analyse than the previously mentioned assays. As such, the use of these types of assays in drug discovery is uncommon but is increasing.
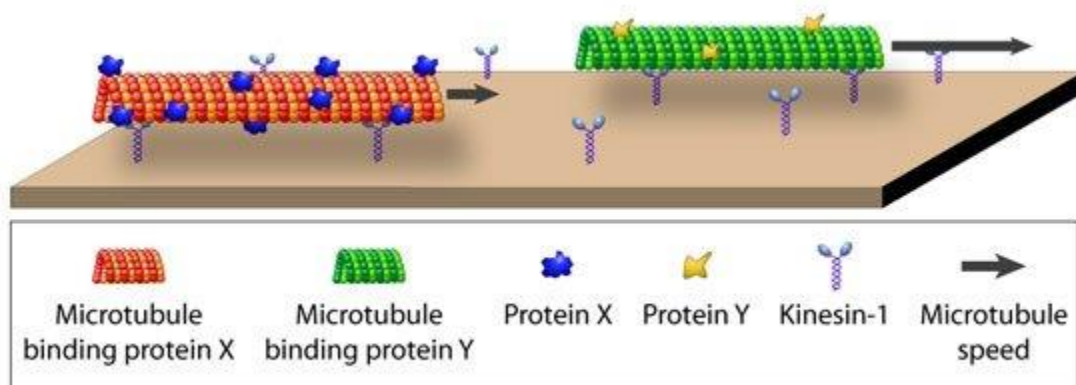
Figure 1.8. Microtubule-gliding assay.
A schematic representation of a microtubule-gliding assay. Motor proteins are affixed onto a glass surface and supplied with microtubules and ATP. Motor proteins will then move microtubules in a unidirectional manner allowing for assessment of motor properties such as run length, velocity, and on-off rate. (Korten and Diez., 2008).

A unique assay that is incredibly powerful in terms of assaying a kinesins ability to transport cargo is the Golgi/peroxisome-dispersion assay (Figure 1.10; Kapitein et al., 2010; Schimert et al., 2019; Gan et al., 2020). In this assay, a kinesin is tagged with a fluorescent protein along with a rapamycin-binding (FRB) domain and is co-expressed with a fluorescently-tagged, peroxisome-targeted (PEX), or Golgi-targeted (GMAP-210), FK506 binding protein (FKBP). Upon addition of rapamycin, dimerization occurs between the FRB and FKBP domain and the motors are targeted towards the

23

peroxisome or Golgi depending on what targeting sequence is expressed. Motors then redistribute either cargo to the cell periphery. This allows one to determine how efficiently motor activation occurs when bound to cargo, how well it can redistribute cargo, and parameters such as run length, velocity, on/off rate, and pause duration.
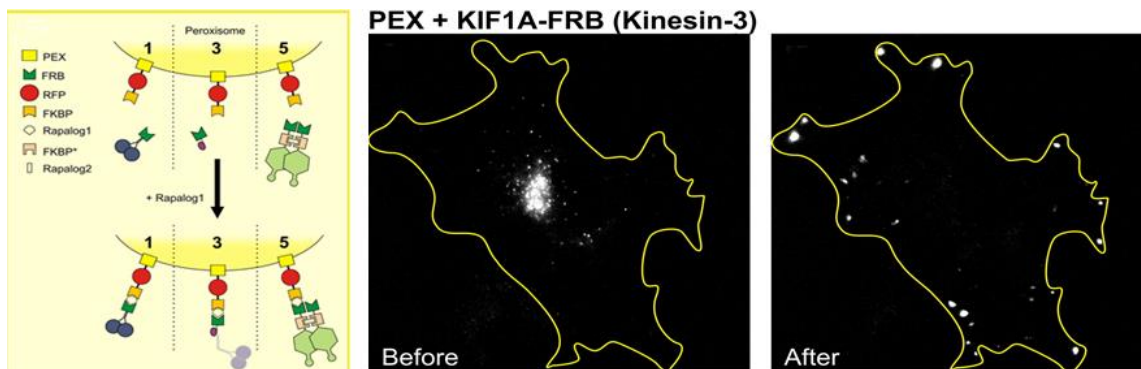
Figure 1.9. Peroxisome/Golgi-dispersion assay.
A motor protein is tagged with a fluorescent protein along with a rapamycin-binding (FRB) domain and is co-expressed with a fluorescently-tagged, peroxisome-targeted (PEX), or Golgi-targeted (GMAP-210), FK506 binding protein (FKBP). Upon addition of rapamycin, dimerization occurs between the FRB and FKBP domain and the motor proteins are targeted towards the peroxisome or Golgi depending on what targeting sequence is expressed. Motor proteins are then redistributed either cargo to the perinuclearly or to the cell periphery depending on directionality of the motor protein. (Kapitein et al., 2010).

1.6. High-Throughput Screening of Kinesins in Drug Discovery

High-throughput screening is an experimental platform for large-scale assaying and discovery of pre-existing and novel drug effects on biological phenomenon using robotics, platform-specific software, and optimized and validated assays. The developmental pipeline of a high-throughput screen involves seven main components; target identification, assay development and optimization, assay validation, a pilot screen, a primary screen, confirmation and validation of hits (molecules that confer the expected change in the assay), and orthogonal assaying and hit optimization (Figure 1.11; Sittampalam et al., 2004). Designing a robust high-throughput screen that accurately allows for discovery of new therapeutic and tool compounds depends greatly on the quality of the biological assay used for drug screening. The Assay Guidance Manual by the NIH is a key resource regarding assay development and optimization for

high-throughput screening (Sittampalam et al., 2004). Succinctly, parameters that constitute a high-quality assay include optimized assay reagents such as plasmids, cell lines and chemical reagents. Moreover, a viable high-throughput assay needs an optimal signal to noise ratio, robust analyses, positive and negative controls, good plate design to identify systemic errors, and potential for streamlined automation of the assay pipeline.

Figure 1.10. Schematic of a high-throughput screening workflow.
A schematic of a high-throughput screening workflow. Assay design, optimization and validation is key to developing a robust screen. A pilot screen precedes the primary screen and allows for further optimization and validity testing. A primary screen follows with subsequent hits needing to be confirmed with orthogonal and secondary assays. (Rockefeller University, HTSRC, 2019).

The assay must be validated by means of a measure of the assay's performance. Many traditional measurements exist including signal to noise ratios, signal to background ratios, and the most commonly used measurement: the Z'-factor (Sittampalam et al., 2004, Inglese et al., 2007). The Z' is a measure of the separation window between the positive and negative control data and ranges between the value of 0 and 1, with higher values indicating a more robust assay, 1 being the ideal assay (Figure 1.12). Generally, various assays have recommended Z'-factors to be considered a valid assay. For example, in a cell-based, phenotypic screen, an assay above 0.2 is considered valid for high-throughput screening, as these types of assays typically describe complex biological phenomenon with complex analyses to go with them (Sittampalam et al., 2004). Conversely, assays that are generally less complex with analyses that are relatively standardized such as nuclear translocation assays, typically show Z' of 0.7 or greater (Sittampalam et al., 2004). This does not mean that an assay with a Z' of less than the recommended measure will not identify hits, however, it does mean that the reliability of those hits will not be as robust as that of a higher Z' assay. Following validation by generation of a Z'-factor, a pilot screen is typically done using a pre-determined chemical or biologic library to screen for problems in assay design and analysis shortfalls as full-scale primary screens are generally a high-cost, low-reward endeavour. Primary screens follow, barring problems with the pilot screen, followed by

identification of hits, dose-response curve generation, and orthogonal assays to confirm hits and generate lead compounds.

$$Z' = 1 - \frac{3(\sigma_p + \sigma_n)}{|\mu_p - \mu_n|}$$
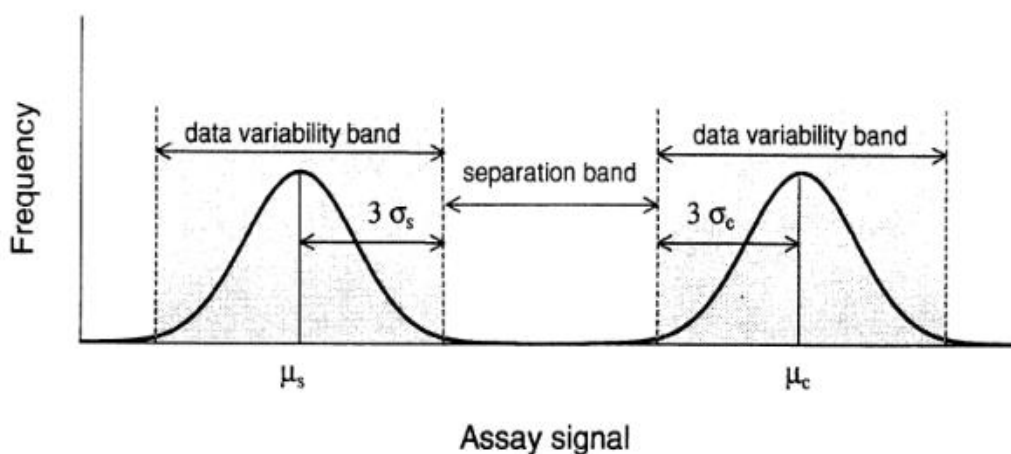
Figure 1.11. Z' equation and schematic
Z', or Z-factor, is a statistical parameter that measures statistical effect size. In high-throughput screening it is used as a measure to evaluate the robustness of the assay being used. It measures the separation between three times the standard deviation of the positive and negative control signal. (Zhang et al., 1999). σ_p, standard deviation of positive control; σ_n, standard deviation of negative control; μ_p, mean of positive control; μ_n, mean of negative control.

High-throughput screens involving kinesins are abundant, however, they generally involve mitotic kinesins such as Eg5 and KIFC1. Indeed, the first kinesin to be screened for possible modulators was the mitotic kinesin EG5 (Mayer et al.,1999). This particular screen was a phenotypic screen that used two assays; one whole-cell immunofluorescence assay, which exploited a post-translational modification on a nucleolar protein that is phosphorylated during mitosis, and a second that identified changes in mitotic spindle conformation. Notably, it identified a molecule, Monastrol, that acted on helix α2/loop L5 and helix α3 which composed a specific inhibitor binding pocket of Eg5 that allosterically inhibited its ATPase activity (Tcherniuk et al., 2010). Despite the high degree of sequence conservation seen in the motor domain of kinesins, Monastrol was able to bind an Eg5-specific region showing that the motor domain may still be a viable target in other kinesins (Bergnes et al., 2005). Interestingly, this gave rise to a host of screens that attempted to exploit potential specific regions in the motor domains of kinesins, although these screens mainly targeted the highly conserved

26

ATPase domain. One such example is that of the mitotic motor KIFC1, in which scientists at AstraZeneca used a Malachite Green ATPase assay and followed up hit identification with structural activity studies (SAR) to generate a variety of compounds that act as specific inhibitors of KIFC1 ATPase activity (Yang et al., 2014). Another example includes the transport motor KIF5B, in which two ATPase assays; one that measured inorganic phosphate levels, and an orthogonal assay which measured ADP levels, was used to identify hits from the Library of Pharmacologically Active Compounds (LOPAC) library of compounds (Kadakkuzha et al., 2014). Although activators and inhibitors of ATPase activity were found for this transport kinesin, follow up studies have not been published and therefore it is unknown whether these hits were confirmed as lead compounds and specific to KIF5B.

More recently, newer screens have been published which include transport kinesins such as kinesin-1 and, dynein. Interestingly, the kinesin-1 screen employed a novel FRET-based assay that identified molecules that disrupt the interaction between kinesin-1 and short linear peptide motifs in organelle-specific cargo adaptors (Randall et al., 2017). As mentioned previously, regulation via cargo adaptors constitutes one regulatory pathway for relief of autoinhibition of kinesins, and to date, no known compounds specifically target these interactions. This screen identified a small molecule, Kinesore, as an *in vitro* inhibitor of the kinesin light-chain and lysosomal cargo adaptor SKIP. In turn, this molecule allowed for a conformational change that led to motor activation. Another interesting assay was utilized in a dynein screen and employed a peroxisome-distribution assay (Kapitein et al., 2010; Schimert et al., 2019; Vincent et al., 2020). This screen identified several potential activators and inhibitors of dynein-based cargo transport that seem to be independent of microtubule-based effects. This would lead further credence to the idea that small molecules may be able to directly target transport motors. Taken together, compounds have been found that specifically affect the various domains and regulatory mechanisms of the transport motors kinesin-I and dynein. As such, it may be possible to find small molecule compounds or biologics that directly target KIF1A and its disease-causing mutants leading to potential tool compound and therapeutic development.

1.7. Project Overview

The overarching goal of my thesis was to develop a high-throughput screen for small molecule modulators of the molecular motor, KIF1A. As KIF1A is neuron-enriched, with low expression in other organ systems, therapeutics that specifically target KIF1A would potentially have minimal off-target effects. To accomplish this, I developed and optimized an assay that allows one to distinguish between inactive, autoinhibited KIF1A and the active, microtubule-bound KIF1A. In its inactive form, KIF1A exists in an autoinhibited, monomeric form, although some research indicates it also may exist in an autoinhibited dimer conformation. This autoinhibited form, when expressed in cells, is seen as a soluble, diffuse signal. Upon activation through cargo binding or by introduction of a hyper-activating mutation such as the V8M mutation, KIF1A binds the microtubules and transports to the cell periphery. I had three major goals in terms of developing this high-throughput screen.

1) Develop and optimize a cell-based, phenotypic assay for a high-content, high-throughput screening platform.

    This goal consisted of generation and validation of required reagents and cell lines, i.e. plasmids, cell lines (neuronal and non-neuronal), identification of positive and negative controls for downstream determination of Z-score, identification of phenotypes (soluble and diffuse signal versus peripherally accumulated and microtubule-bound, tubular signal), and generation of stable cell lines expressing my positive and negative controls.

2) Generate a robust, high-throughput analysis for peripheral accumulation of KIF1A and colocalization of KIF1A and the microtubule marker EB3.

    For robust assaying of activated versus non-activated phenotypes, image analyses must be optimized for the phenotype one wishes to assess. This includes segmentation of cells, accurate identification of parameters that represent the phenotype being assayed (e.g. mean fluorescence intensity, Pearson's correlation coefficient, etc.), background subtraction, and identification of primary and secondary structures within cells. In this case, I was able to generate an analysis that allows for identification of raw and normalized fluorescence intensity levels in segmented areas of the cell.

28

This work is significant as currently there are no known therapeutics or cell-permeable tool compounds that exist for KIF1A. This phenotypic screen allows for relatively low-cost, high-throughput assaying of small molecule modulators of KIF1A and allows for multiple parameters of KIF1A function to be assessed including activation, microtubule-binding capacity, and efficiency of transport. Ultimately, I hope this high-throughput screen yields KIF1A-specific hit compounds that can be developed into lead compounds for clinical testing or experimental use.

Chapter 2.   Materials and Methods

2.1. Plasmid Generation

Wild-type (WT) KIF1A-GFP and V8M mutant KIF1A-GFP cDNA's were excised from pEGFP-N1-KIF1A-GFP and pEGFP-N1-V8M-KIF1A-GFP (a kind gift from Dr. Shinsuke Niwa, Tohoku University) using *EcoRI* and *NotI* restriction endonucleases (New England Biolabs, Ipswich, MA, USA). pTetOne Doxycycline-On (Takara Bio, Kyoto, Japan) and pEF-GFP (Addgene: #11154) vectors were digested using *EcoRI* and *NotI* restriction endonucleases and subsequently treated with Quick calf intestinal alkaline phosphatase (Quick CIP; New England Biolabs, Ipswich, MA, USA) to prevent subsequent self-ligation of vector. Restriction fragments were size separated by agarose gel electrophoresis and desired fragments excised and purified using QIAquick Gel Extraction Kit (Qiagen, Venlo, Netherlands). Wild-type KIF1A-GFP and V8M mutant KIF1A-GFP fragments were ligated with both pTetOne Doxycycline-On and pEF-GFP vector fragments using T4 DNA Ligase (New England Biolabs, Ipswich, MA, USA) at 16°C overnight. High-efficiency DH5α competent *E.coli* (New England Biolabs, Ipswich, MA, USA) were transformed by chemical transformation. 10 µL ligated DNA mixture was added to 50 µL *E.coli* on ice and incubated for 2 minutes. The mixture placed in 42°C for 30 seconds and returned to ice for 5 minutes. 950 mL LB media was added and placed in an incubating shaker for 60 minutes at 37°C at 250 rpm. 100 µL of mixture was spread onto ampicillin agar plates for both pTetOne Doxycycline-On and pEF-GFP vectors and incubated for 16 hours. Colonies from each condition were picked and placed in liquid LB cultures containing 1:1000 dilution of 100ug/mL ampicillin and placed in an incubating shaker for 16 hours at 37°C at 250 rpm. Plasmids were extracted using QIAprep Spin Miniprep Kit (Qiagen, Venlo, Netherlands) and cloned plasmids were subsequently confirmed by sequencing and agarose gel electrophoresis via restriction digestion using *SacI, EcoRI, and NotI* restriction endonucleases (New England Biolabs, Ipswich, MA, USA). The microtubule marker, EB3-mKate2, was a kind gift from Julian Guttman, Simon Fraser University.

2.2. Cell Culture and Transient Transgene Expression

COS-7 cells were grown and maintained in Dulbecco's Modified Eagle Medium (DMEM) and 10% fetal bovine serum (FBS) at 37°C/5% CO_2 conditions. SK-N-SH cells were grown and maintained in Eagle's Minimum Essential Media (EMEM) and 10% FBS at 37°C/5% CO_2 conditions. For phenotypic assessment in COS-7 and SK-N-SH, 150 000 cells were plated onto glass coverslips in a 6 cm dish and incubated overnight at 37°C, 5% CO_2 conditions. The following day, transient transfections were carried out using liposomal-mediated gene delivery or through electroporation. For liposomal-mediated gene delivery, jetPRIME transfection reagent (Polyplus-transfection SA, New York, NY, USA) was used. 2µg total of plasmids were mixed with 200µL jetPRIME buffer with subsequent addition of 4µL jetPRIME reagent. The mixture was incubated for 10 minutes at room temperature and added to cells in serum-containing media. Cells were incubated at 37°C/5% CO_2 conditions for 4 hours, after which media was exchanged and cells re-incubated at 37°C/5% CO_2 conditions for 24 hours. For gene delivery through electroporation the Amaxa Cell Line Nucleofector Kit V (Lonza, Basel, Switzerland) with corresponding Amaxa Nucleofector IIb (Lonza, Basel, Switzerland) was used. Cells were detached using HyClone Trypsin, 0.25% (Danaher, Washington D.C., USA) and resuspended in the respective media. 1 x 10^6 cells were isolated and spun down at 200xg for 10 minutes at room temperature. Cells were resuspended in 100 µL Nucleofector solution and 2µg total plasmid was added to the mixture. Suspensions were transferred to cuvettes and electroporated with the respective programs (W-001 for COS-7 and X-005 for SK-N-SH). Cells were subsequently resuspended in 500 µL of their respective medias, plated, and incubated for 24 hours at 37°C/5% CO_2 conditions.

2.3. Doxycycline-Inducible KIF1A Expression

To assess doxycycline-inducible KIF1A expression at various times and concentrations, 150 000 COS-7 cells were plated onto glass coverslips in a 6 cm dish and incubated overnight at 37°C, 5% CO_2 conditions. The following day, transient transfections were carried out using jetPRIME transfection reagent (Polyplus-transfection SA, New York, NY, USA) for liposomal-mediated gene delivery. 2µg total of pTetOne-WT-KIF1A-GFP were mixed with 200µL jetPRIME buffer with subsequent addition of 4µL jetPRIME reagent. The mixture was incubated for 10 minutes at room

temperature and added to cells in serum-containing media. Cells were incubated at 37°C/5% CO_2 conditions for 4 hours, after which media was exchanged and cells were allowed to express 24 hours. Subsequently, media was removed and replaced with three dilutions of 1mg/mL stock doxycycline (1:10000, 1:5000, 1:1000). Cells were allowed to express for 4, 8, and 24 hours post-induction of transgene expression via doxycycline addition. Following those time points, glass coverslips with adhered cells were removed and washed with 1 x Dulbecco's Phosphate Buffered Saline (dPBS). dPBS was removed and cells were fixed with 4% paraformaldehyde (PFA) solution for 15 minutes at 37°C. PFA was removed and cells were washed two times in one minute intervals with dPBS. Cells were subsequently incubated at room temperature for 5 minutes with a 300 nM 4′,6-diamidino-2-phenylindole (DAPI) solution in dPBS for staining of nuclei. Cells were washed with dPBS 3 times in 5 minute intervals and mounted using elvanol and subsequently imaged using widefield fluorescence microscopy.

2.4. Lentiviral Transduction and Stable Cell Line Generation

Lentiviruses were generated and packaged by Applied Biological Materials (Applied Biological Materials Inc, Richmond, BC, Canada) with a custom made EB3-mKate2 plasmid generated by Applied Biological Materials (Applied Biological Materials Inc, Richmond, BC, Canada). For transduction of both cell lines, COS-7 and SK-N-SH, cells were detached using HyClone Trypsin, 0.25% (Danaher, Washington D.C., USA) and resuspended in their respective media. Cells were plated at 10000 cells per well of a 12-well plate and incubated overnight at 37°C/5% CO_2 conditions. Media was removed, and a mixture containing 8µg/mL of polybrene, media corresponding to the cell type, and differing multiplicity of infections (MOIs) of lentiviruses (titre of 1 x 10^6) totalling 1 mL was added. Plates containing cells and lentiviral mixtures were subsequently spun down at 800g for 60 minutes at room temperature and incubated at 37°C/5% CO_2 conditions for 8 hours. Following incubation, lentiviral media was exchanged for media corresponding to the cell line transduced and incubated for 24 to 48 hours at 37°C/5% CO_2 conditions. Cells were subsequently assessed for transduction using fluorescence microscopy.

For the generation of polyclonal stable cell lines, transduced cells underwent a media exchange for selection media containing predetermined killing concentrations of puromycin (0.8µg/mL for COS-7; 0.7µg/mL for SK-N-SH). Selection media was exchanged every 72 hours and cells were regularly assessed for fluorescence-

expressing colonies. Once formed and sufficiently dense, colonies were detached using HyClone Trypsin, 0.25% (Danaher, Washington D.C., USA), resuspended in their respective selection media and expanded in progressively higher surface area flasks. Cells were regularly assessed for fluorescence using fluorescence microscopy. Once sufficiently expanded, polyclonal lines were frozen down in a 5% DMSO-containing solution of their respective non-selection media.

2.5. Immunoblotting of Endogenous and Expressed KIF1A

COS-7 cells transfected with pEF-KIF1A-GFP, pEF-V8M-KIF1A-GFP, pTetOne KIF1A-GFP and pTetOne V8M-KIF1A-GFP, along with non-transfected COS-7, HeLa, and SK-N-SH cells were lysed in ice-cold radioimmunoprecipitation assay (RIPA) buffer (50 mM Tris;pH 7.5, 5 mM EDTA, 150 mM NaCl, 1% Triton X-100) containing Roche cOmplete protease inhibitor cocktail (Hoffman-La Roche AG, Basel, Switzerland). Primary hippocampal neuronal cell lysates were previously prepared (Gan et al., 2020). For detection of endogenous KIF1A, total protein isolated from cell lysates (15μg) were separated on a precast 4-15% gradient gel (Bio-Rad Laboratories, Hercules, CA, USA) and subsequently transferred to a PVDF membrane. Membranes were blocked using a 3% BSA solution in TBS-Tween and blotting was performed using primary antibodies in blocking solution against KIF1A (1:500; BD Transduction Laboratories, Franklin Lakes, NJ, USA) and the loading control, GAPDH (1:1000; Novus Biologicals, Centennial, CO, USA; catalog #NB300-327). Immunoreactive bands were visualized using enhanced chemiluminescent substrate (SuperSignal West Pico PLUS Chemiluminescent Substrate: ThermoFisher Scientific, Waltham, MA, USA) for detection of peroxidase activity from HRP-conjugated secondary antibodies (1:20000; Bio-Rad, Hercules, CA, USA). Blotting was performed in triplicate using two different cell lysate samples. Protocols were identical for transfected COS-7 lysates, but primary antibodies against GFP (1:2000; Invitrogen, Waltham, MA, USA) and the loading control β-actin (1:1000; Santa Cruz Biotechnology, Santa Cruz, CA, USA) were used.

2.6. Fluorescent Microscopy

For imaging of cellular phenotypes and doxycycline-inducible expression studies, following transfection, glass coverslips with adhered cells were removed and washed

with 1x dPBS. dPBS was removed and cells were fixed with 4% PFA solution for 15 minutes at 37°C. PFA was removed and cells were washed two times in one minute intervals with dPBS. Cells were subsequently incubated at room temperature for 5 minutes with a 300 nM 4′,6-diamidino-2-phenylindole (DAPI) solution in dPBS for staining of nuclei, washed with dPBS 3 times in 5 minute intervals and mounted using elvanol. Cells were imaged using a wide-field fluorescent microscope (Leica, DMI, 6000B; Leica, Wetzlar, Germany) equipped with a CCD camera (Hamamatsu ORCA-ER-1394; Shizuoka, Japan). Images were captured at 400X magnification with a 40X/0.9NA lens.

For screening of stable cell line fluorescence, growth media was removed and replaced with pre-warmed 1x dPBS. Cells were subsequently imaged using a wide-field fluorescent microscope with integrated CMOS cameras (EVOS M7000 Imaging System; ThermoFisher Scientific, Waltham, MA, USA) at 200X magnification using a 20X/0.4NA long working distance (LWD) lens.

2.7. Image Analysis

All images acquired were analyzed using *CellProfiler 3.0* cell image analysis software (McQuin et al., 2018). A custom fluorescence intensity distribution analysis pipeline was constructed as follows. A greyscale image of the green channel corresponding to KIF1A-GFP variants was imported along with a greyscale image of the blue channel corresponding to DAPI (nuclei). Segmentation was done using an automatic global thresholding strategy. Primary objects (nuclei) were identified using automatic global thresholding utilizing a minimal cross entropy strategy and Gaussian smoothing with a sigma of 1. Nuclei were determined to have a range of diameters from 60 to 160 pixel units and separated by shape. Objects outside this range were discarded and holes filled following thresholding and declumping. Secondary object (cytoplasm) detection was accomplished using an automatic global thresholding strategy utilizing an Otsu three-class method to move objects below the threshold to the background. No smoothing was applied, and thresholding was corrected by a factor of 0.6. Secondary objects touching the border of the image were discarded along with associated primary objects. Object intensity and object intensity distribution modules were used to identify the mean fluorescence intensities across the cytoplasm as well as the distribution of the fluorescence intensities across the cytoplasm. Fluorescence intensity distribution was

determined using 4 radial sections (bins) of the cytoplasm automatically scaled for cell size, beginning from the edge of the associated primary object (nuclei). Values for mean fluorescence intensity, fraction at a distance (FraAtD) of the outermost bin, mean fraction at a distance (Mean FracAtD) of the outermost bin, and radial coefficient of variation (Radial CV) of the outermost bin were exported to a *Microsoft Excel* (Microsoft, Redmond, WA, USA) spreadsheet. FraAtD is defined as the fluorescence intensity in the specified bin divided by the total fluorescence. Mean FracAtD is defined as FraAtD normalized by the amount of pixels within the specified bin. Radial CV is defined as the ratio of the standard deviation of pixel intensities to the mean, or the variability in pixel intensity distribution across the specified bin. Objects whose diameters were below 80 μm or exceeded 300μm were filtered out in Excel as these were considered artifacts or dying cells.

A custom colocalization and overlap analysis pipeline was constructed as follows. A greyscale image of the green channel corresponding to KIF1A-GFP variants was imported along with a greyscale image of the red channel corresponding to EB3-mKate2. A Laplacian of Gaussian (LoG) filter was applied to both images to enhance edges of cellular structures to help identify tubular structures. The sigma of the Gaussian function was applied automatically. Following LoG processing, a morphological operation module was applied to both images consisting of an erosion and dilation function to return parts of the image with linear structures. A line length of 2 was chosen to reflect the average width of tubular structures within cells. An automatic global threshold utilizing a minimum cross entropy strategy was then applied to the resulting images for binarization. Images were not smoothed (Gaussian of 0) and no threshold correction was applied. A colocalization module was run across the entire masked image using a 15 percent of max intensity threshold to identify the Pearson's correlation coefficient for quantification of correlation. An image overlap module was run alongside the colocalization module to generate an F-factor for quantification of the degree of overlap of binarized pixels in red and green channels. Pearson's correlation coefficient is defined as the covariance between pixels in the red and green channels divided by the sum of their standard deviations. F-factor is defined as two times the product of the precision and recall divided by the sum of the precision and recall. The precision is defined as the number of true positive pixels divided by the sum of the number of true positive pixels and false positive pixels. The recall is defined as the number of true

positive pixels divided by the sum of true positive pixels and false positive pixels. Values are exported to a *Microsoft Excel* spreadsheet.

2.8. Statistical Analysis

Data obtained from all experiments was exported to a *Microsoft Excel* spreadsheet and imported to *GraphPad Prism 9* (GraphPad Software, San Diego, CA, USA) for further analysis. For doxycycline-induced KIF1A expression experiments, data was presented as mean ± SEM. All experiments were performed on at least 5 cells from three independent cultures. All statistical analyses were performed using one-way ANOVAs with Tukey's *post hoc* tests, comparing 4 hour conditions with 8 and 24 hour conditions. For fluorescent intensity distribution experiments assessing the peripheral accumulation in COS-7 and SK-N-SH cells, data was presented as mean ± SEM. All experiments involving constitutively-active plasmids were performed on at least 15 cells. All experiments involving doxycycline-inducible plasmids were performed on at least 3 cells. All statistical analyses were performed using a two-tailed unpaired Student's *t*-test.

Chapter 3.   Results

3.1. Characterization of Cellular Phenotypes

3.1.1. Endogenous KIF1A Expression and Confirmation of Cloned Plasmids

My goal was to design a high-throughput screen for small molecule modulators of the molecular motor KIF1A based on an assay that allows for one to easily distinguish between an activated and non-activated motor. KIF1A is present in an autoinhibited form that presents as a diffuse, cytoplasmic signal *in vivo*, and upon activation, KIF1A binds to microtubules resulting in a tubular phenotype *in vivo* (Hammond et al., 2009). Furthermore, upon activation KIF1A distributes peripherally to cell edges and distal neurites (Lee et al., 2015; Chiba et al., 2019; Kaur et al., 2020). To begin designing a microtubule-binding and peripheral accumulation assay optimized for a high-throughput screen, I characterized a suitable positive and negative control, cell lines and plasmid constructs. For the positive control, ideally a chemical control would be used; however, no such compounds are currently known to activate KIF1A. One potential compound, kinetin, was tested but did not yield the desired phenotypes (Appendix, Figure A1.). The motor mutant V8M hyperactivates KIF1A resulting in peripheral accumulation and microtubule-binding (Niwa et al., 2016; Chiba et al., 2019). As such, I tested the V8M mutant as a potential positive genetic control. For the negative control, I used WT KIF1A as it is monomeric, soluble, and diffuse in the cytoplasm (Hammond et al., 2009). Desired cell lines need to have a flat morphology and large cytoplasm for clear identification of peripheral KIF1A aggregates and identification of tubular structures (Cai et al., 2007). Two cell lines were chosen that fit these criteria: a neuronal cell line, SK-N-SH, and a non-neuronal cell line, COS-7. A neuronal cell line was chosen as it may allow for the discovery of more physiologically relevant hits. Paradoxically, this could also be a hindrance in hit discovery due to the potential off-target effects on neuron-specific factors that may affect KIF1A function as it is a neuron-enriched motor. For this reason, a non-neuronal cell line was also chosen as it removes that potential conflating factor in downstream hit validation. Furthermore, the COS-7 cell line has been used extensively for microtubule-binding studies due to its ease of transfection and large cytoplasm (Hammond et al., 2009; Niwa et al., 2016).

Due to the dimeric nature of active KIF1A, endogenous KIF1A monomers may dimerize with the transiently expressed KIF1A-V8M and interfere with the functionality of the assay. As such, I conducted an immunoblot on whole cell lysates to determine if the cell lines I chose endogenously express KIF1A. COS-7 did not express KIF1A, however, the SK-N-SH immunoblot showed two bands at around 200 and 215 kDa (Figure 3.1A). Splice variants of KIF1A exist with 3 isoforms that have been defined and 13 potential isoforms which explains the second band on the immunoblot (The Uniprot Consortium, 2019). I immunoblotted primary neuron lysate as a positive control, HeLa cells as a negative control, and GADPH as a loading control. Ultimately, phenotypic characterization, i.e., motor distribution, is needed to determine if the endogenous KIF1A affected V8M phenotypes in SK-N-SH cells.

Table 3.1. Cloned KIF1A-GFP Plasmids and Expected Cellular Phenotypes

Plasmid	Expected Phenotype
pEF-WT-KIF1A-GFP	Soluble, Diffuse
pEF-V8M-KIF1A-GFP	Peripherally Accumulated, Microtubule-Bound
pTetOne-WT-KIF1A-GFP	Soluble, Diffuse
pTetOne-V8M-KIF1A-GFP	Peripherally Accumulated, Microtubule-Bound

Summary of all KIF1A plasmids that were cloned along with the phenotypes expected to be seen when expressed in COS-7 and SK-N-SH cells. pEF plasmids drive transgene expression through a human EF1α promoter. pTetOne plasmids drive transgene expression through a CMV promoter.

Next, I successfully cloned four separate plasmids containing both the positive control KIF1A-V8M mutant and the negative control WT KIF1A (Table 3.1). To assess whether the plasmids drive expression of the cloned transgenes, cells were transfected via a liposomal-mediated gene delivery method and allowed to express for 24 hours. Cell lysates were generated from cells expressing the constitutively-active pEF plasmids. For doxycycline-inducible plasmids, 24 hours post transfection medium was exchanged for medium containing a 1:1000 dilution of 1 mg/mL doxycycline stock and allowed to express for 24 hours and cell lysates were harvested. Lysates were immunoblotted and

all four constructs showed strong bands at approximately 240 kDa, the expected size of a KIF1A-GFP fusion construct (3.1B). This confirmed the size of all four fusion proteins. In the upcoming sections, I group results based on the characterization of the cellular phenotypes seen for each of the KIF1A variants.
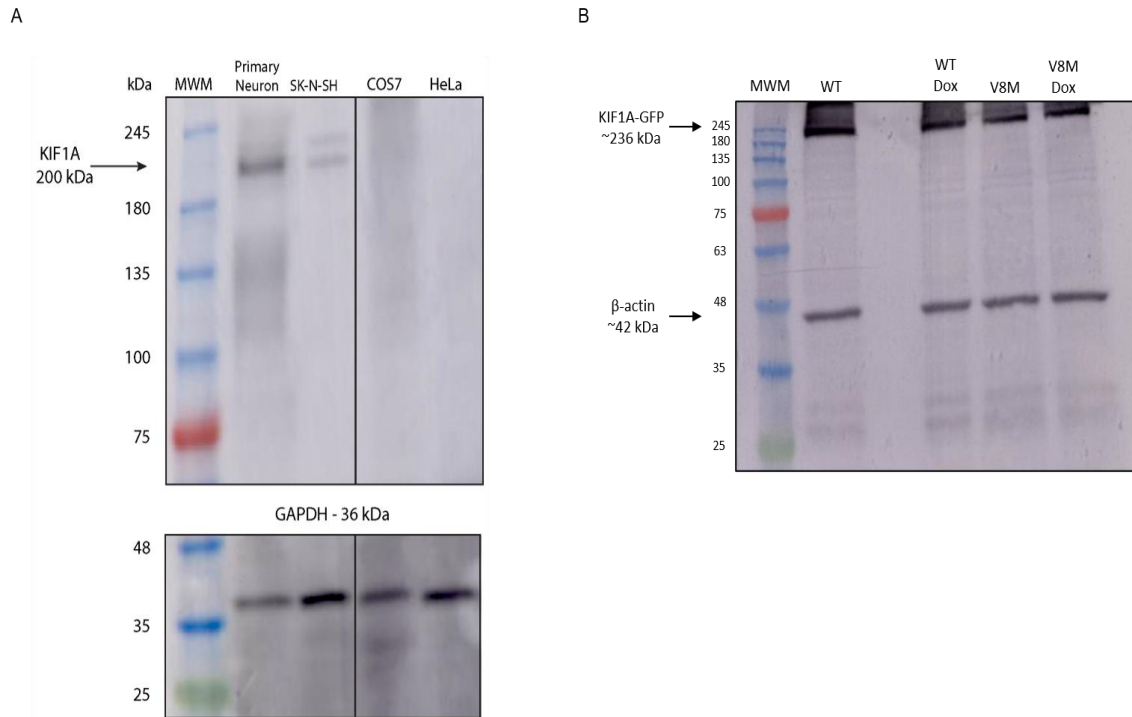
Figure 3.1. Representative immunoblots for endogenous KIF1A expression and verification of functionality of cloned plasmids
A) KIF1A is undetectable in COS7 cells. Immunoblot analysis of endogenous KIF1A expression in neuronal and non-neuronal cells. KIF1A is detectable in primary hippocampal neurons and SK-N-SH lysates. A second band is detected in the SK-N-SH cells which may indicate the presence of a KIF1A isoform, for which at least five have been identified (https://www.ncbi.nlm.nih.gov/genbank/). B) All four plasmids (pEF and pTetOne vector backbones) express the associated wild-type (WT) and V8M mutant KIF1A. Lane three is left intentionally blank. Note the absence of KIF1A in COS-7 (Figure 3.1A).

3.1.2. Phenotypic Characterization of pEF Constructs in COS-7 and SK-N-SH

To ask whether the constitutively-active WT- and V8M-KIF1A-GFP constructs were suitable controls for the peripheral accumulation assay, I wanted to determine whether there was any difference in the degree of peripheral accumulation between them. To accomplish this, I transfected COS-7 and SK-N-SH cells seeded onto glass coverslips with the WT- and V8M-KIF1A-GFP constructs. Following 24 hours of expression, cells were fixed and mounted onto glass slides and imaged using a

widefield, fluorescent microscope. Images were subsequently analyzed using a custom *CellProfiler* pipeline that allowed for determination of the fluorescence intensity distribution across four radial cross sections of each cell. Graphs were generated that showed the fraction of the total intensity in the outermost cross section (FracAtD), along with the fraction of the total intensity normalized for the number of pixels in the specified cross section (Mean FracAtD). Mean FracAtD was used to normalize for the varying sizes between cells.

For COS-7, WT-KIF1A-GFP weak fluorescence accumulates at the cell periphery (Figure 3.2A). However, V8M-KIF1A-GFP is distributed and accumulates in protruding cell processes (Figure 3.2A). V8M-KIF1A-GFP had significantly more ($p<0.05$) peripheral accumulation as compared to WT-KIF1A-GFP (Figure 3.2C), even when normalized for cell size (Figure 3.2D). This result shows that active KIF1A peripherally accumulates distally and may be suitable as a potential assay for KIF1A activation in COS-7 cells.

For SK-N-SH, WT-KIF1A-GFP accumulation in the cell periphery was seemingly reduced (Figure 3.3A) when compared to KIF1A-V8M-GFP as the latter was readily seen distributed in protruding cell processes (Figure 3.3B). However, when quantified, there was no significant difference between the WT- and V8M-KIF1A (Figure 3.3C), even when normalized for differing cell sizes (Figure 3.3D).

Next, I wanted to confirm that activation of KIF1A results in a microtubule-bound phenotype that may be subsequently quantified. For this, I would look for colocalization of KIF1A with a microtubule-marker. I co-transfected either the constitutively-active WT- or V8M-KIF1A-GFP constructs along with the microtubule marker EB3-mKate2. Cells expressed for 24 hours after which they were fixed, mounted and imaged using fluorescence microscopy.

For COS-7, in the WT-KIF1A-GFP, a diffuse signal was seen throughout the cell with no clear colocalization of the KIF1A with EB3 (Figure 3.2B). However, V8M-KIF1A-GFP accumulated distally and showed a tubular phenotype that colocalized with EB3 (Figure 3.2B). Although visually the microtubule-bound phenotype was clear, quantification of colocalization and degree of overlap was not performed as the analysis is being optimized and be pursued in future studies (Figure 3.9). This result shows that

active KIF1A binds microtubules in the peripheral regions of COS-7 and may be suitable as a potential assay for KIF1A activation.

For SK-N-SH, in the WT-KIF1A-GFP, a diffuse signal was seen throughout the cell with no clear colocalization of the KIF1A with EB3, albeit slight peripheral accumulation at distal tips (Figure 3.3B). However, the V8M-KIF1A-GFP accumulated distally and showed a tubular phenotype that colocalized with EB3-mKate3 (Figure 3.3B). Although visually the microtubule-bound phenotype was clear, quantification of colocalization and degree of overlap was not performed as the analysis is in progress (Figure 3.9). This result shows that active KIF1A binds microtubules in the peripheral regions of SK-N-SH cells and may be suitable as a potential assay for KIF1A activation in SK-N-SH cells.

A

WT KIF1A-GFP   V8M KIF1A-GFP

B

WT KIF1A-GFP   EB3-mKate2   Overlay

V8M KIF1A-GFP   EB3-mKate2   Overlay
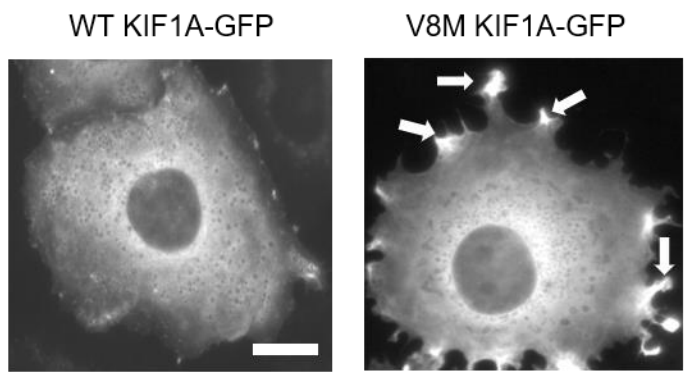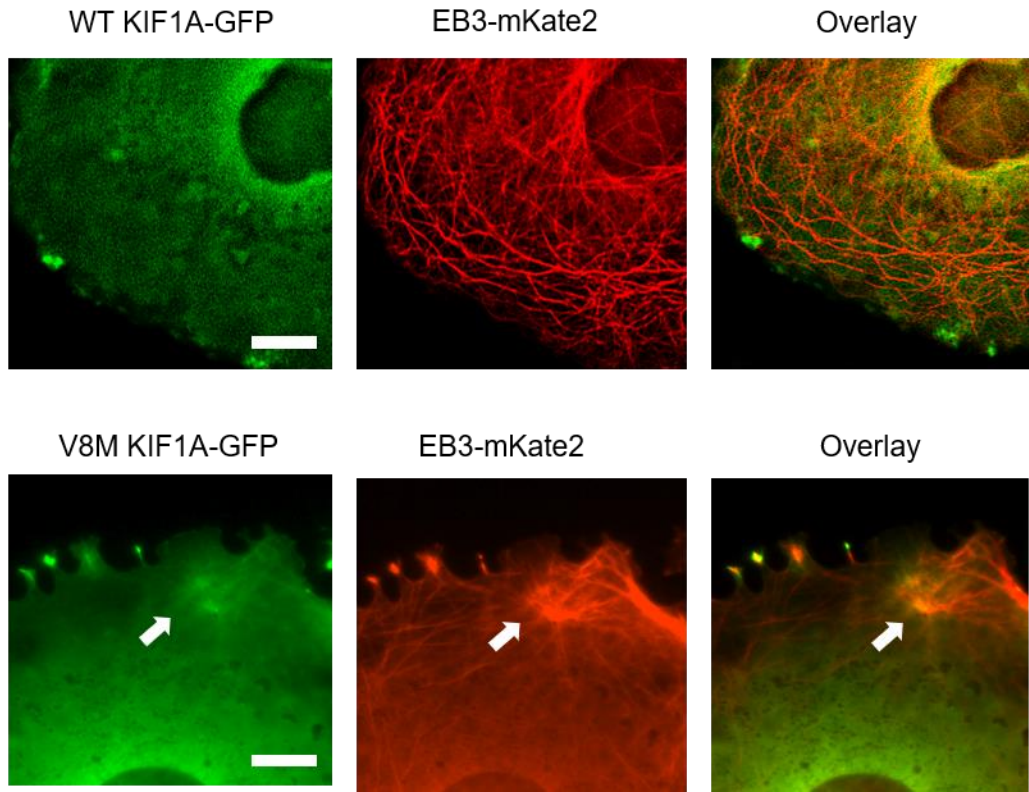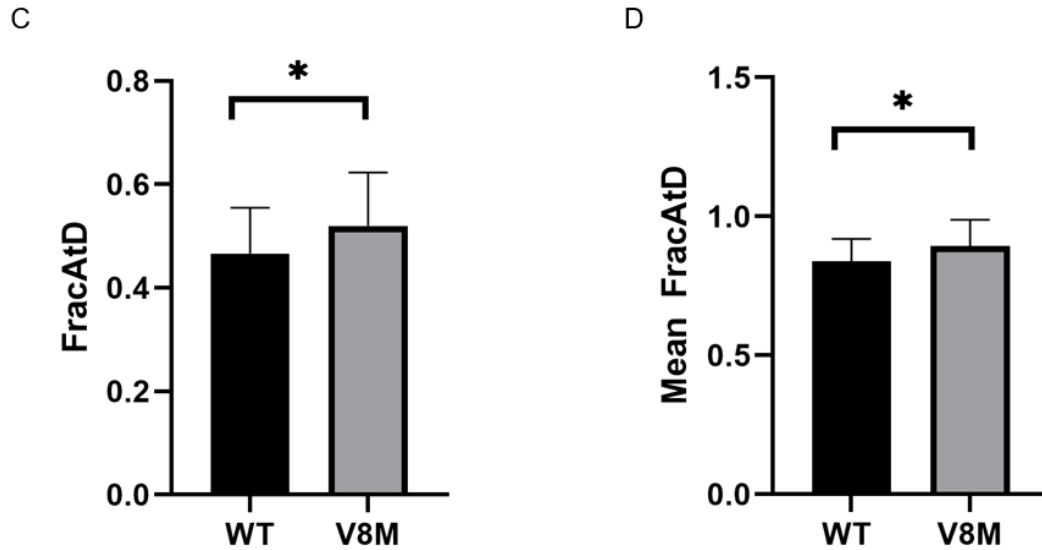
Figure 3.2. Peripheral accumulation and microtubule-binding using pEF constructs in COS-7 cells.

A) Representative image of COS-7 cells expressing wild-type (WT)-KIF1A-GFP and V8M-KIF1A-GFP. V8M-KIF1A-GFP shows peripheral accumulation while the WT-KIF1A-GFP shows a diffuse signal. White arrows identify peripheral accumulation of KIF1A. Scale bar:10μm. B) Representative image of COS-7 cells expressing WT-KIF1A-GFP and V8M-KIF1A-GFP with EB3-mKate2. V8M-KIF1A-GFP shows colocalization with EB3-mKate2 while WT-KIF1A-GFP does not. White arrows identify microtubule colocalization. Scale bar:40μm. C) Fraction at distance (FracAtD) of WT-KIF1A-GFP compared to V8M-KIF1A-GFP. V8M-KIF1A-GFP shows a significant difference in peripheral accumulation. *p<0.05. n=36 cells, WT; n=23 cells, V8M D) Mean fraction at distance (Mean FracAtD) of WT-KIF1A-GFP compared to V8M-KIF1A-GFP. V8M-KIF1A-GFP shows a significant difference in peripheral accumulation normalized for cell size. *p<0.05. n=36 cells, WT; n=23 cells, V8M

A

WT KIF1A-GFP   V8M KIF1A-GFP

B

WT KIF1A-GFP   EB3-mKate2   Overlay

V8M KIF1A-GFP   EB3-mKate2   Overlay

Figure 3.3. Peripheral accumulation and microtubule-binding using pEF constructs in SK-N-SH cells.
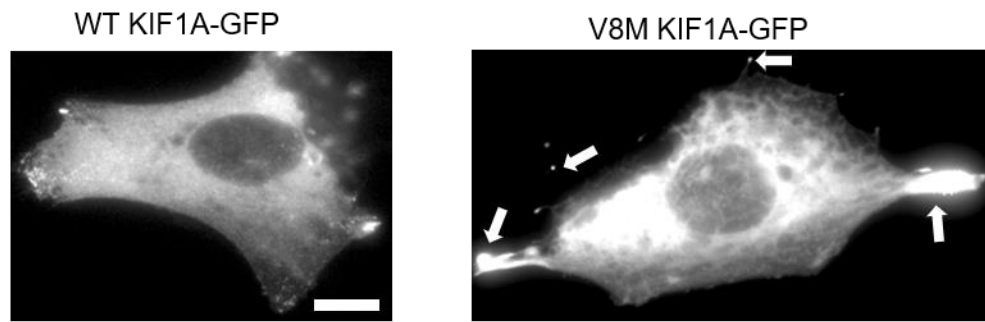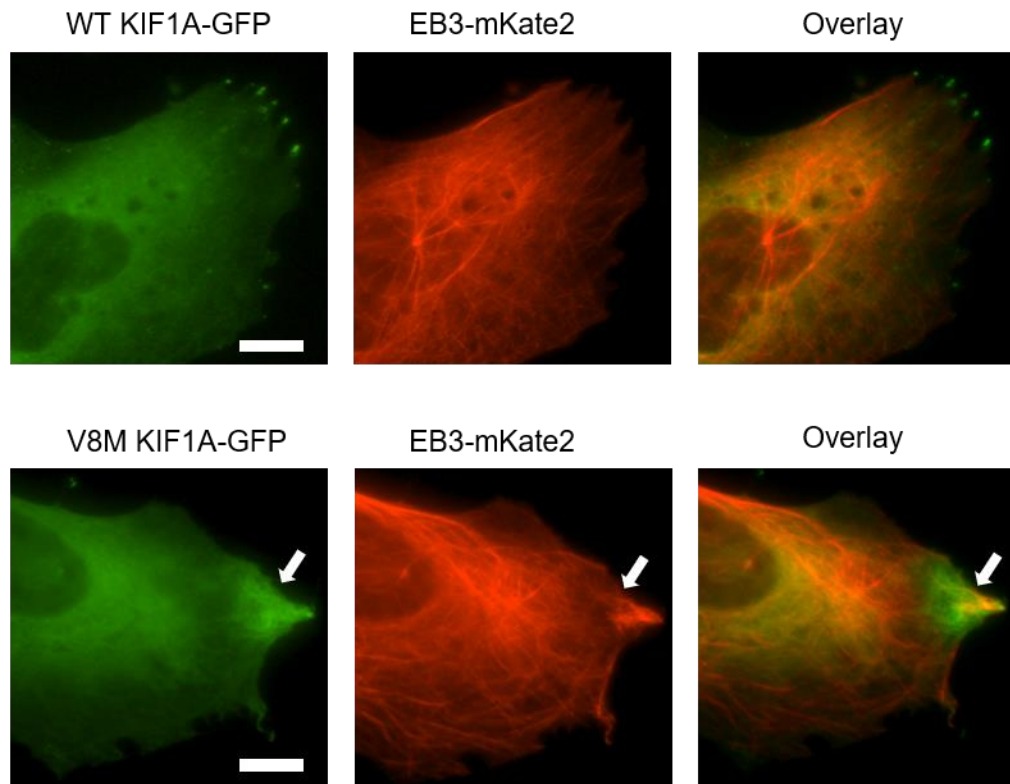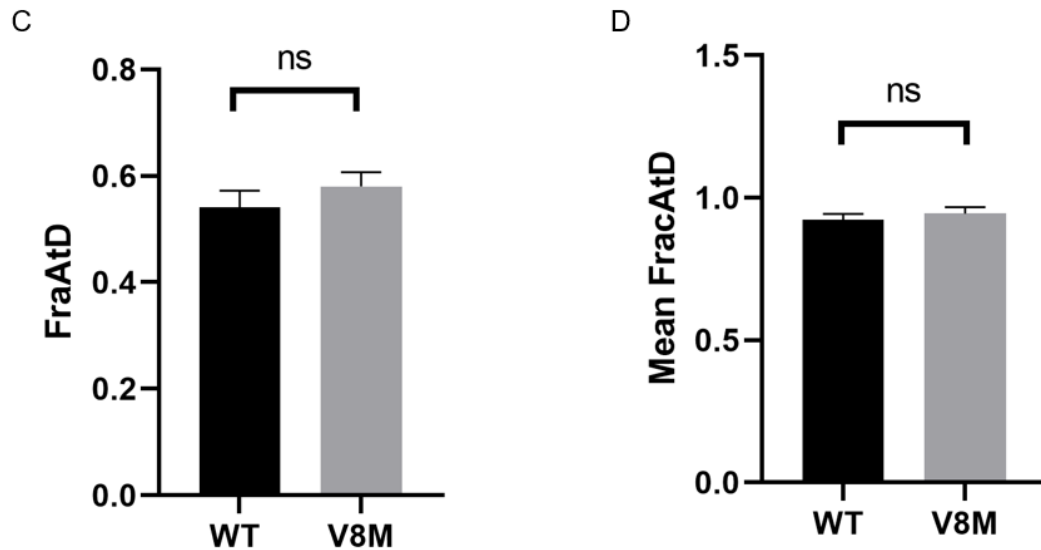A) Representative image of SK-N-SH cells expressing wild-type (WT)-KIF1A-GFP and V8M-KIF1A-GFP. V8M-KIF1A-GFP shows peripheral accumulation while WT-KIF1A-GFP shows a diffuse signal. White arrows identify peripheral accumulation of KIF1A. Scale bar:10μm. B) Representative image of SK-N-SH cells expressing WT-KIF1A-GFP and V8M-KIF1A-GFP with EB3-mKate2. V8M-KIF1A-GFP shows colocalization with EB3-mKate2 while the WT-KIF1A-GFP does not. White arrows identify microtubule colocalization. Scale bar:40μm. C) Fraction at distance (FracAtD) of WT-KIF1A-GFP compared to V8M-KIF1A-GFP. V8M-KIF1A-GFP shows no significant difference in peripheral accumulation. ns: p>0.05. n=11 cells, WT; n=14 cells, V8M D) Mean fraction at distance (Mean FracAtD) of WT-KIF1A-GFP compared to V8M-KIF1A-GFP. V8M-KIF1A-GFP shows no significant difference in peripheral accumulation normalized for cell size. ns: p>0.05. n=11 cells, WT; n=14 cells, V8M

3.1.3. Doxycycline-Inducible KIF1A Time-Course and Concentration Study

Doxycycline-inducible systems (i.e., pTetOne) allow for transcriptional control of transgenes through addition of tetracyclines such as doxycycline. Advantages of using such promoters include temporal control of transgene expression, as well as the amount of transgene expression one wishes to see, which is particular useful where high levels of expression result in toxicity of the cell (Wüst et al., 2020). I wanted to utilize such a system to see how finely I can control KIF1A expression so that I could reduce background within cells, increasing my signal to noise ratio for easier identification of cellular phenotypes. For this, I needed to assess whether doxycycline-induced

expression of KIF1A was altered at different concentrations of doxycycline, and whether the expression time would affect KIF1A expression in such a system.

To assess whether expression differs at different time points after addition of doxycycline, COS-7 cells were transfected with doxycycline-inducible plasmids containing the wild-type KIF1A-GFP transgene and allowed to express for 24 hours at which point differing concentrations of 1 mg/mL doxycycline stock solution was added (1:10000, 1:5000, 1:1000). Following addition of doxycycline, cells were allowed to express the transgene for four hours, eight hours, or 24 hours. Subsequently, cells were fixed, mounted on glass slides and imaged using fluorescent microscopy. At four hours, only endogenous staining was seen at all dilution factors (Figure 3.4A). However, at eight hours and 24 hours, expression of KIF1A-GFP was seen (Figure 3.4A). At the eight and 24 hour time points, mean fluorescent intensities were significantly increased across all conditions as compared to all four hour conditions (Figure 3.4B). Furthermore, there was significant increases in the variation of fluorescent intensities across cells in each eight and 24 hour time point as compared to all four hour conditions (Figure 3.4C). In addition, eight and 24 hour conditions were compared to see whether there were significant differences in fluorescent intensities and radial distributions of fluorescence. All 24 hour conditions had significantly higher mean fluorescent intensities as compared to the eight hour 1:1000 condition (Figure 3.4D). Moreover, a significant difference was seen between the eight hour 1:10000 condition and the 24 hour 1:1000 condition. No significant differences were seen in the radial distributions of fluorescence intensities across all conditions (Figure 3.4E). Ultimately, the doxycycline-inducible construct acts as expected with increasing concentrations and time periods generally resulting in an increase of KIF1A expression. However, for the proposed assays, this plasmid seems to have no benefit as compared to the constitutively-active construct since expression levels do not seem to influence the phenotype of KIF1A. Furthermore, transgene expression is still reliant on transcription and translation leading to a lag time in protein production which confers no benefit over constitutively-active constructs.
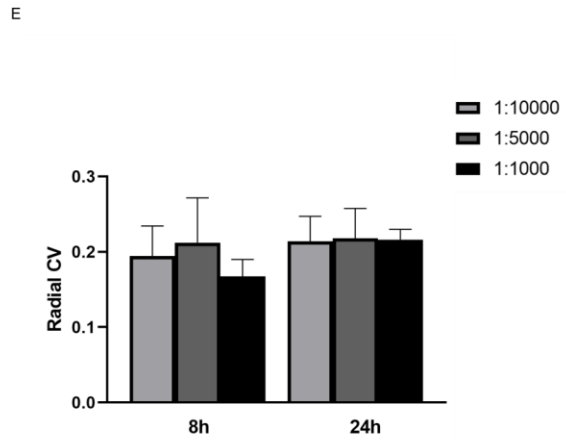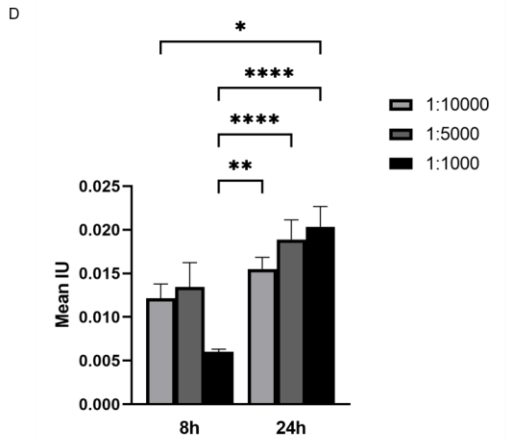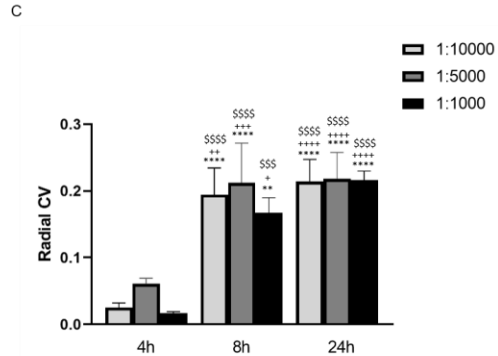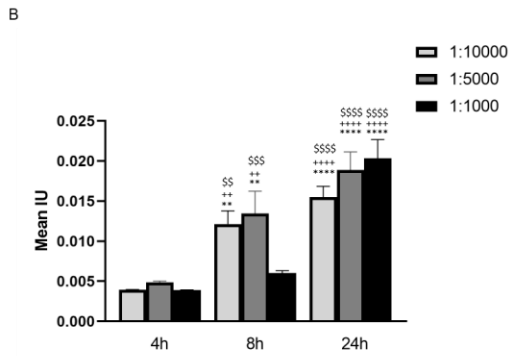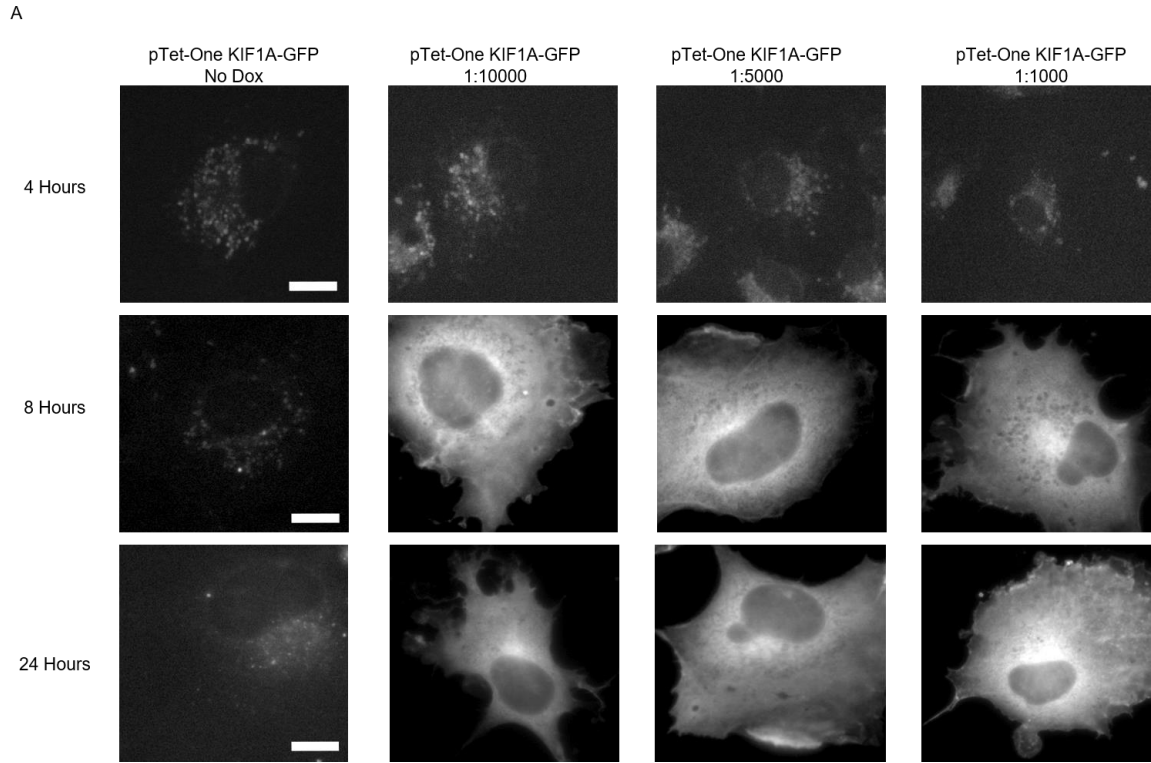
Figure 3.4. Time-course and concentration dependent expression by doxycycline-inducible constructs.

A) Representative images of pTetOne wild-type KIF1A-GFP transfected COS-7 cells at differing time points (4, 8 and 24 hours) and dilutions of 1mg/mL doxycycline stock solution (1:10000, 1:5000, 1:1000). At 4 hours, no expression is seen at all dilutions, while at 8 and 24 hours expression of KIF1A-GFP is seen. Expression seems to increase at increasing concentrations of doxycycline and longer time points. Scale bar:10µm. B&C) Comparison of mean fluorescence intensity (mean IU) and radial coefficient of variation (radial CV) between 4 hours of expression and 8 and 24 hours at all dilutions. All time points and dilutions showed significant differences in mean fluorescence intensity. *$p < 0.05$, **$p < 0.01$, ***$p < 0.001$, ****$p < 0.0001$ when compared to 4h 1:10000 dilution, +$p < 0.05$, ++$p < 0.01$, +++$p < 0.001$, ++++$p < 0.0001$ when compared to 4h 1:5000 dilution, $p < 0.05$, $$p < 0.01$, $$$p < 0.001$, $$$$p < 0.0001$ when compared to 4h 1:1000 dilution. $n \geq 6$. D&E) Comparison of mean fluorescence intensity (mean IU) and radial coefficient of variation (radial CV) between 8 and 24 hours at all dilutions. *$p < 0.05$, **$p < 0.01$, ***$p < 0.001$, ****$p < 0.0001$. $n \geq 6$ cells.

3.1.4. Phenotypic Characterization of pTetOne Constructs in COS-7 and SK-N-SH

To ask whether the constitutively-active WT- and V8M-KIF1A-GFP constructs were suitable controls for the peripheral accumulation assay, I wanted to determine whether there was any difference in the degree of peripheral accumulation between them. To accomplish this, I transfected COS-7 and SK-N-SH cells seeded onto glass coverslips with the WT and V8M KIF1A-GFP constructs. Following 24 hours of expression, media was exchanged for media containing doxycycline at a 1:10000 dilution of 1mg/mL stock and allowed to express for 24 hours. A 1:10000 dilution was used as it provided similar expression levels to higher concentrations of doxycycline at the same time point (Figure 3.4D) and higher concentrations of doxycycline are cytotoxic (Ermak et al., 2003). Cells were fixed, imaged, and subsequently analyzed using a custom *CellProfiler* pipeline.

For COS-7, WT-KIF1A-GFP weakly accumulates at the cell periphery (Figure 3.5A). However, V8M-KIF1A-GFP distributes and accumulates in protruding cell processes (Figure 3.5A). When quantified, there was no significant difference in peripheral accumulation (Figure 3.5C), even when normalized for differing cell sizes (Figure 3.5D). Ultimately, this may be due to relatively low sample sizes (n=7, WT; n=9, V8M) as the phenotype is clear via visual assessment. This result shows that active KIF1A peripherally accumulates distally, however, this doxycycline-inducible construct may not be suitable for downstream peripheral accumulation assay development. Larger sample sizes would be needed to determine suitability for this peripheral accumulation assay.

For SK-N-SH, WT-KIF1A-GFP showed little accumulation in the cell periphery (Figure 3.6A). However, V8M-KIF1A-GFP was clearly distributed and accumulated in protruding cell processes (Figure 3.6A). When quantified, there was no significant difference in peripheral accumulation (Figure 3.6C), even when normalized for differing cell sizes (Figure 3.6D). Ultimately, this may be due to low sample sizes (n=3, WT; n=4, V8M) as the phenotype is clear via visual assessment. Conversely, as with the constitutively-active SK-N-SH, the irregular shape of the SK-N-SH cells may affect the output of the assay since the nucleus tends to be located close to the cell periphery. Furthermore, dimerization between the V8M mutant and endogenously expressed KIF1A may occur resulting in decreased motility and subsequent peripheral accumulation (Figure 3.1A). This result shows that active KIF1A peripherally accumulates distally, however, this doxycycline-inducible construct may not be suitable for downstream peripheral accumulation assay development. Higher sample sizes would be needed to determine suitability for peripheral accumulation assaying.

Next, I wanted to confirm that activation of KIF1A results in a microtubule-bound phenotype. I co-transfected either the doxycycline-inducible WT- or V8M-KIF1A-GFP constructs along with the microtubule marker EB3-mKate2. Cells expressed the plasmids for 24 hours after which they were fixed, mounted and imaged using fluorescence microscopy.

For COS-7, WT-KIF1A-GFP shows a diffuse signal throughout the cell with no clear colocalization of the KIF1A with EB3 (Figure 3.5B). However, V8M-KIF1A-GFP accumulates distally and shows a tubular phenotype that colocalizes with EB3-mKate2 (Figure 3.5B). Although visually the microtubule-bound phenotype was clear, quantification of colocalization and degree of overlap was not performed as the analysis is in progress (Figure 3.9). This result shows that active KIF1A binds microtubules in the peripheral regions of the COS-7's and may be suitable as a potential assay for KIF1A activation in COS-7 cells.

For SK-N-SH, WT-KIF1A-GFP shows a diffuse signal throughout the cell with no clear colocalization of the KIF1A with EB3 (Figure 3.6B). However, the V8M mutant accumulates distally and shows a tubular phenotype that colocalizes with EB3-mKate2 (Figure 3.6B). Although visually the microtubule-bound phenotype was clear, quantification of colocalization and degree of overlap was not performed as the analysis

is in progress (Figure 3.9). This result shows that active KIF1A binds microtubules in the peripheral regions of SK-N-SH cells and may be suitable as a potential assay for KIF1A activation in SK-N-SH cells.

A

WT KIF1A-GFP   V8M KIF1A-GFP

B

WT KIF1A-GFP   EB3-mKate2   Overlay

V8M KIF1A-GFP   EB3-mKate2   Overlay
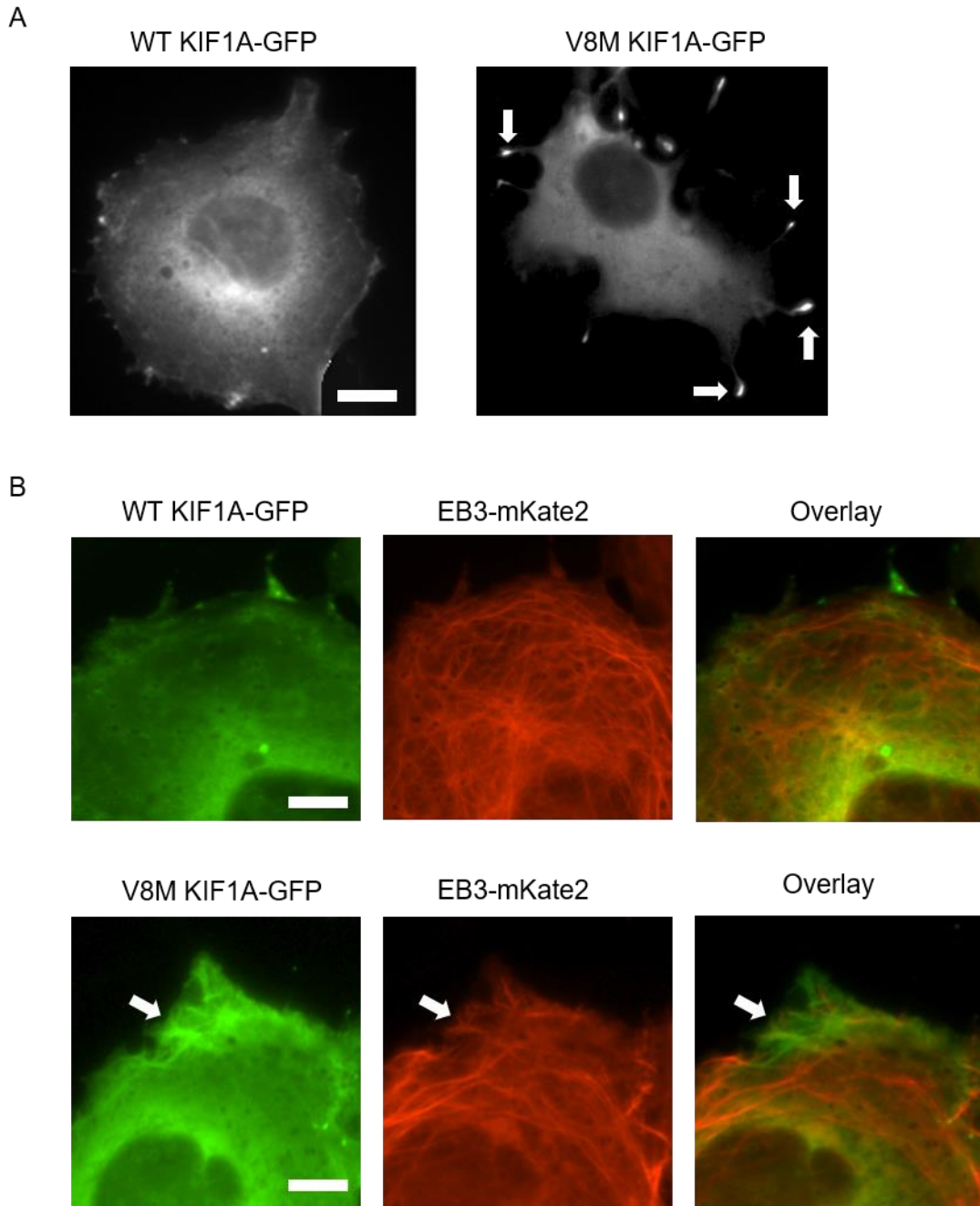
C
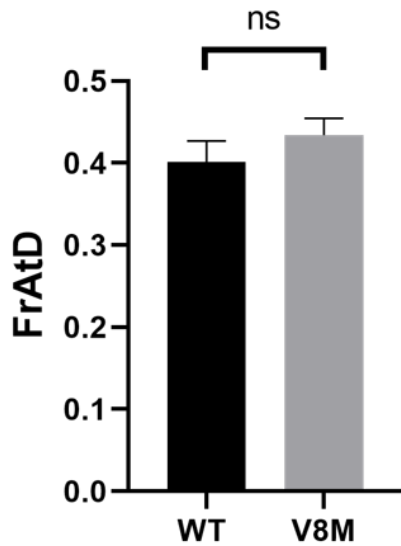
D
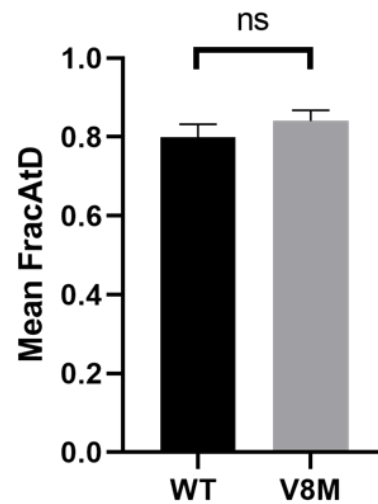
Figure 3.5. Peripheral accumulation and microtubule-binding using pTetOne constructs in COS-7 cells.
A) Representative image of COS-7 cells expressing doxycycline-inducible wild-type (WT) KIF1A and V8M mutant KIF1A. The V8M mutant KIF1A-GFP shows peripheral accumulation while the WT KIF1A-GFP shows a diffuse signal. White arrows identify peripheral accumulation of KIF1A. Scale bar:10µm. B) Representative image of COS-7 cells expressing WT KIF1A and V8M mutant KIF1A with EB3-mKate2. The V8M mutant KIF1A-GFP shows colocalization with EB3-mKate2 while the WT KIF1A-GFP does not. White arrows identify microtubule colocalization. Scale bar:10µm. C) Fraction at distance (FracAtD) of WT KIF1A compared to V8M KIF1A. V8M KIF1A shows no significant difference in peripheral accumulation. ns: p>0.05. n=7 cells, WT; n=9 cells, V8M D) Mean fraction at distance (Mean FracAtD) of WT KIF1A compared to V8M KIF1A. V8M KIF1A shows no significant difference in peripheral accumulation normalized for cell size. ns: p>0.05. n=7 cells, WT; n=9 cells, V8M

A

WT KIF1A-GFP   V8M KIF1A-GFP

B

WT KIF1A-GFP   EB3-mKate2   Overlay

V8M KIF1A-GFP   EB3-mKate2   Overlay
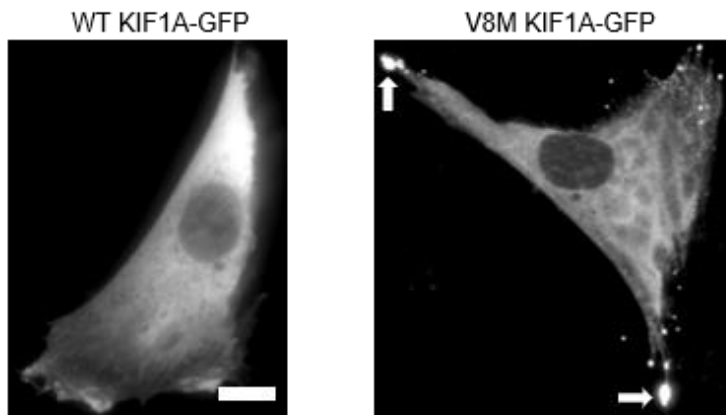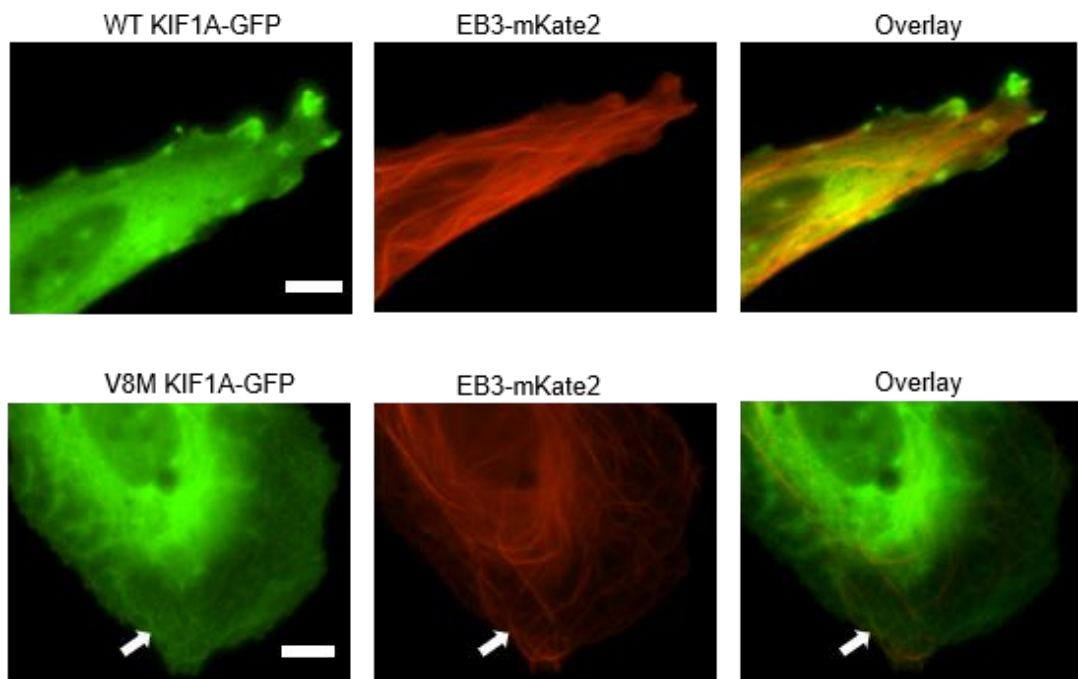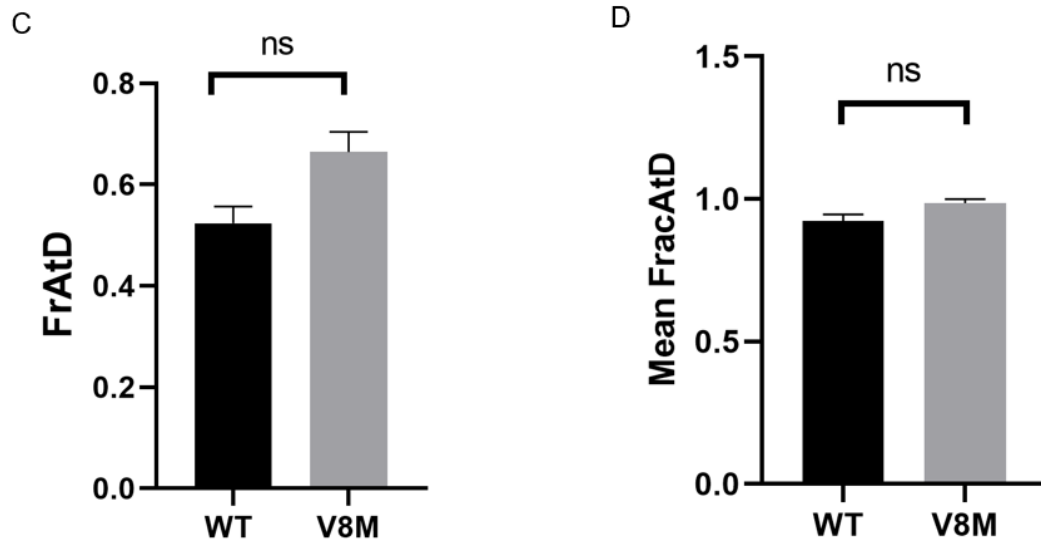
Figure 3.6. Peripheral accumulation and microtubule-binding using pTetOne constructs in SK-N-SH cells.
A) Representative image of SK-N-SH cells expressing doxycycline-inducible wild-type (WT) KIF1A and V8M mutant KIF1A. The V8M mutant KIF1A-GFP shows peripheral accumulation while the WT KIF1A-GFP shows a diffuse signal. White arrows identify peripheral accumulation of KIF1A. Scale bar:10μm. B) Representative image of SK-N-SH cells expressing WT KIF1A and V8M mutant KIF1A with EB3-mKate2. The V8M mutant KIF1A-GFP shows colocalization with EB3-mKate2 while the WT KIF1A-GFP does not. White arrows identify microtubule colocalization. Scale bar:10μm. C) Fraction at distance (FracAtD) of WT KIF1A compared to V8M KIF1A. V8M KIF1A shows no significant difference in peripheral accumulation. ns: p>0.05, n=3 cells, WT; n=4 cells, V8M D) Mean fraction at distance (Mean FracAtD) of WT KIF1A compared to V8M KIF1A. V8M KIF1A shows no significant difference in peripheral accumulation normalized for cell size. ns: p>0.05, n=3 cells, WT; n=4 cells, V8M

3.1.5. Stable Cell Line Generation

Designing a cell-based, phenotypic assay suitable for high-throughput screening is reliant on reducing variability in your assay, particularly cell to cell variability, allowing for a robust Z' (Figure 1.12; Macarron & Hertzberg, 2009). As such, generation of monoclonal stable cell lines is crucial as this allows for consistent expression levels of the proteins of interest, in this case, KIF1A and EB3. Furthermore, this is critical for downstream optimization of analysis parameters as you increase the amount of cell samples containing your proteins of interest thereby allowing for a more robust analysis and generation of Z'. I planned to generate eight total cell lines, four for both COS-7 and SK-N-SH (Table 3.2).

Table 3.2. Generation of Stably Expressing Monoclonal Cell Lines

Cell line	pEF-WT-KIF1A-GFP	pEF-V8M-KIF1A-GFP	pTetOne-WT-KIF1A-GFP	pTetOne-V8M-KIF1A-GFP	EB3-mKate2
COS-7	X				X
		X			X
			X		X
				X	X
SK-N-SH	X				X
		X			X
			X		X
				X	X

A table showing all potential stable cell lines I plan to generate. X demarks the transgenes that will be stably incorporated into COS-7 and SK-N-SH. Currently, I have generated polyclonal lines expressing EB3-mKate 2.

To start, I wanted to begin by generating a monoclonal cell line with optimal expression levels for the microtubule marker EB3-mKate2 as every cell line generated would have this for the microtubule-binding assay. This would reduce the variability from cell to cell and between WT and V8M conditions of each cell line. To do this, lentiviruses were packaged with a custom generated EB3-mKate2 plasmid. Both COS-7 and SK-N-SH were transduced with the lentivirus for 48 hours. Cells were subsequently screened for expression of fluorescence. Viral media was exchanged for selection media containing puromycin (0.8μg, COS-7; 0.7μg, SK-N-SH) and allowed to select and form colonies. Selection media was exchanged every three days and transduced cells were screened for fluorescence. Once fluorescent colonies grew to confluence, cells were seeded onto coverslips and imaged using fluorescent microscopy. Polyclonal cell lines expressing EB3-mKate2 were generated for both COS-7 and SK-N-SH cells (Figure 3.7). Monoclonal cell lines are currently being generated.

	Phase-Contrast	EB3-mKate2
SK-N-SH		
COS-7		
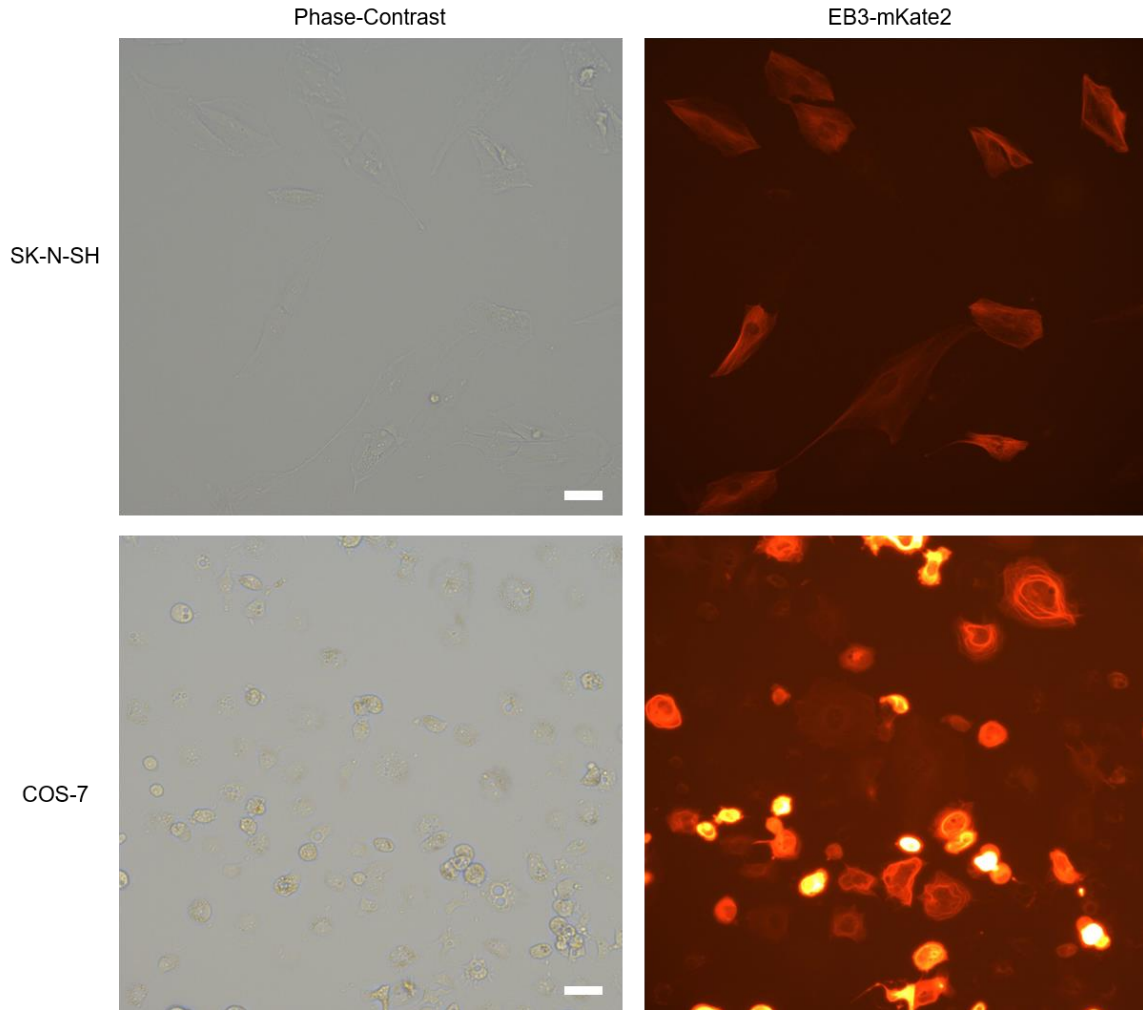
Figure 3.7. Polyclonal SK-N-SH and COS-7 cells stably expressing EB3-mKate2.
A representative phase and fluorescent image of polyclonal SK-N-SH and COS-7 cells stably expressing EB3-mKate2. Scale bar:100µm

3.2. Generation of High-Throughput Analyses

3.2.1. Fluorescence Intensity Distribution Analysis Workflow for Peripheral Accumulation Assay

Automation of analyses is critical for a viable high-throughput workflow. I focused on generating a fluorescence intensity distribution analysis for assaying of peripheral accumulation of KIF1A. Primarily this analysis depends on accurate segmentation of cellular compartments, in this case, the nuclei and the cytoplasm. As KIF1A accumulates

peripherally, if the cytoplasm was not completely delineated including distal processes, high intensity fluorescence generated by aggregation of KIF1A would be excluded from the analysis. To accomplish proper segmentation, I generated a custom pipeline in *CellProfiler*. Primary objects, in this case nuclei, needed to be identified and segmented properly for the program to accurately apply automatic thresholds in downstream modules. Nuclei were identified by applying size exclusion whereby the average nuclei size diameter was identified and a percentage range was applied to include nuclei of differing sizes within that range (in this case 60 pixel units to 160 pixel units). An automatic threshold was then applied using a minimum cross entropy method whereby probability maps are applied to the object being identified to try to accurately outline it. A Gaussian smooth was needed at a sigma of 1 to allow proper distinguishing of nuclei.

Once nuclei were properly identified, a second thresholding module was applied that utilized another form of automatic global thresholding, the Otsu three class method, in which pixels are separated into three classes, foreground, background, and middle. The option to move the middle pixels to the background was applied which allowed for robust identification of cellular cytoplasm. However, if the pixel intensities fell under a given range, unwanted portions of the cytoplasm were moved to the background. This can be seen in the "identify cytoplasm" portion of Figure 3.8 in which a portion of the orange highlighted cell was moved to the background due to the high degree of separation between pixel intensities between perinuclear cytoplasm, periphery, and the rest of the cell. Ideally, a whole cell stain would be used during the screen which would forego this segmentation issue.

Lastly, after identification of the cytoplasm, two analyses were conducted: fluorescence intensity and fluorescence intensity distribution. The fluorescence intensity module gives a range of values including mean intensity (total intensity normalized by the amount of pixels in the cell), total intensity (total intensity in the cell), median, maximum, and more. For the fluorescence intensity distribution analysis, the cytoplasm is highlighted and segregated into a number of concentric rings named bins that can be scaled for cell size. For each bin, a range of values is given, including fraction at a distance (FracAtD; fluorescence intensity of a bin as a fraction of total intensity), mean fraction at a distance (Mean FracAtD; FracAtD normalized by number of picture in a bin), and radial coefficient of variation (Radial CV; measure of intensity differentials at different portions of a selected bin). Ultimately, this analysis is easily automated for a

high-throughput screening format and robust in terms of fluorescence distribution analysis. However, it would benefit from a whole cell stain to ensure almost perfect segmentation for even better analysis of peripheral distribution.

Nuclei - DAPI
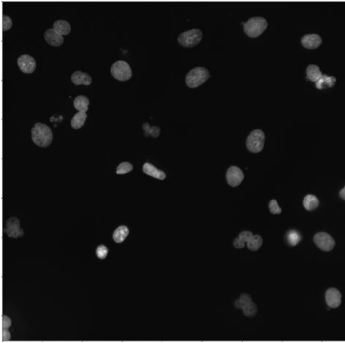
V8M KIF1A GFP
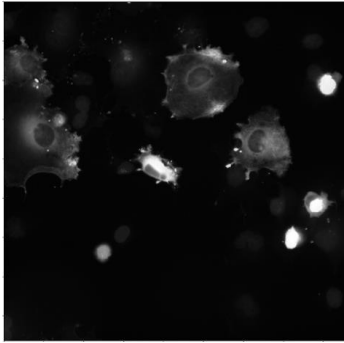
Analysis Workflow
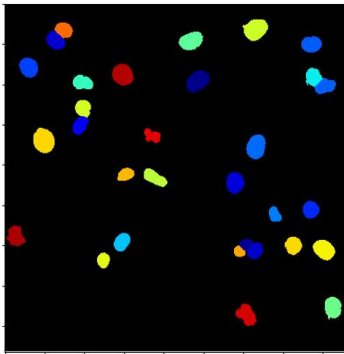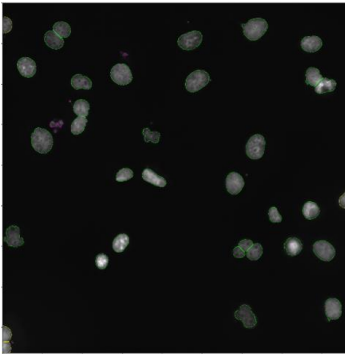
Identify Nuclei
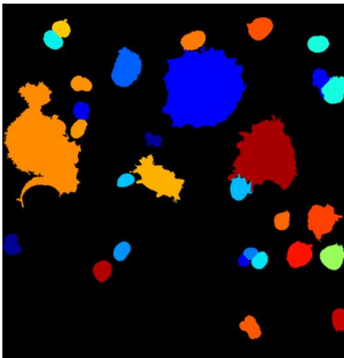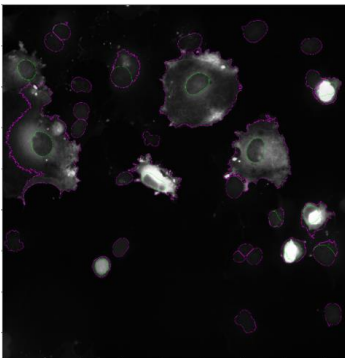
Identify Cytoplasm

Heat map generation and intensity calculation
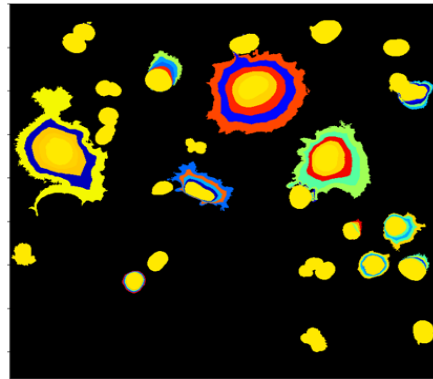
OUTPUT

Fluorescence Intensity Analysis

Image	Object	Feature	Mean	Median	STD
KIF1A	Cytoplasm	IntegratedIntensity	5295.232	853.125	8936.101
KIF1A	Cytoplasm	MeanIntensity	0.149	0.084	0.144
KIF1A	Cytoplasm	StdIntensity	0.07	0.015	0.103
KIF1A	Cytoplasm	MinIntensity	0.047	0.041	0.013
KIF1A	Cytoplasm	MaxIntensity	0.386	0.164	0.34
KIF1A	Cytoplasm	IntegratedIntensityEdge	57.448	25.121	78.291
KIF1A	Cytoplasm	MeanIntensityEdge	0.07	0.07	0.024
KIF1A	Cytoplasm	StdIntensityEdge	0.021	0.008	0.03
KIF1A	Cytoplasm	MinIntensityEdge	0.05	0.042	0.017
KIF1A	Cytoplasm	MaxIntensityEdge	0.184	0.093	0.198
KIF1A	Cytoplasm	MassDisplacement	4.362	2.116	5.061
KIF1A	Cytoplasm	LowerQuartileIntensity	0.091	0.074	0.049
KIF1A	Cytoplasm	MedianIntensity	0.139	0.085	0.133
KIF1A	Cytoplasm	MADIntensity	0.049	0.009	0.088
KIF1A	Cytoplasm	UpperQuartileIntensity	0.199	0.093	0.241
KIF1A	Cytoplasm	CenterMassIntensity_X	1198.052	1354.235	616.432
KIF1A	Cytoplasm	CenterMassIntensity_Y	973.544	988.5	539.387
KIF1A	Cytoplasm	CenterMassIntensity_Z	0.0	0.0	0.0
KIF1A	Cytoplasm	MaxIntensity_X	1202.833	1403.0	610.846
KIF1A	Cytoplasm	MaxIntensity_Y	984.9	1044.0	536.018
KIF1A	Cytoplasm	MaxIntensity_Z	0.0	0.0	0.0

Fluorescence Intensity Distribution Analysis

Image	Objects	Bin # (innermost=1)	Bin count	Fraction	Intensity	COV
KIF1A	Cytoplasm	1	4	0.1761	1.3505	0.2489
KIF1A	Cytoplasm	2	4	0.2924	1.1726	0.288
KIF1A	Cytoplasm	3	4	0.2769	0.9857	0.3096
KIF1A	Cytoplasm	4	4	0.3017	0.7627	0.2079

Figure 3.8. High-throughput fluorescent intensity distribution analysis workflow.
A schematic of the fluorescent intensity distribution analysis workflow for peripheral accumulation analyses. Greyscale images of the green and blue channels are added and subsequently two sets of thresholds are applied to identify primary objects (nuclei) and secondary objects (cytoplasm). The cytoplasm is radially segmented (binned), and a heat map is generated with varying colors for differing fluorescent intensities. Values are output in *CellProfiler* and in an *Excel* spreadsheet.

3.2.2. Colocalization and Overlap Analyses Workflow for Microtubule-Binding Assay

Unlike the fluorescence intensity distribution assay where segmentation is needed for large objects such as the cytoplasm, a robust colocalization analysis needs to be able to recognize distinct cellular objects such as puncta, or in the case of my assay, microtubular structures. These types of structures can be extremely hard to identify using traditional thresholding methods and as such, enhancements need to be made to identify these structures.

I started the design of a custom pipeline on *CellProfiler* that allows for analysis of colocalization and overlap between KIF1A-GFP and EB3-mKate2. First, a Laplacian of Gaussian (LoG) function is applied to both greyscale images to be able to identify edges within the cell, such as the microtubules. The LoG function is ideal for detection of areas that exhibit rapid changes in intensity, such as the microtubules. It allows for detection of the complete microtubular structure since the microtubules have a relatively consistent intensity across their length with large drop offs of intensity along their edges. A large degree of noise is often seen along their length, as seen in the V8M-KIF1A-GFP mutant (Figure 3.3B), of which the LoG is sensitive to. As such, this function applies a Gaussian smooth on top of the edge detection to better identify areas of differing intensity. The values used for the LoG function are automatically generated by *CellProfiler* and seem to identify edges well.

Next, a morphological function (*openlines)* is applied in which pixels around those edges are eroded to further reduce noise and then the final pixels that make up the edges are dilated allowing for easier identification of microtubular structures. A line length of two pixels seems to identify microtubular structures quite well. The line length is predetermined and is based on the minimum width of the microtubules (approximately 2 pixels). Minimum width was chosen as due to the high degree of noise that is present near the microtubular structures, particularly along the periphery of the cell, an LoG

function may over process the image reducing average microtubule size (measured to be around 3 pixels). As such, using a width smaller than that of average allows for a larger number of microtubular structures to be detected. Unfortunately, this function also detects cellular structures such as edges of nuclei, the cell periphery, and vesicular-like structures within cells as these structures typically fall into the line length range of the microtubules. This is a detriment to the next step, in which a global threshold is applied to both morphed images to allow for binarization of the identified cellular structures. In this case, you can see that vesicular structures, cell edges, nuclei edges, and other artifacts are identified alongside the microtubules (Figure 3.9). Currently, this is the bottleneck in image processing as it disallows proper colocalization and overlap measurements. Currently, a sigma of 1 for the thresholding value seems to highlight microtubules the best while minimizing other foreground objects such as vesicular structures and cell edges. However, these objects are still present. Due to the identification of such vesicular structures, cell edges, nuclei edges, and other artifacts in both the KIF1A-GFP and EB3-mKate2 images, the degree of colocalization and overlap identified by the software is skewed high. Ultimately, for an analysis like this to be utilized for colocalization and overlap quantification, an ability to filter out unwanted structures would be needed.

KIF1A-GFP	EB3-mKate2	Analysis Workflow

Images
Metadata
NamesAndTypes
Groups
EnhanceEdges
EnhanceEdges
Morph
Morph
GrayToColor
Threshold
Threshold
MeasureColocalization
MeasureImageOverlap
ExportToSpreadsheet

Enhance
Edges

Morph
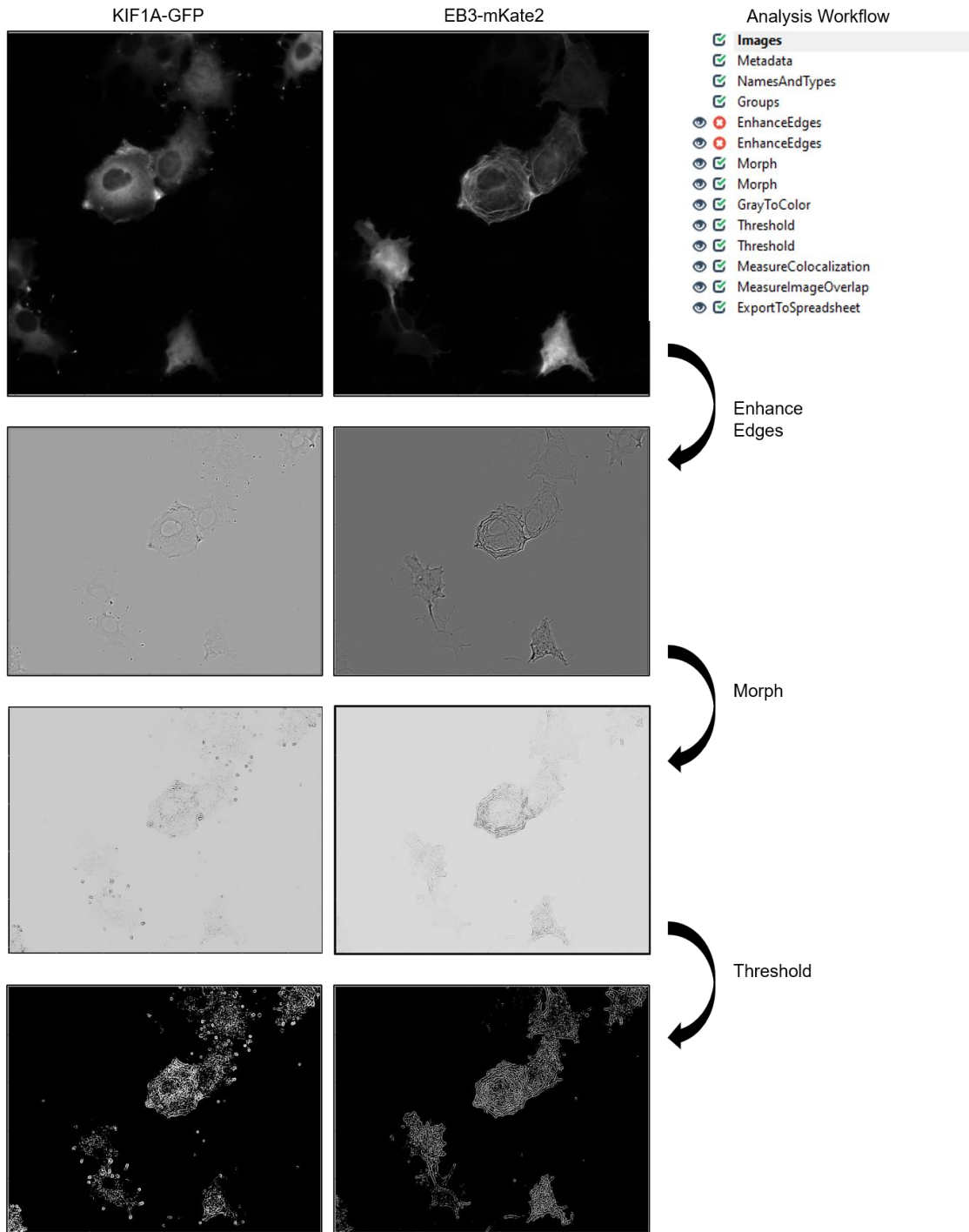
Threshold

OUTPUT

↓

Colocalization Analysis

First image	Second image	Objects	Measurement	Value
Threshold	ThresholdGreen	-	Correlation	0.381
Threshold	ThresholdGreen	-	Slope	0.389
Threshold	ThresholdGreen	-	Manders Coefficient	0.411
ThresholdGreen	Threshold	-	Manders Coefficient	0.393
Threshold	ThresholdGreen	-	RWC Coefficient	0.411
ThresholdGreen	Threshold	-	RWC Coefficient	0.393
Threshold	ThresholdGreen	-	Overlap Coefficient	1.000
Threshold	ThresholdGreen	-	Manders Coefficient (Costes)	nan
ThresholdGreen	Threshold	-	Manders Coefficient (Costes)	0.000

Overlap Analysis

Measurement	Value
Ffactor	0.401835274489
Precision	0.393415844694
Recall	0.41062295082
FalsePosRate	0.0217699131007
FalseNegRate	0.58937704918
RandIndex	0.9222911266189224
AdjustedRandIndex	0.37639040984143884

Figure 3.9. High-throughput colocalization and overlap analysis workflow.
A schematic for a high-throughput colocalization and overlap analysis workflow. Greyscale images for both red (EB3-mKate2) and green (KIF1A-GFP) channels are imported into *CellProfiler*. Both images are run through a Laplacian of Gaussian (LoG) function to enhance object edges for identification of microtubular structures. Morphological operations (erosion and dilation) that further enhance edges are run on both images. Subsequent thresholding allows for binarization of images. Binarized images are overlapped and colocalization and overlap analyses are run to identify degree of colocalization and overlap of images. Values are output in *CellProfiler* and in an *Excel* spreadsheet.

63

Chapter 4.   Discussion

4.1. Summary

Neurons are highly polarized cells comprised of morphologically, biochemically, and functionally distinct extensions of the cell body: the axon and dendrites. Establishing and maintaining of these domains depends on the bidirectional transport of cargos within these microtubule-based structures. Active transport utilizes motor proteins, namely the kinesin superfamily (KIFs) for anterograde transport. When any aspect of this process is dysregulated the resulting "transportopathy" contributes to neurological disorders, such as Huntington's, Alzheimer's, and Parkinson's disease (Millecamps & Julien, 2013). The kinesin-3 family member KIF1A is an anterograde motor that is enriched in neurons and functions in the transport of cargo such as DCVs and SVPs critical for neuron development, maintenance, and viability. Mutations in KIF1A are implicated in the pathogenesis of neurological disorders such as HSP. Unfortunately, tool compounds and therapies that specifically target KIF1A or transport-related disorders do not exist. One potential avenue for discovering such therapeutics and tool compounds is high-throughput screening. High-throughput screening is a powerful platform that allows one to utilize various enzymatic and phenotypic assays to screen numerous small molecules and biologics for their effects on a given system.

As such, my main goal of my project was to design a high-throughput screen for small molecule modulators of KIF1A. I focused on designing an assay that could robustly differentiate inactive, autoinhibited motors from active microtubule-bound motors. A microtubule-binding assay and peripheral accumulation assay were chosen as potential assays to be used in a high-throughput screen due to their extensive use in assessing motor activation (Hammond et al., 2009; Niwa et al., 2016). Two cell lines, one neuronal (SK-N-SH) and one non-neuronal (COS-7), were chosen for these assays due to their flat morphologies and large cytoplasm. I was able to generate four plasmids that incorporate a GFP-tagged, full length KIF1A motor (Table 3.1).

Doxycycline-inducible plasmids were assayed for differences in expression at varying time points and concentrations to assess their suitability in reducing background noise due to overexpression of KIF1A. Significant differences were seen in expression levels in the eight and 24 hour conditions compared with that of the four hour condition,

in which little to no expression was seen (Figure 3.4). Furthermore, expression levels between all time points and concentrations were similar, except between the 1:1000 eight hour condition and all 24 hour conditions, as well as 1:10000 eight hour time point and 1:1000 24 hour condition. Ultimately, doxycycline-inducible plasmids were determined to confer no benefit over constitutively-active plasmids in the context of my assays as expression times are similar between plasmids and expression levels generally were not significantly altered in most conditions.

Two suitable controls were determined, a wild-type KIF1A for the negative control, and a hyperactive mutant, V8M KIF1A, for the positive control. I characterized the phenotypes of all four plasmids when co-expressed with EB3-mKate2, a microtubule marker, and found that in the wild-type conditions, motors displayed a diffuse localisation in the cytoplasm (Figure 3.2; 3.3; 3.5; 3.6). Conversely, in the V8M mutant motors peripherally accumulated and colocalized with EB3-mKate2 (Figure 3.2; 3.3; 3.5; 3.6). These phenotypes were visually seen in both COS-7 and SK-N-SH. However, when quantified, there was only a significant difference in peripheral accumulation between WT KIF1A and V8M KIF1A in one condition, COS-7 with pEF-KIF1A-GFP plasmids (Figure 3.2C and D). This may have been the result of lower sample sizes in the SK-N-SH and pTetOne conditions. Conversely, in SK-N-SH, problems with the fluorescent distribution analysis may be a result of the irregular morphologies of SK-N-SH which situate the highly-fluorescent perinuclear area, close to the cell periphery. Moreover, there may be a decrease in the degree of transport due to hampering of the hyperactive V8M mutant by dimerization with endogenous KIF1A (Figure 3.1A). Microtubule-binding, although present in all V8M mutant conditions, was not quantifiable due to problems encountered in the design of the analysis. Ultimately, these results suggest COS-7 and pEF-KIF1A-GFP plasmids as optimal for downstream validation for high-throughput screening.

Furthermore, I was able to generate two polyclonal COS-7 and SK-N-SH stably expressing EB3-mKate2 (Figure 3.7), with monoclonal colony generation being currently underway. Lastly, I was able to construct a high-throughput analysis pipeline using *CellProfiler* software that allows for accurate quantification of fluorescence intensity distribution across cells (Figure 3.8), as well as begin preliminary construction of a high-throughput analysis pipeline for colocalization and overlap between the microtubule marker EB3-mKate2, and the variants of KIF1A-GFP (Figure 3.9).

4.2. Complications in Assay Design

One major bottleneck encountered in optimizing the microtubule-binding and peripheral accumulation assays for a high-throughput screen was the development of stable cell lines incorporating the microtubule marker EB3-mKate2 and the constitutively-expressed or doxycycline-on variants of KIF1A-GFP. In both cell lines, COS-7 and SK-N-SH, similar problems regarding stable integration of the plasmid were seen. Post-transfection and infection with the desired plasmid, cells were allowed to express the transgene and resistance-marker for 24 or 48 hours. Cells were assessed using fluorescence microscopy for expression of the transgene. Selection media was added, and transgene-expressing colonies allowed to form. Although stable colonies were seen to be forming, fluorescence microscopy showed an absence of fluorescence with only the occasional fluorescent cell being detected within the colony.

Stable cell line generation depends on the incorporation of your construct into the cell's genome. The efficiency of this incorporation depends on a host of factors, namely transfection efficiency, selection conditions and the stability of expression by your promoter. Several different transfection methods were used including liposome-mediated methods and electroporation, with consistent 80-90% transfection rates. In addition, selection conditions were chosen through a killing curve in which 100% of non-transfected cells were dead after 4-5 days. Control cells plated alongside transfectants were 100% dead at the time of colony formation. This suggested that the resistance gene was incorporated and that the problem may lie in the expression or integration of the transgene. Interestingly, promoter-mediated silencing of transgenes during selection via methylation of the CpG islands of the promoter is often seen in constructs driven by the cytomegalovirus (CMV) promoter (Teschendorf et al., 2002; Brooks et al., 2004; Zuniga et al., 2019).

Originally, a CMV-promoter driven construct was used for expression of the KIF1A-GFP variants and EB3-mKate2, which could possibly explain the absence of KIF1A-GFP or EB3-mKate2 expression. A variety of alternate promoters exist that are inherently more resistant to methylation-based silencing during stable cell lines formation such as the human eukaryotic translation elongation factor 1 (EF1α) and beta-actin (β-actin) promoter (Teschendorf et al., 2002; Wang et al., 2017; Zuniga et al., 2019). Furthermore, promoters such as the EF1α promoter drive more consistent expression of

transgenes across cells compared to that of the CMV promoter (Wang et al., 2017). This is a benefit for my assay as consistent expression levels from cell to cell reduce variability in fluorescence intensity distribution, an output of my analysis. As such, I cloned the transgenes for the constitutively-expressed KIF1A wildtype and V8M variants into a new vector, one that is driven by the EF1α promoter. Furthermore, I wanted my stable cell lines to be derived from the same monoclonal population of EB3-mKate2 expressing cells (both COS-7 and SK-N-SH) as this would reduce variability of expression levels across all stable cell lines allowing for more robust colocalization or overlap analysis between channels. However, the same problems were seen as that of the KIF1A variants since the transgene was driven by the CMV promoter. To ensure that the EB3-mKate2 transgene was stably incorporated into my cell lines, I employed a lentiviral-mediated strategy as lentiviral-mediated incorporation of transgenes decreases stable cell line generation times, and increases the stability and likelihood of integration events (Tandon et al., 2018). Furthermore, Applied Biological Materials (ABM, Richmond, BC) was employed to clone the transgene into an EF1α promoter driven plasmid to decrease the likelihood of promoter silencing, as well as package the lentivirus. Currently, polyclonal lines expressing EB3-mKate2 for both COS-7 and SK-N-SH have been generated using lentiviral-mediated transgene delivery. Monoclonal cell line generation is currently ongoing.

Unfortunately, due to unforeseen circumstances such as the COVID-19 lockdown, reagent production and delivery times by ABM, as well as reagent quality (inadequate viral titers), the generation of stable cell lines has been the bottleneck in progression of this assay to a suitable high-throughput screening format. Downstream analyses including a high-throughput fluorescence distribution analysis, as well as a colocalization analysis, are dependent on stable cell line generation. Stable cell lines for my positive (V8M KIF1A-GFP) and negative (WT KIF1A-GFP) controls would allow me to generate images at the Center for High-Throughput Chemical Biology which would include a high number of dual-expressing cells (variant of KIF1A-GFP with EB3-mKate2) with consistent expression levels across cells. I have been unable to accomplish this using transient transfection methods as co-transfection yielded a low percentage of dual-expressing cells with varying expression levels of the transgenes. Uniform expression of both fluorescent markers are critical for segmentation of the cytoplasm of the cells from the background and nuclei which is dependent on consistent thresholding: an image

analysis technique that benefits from compartmentalized fluorescent uniformity, particularly in a high-throughput format. With proper segmentation and consistent expression levels within control groups, optimization of a robust, high-throughput fluorescence distribution analysis and colocalization analysis could be achieved.

One of the main problems seen currently in terms of the image analysis is that segmentation, although quite good at detecting cell edges when fluorescence intensity is uniform, can fall apart when a high degree of fluorescence is aggregated in the tips of processes that extend out from the cell (Figure 3.5A). Due to the discrepancy of the fluorescence intensities between the tip of the process and the main cell body, segmentation software will typically remove the highly intense portion and consider that as a separate object compared to the cell body. Particularly in the COS-7 cells which tend to accumulate the KIF1A-GFP in processes extended away from the cell body, this alters the values outputted by the fluorescence distribution analysis. It is a possibility, however, that automated segmentation still will not properly segment cytoplasmic regions in stable cell lines, particularly expressing the positive control V8M KIF1A-GFP mutant, as accumulation at the tips of processes may result in them being considered as a separate object. A solution for this is using a whole-cell live stain such as Cellomics Whole Cell Stain (Thermofisher, Waltham, MA, USA) which would demarcate the entire cell including the processes allowing for easy segmentation of the cytoplasm from the background. Another solution to this problem would be to expand the radial segments used in the fluorescence distribution analysis out past the cells borders (Kapitein et al., 2010). Cell segmentation would not be needed in this case as one could use an average of the cell size to expand a non-scaled radial segment out from the nuclei, an easily segmented cellular compartment. This would allow for capture of peripheral aggregates in the protruding cell processes, albeit losing some accuracy as cell sizes may differ slightly. Conversely, use of a watershed method in which pixel values are treated as local topography may confer advantages over a complete cell segmentation strategy (Meyer, 1994). Using a watershed method, one can identify regions of high intensity corresponding to accumulations of KIF1A-GFP while disregarding regions of low intensity, such as the cytoplasm. Furthermore, this method would allow one to completely forgo segmentation and focus on the number and intensity of punctate KIF1A-GFP aggregates throughout the whole image. These outputs would correspond to the degree of peripheral accumulation seen. However, it is important to note that KIF1A-

GFP intensities tend to be high perinuclearly, so a strategy such as excluding a defined region outside the nuclei or a highly optimized watershed based on average fluorescence intensities in KIF1A-GFP aggregates may be needed.

Another challenge is the segmentation of the microtubules in both the EB3-mKate2 and positive control (V8M KIF1A-GFP). Although thresholding microtubule structures post erosion and dilation of a greyscale image is relatively simple to do, a number of Golgi- and ER- localized vesicular structures, along with cell edges and nuclear edges, are also eroded and dilated with them. Conversely, bleed through of microtubule structures could alter the analysis, however, this was tested for previously (Appendix; Figure A2.). Following binarization via thresholding and overlaying of the microtubule mask with the KIF1A image, colocalization and overlap (quantified via Pearson correlation coefficient and F-score) are affected due to the identical segmentation of vesicular and edge objects giving an unreliable correlation or overlap between microtubules and KIF1A (Figure 3.9). One way to overcome this would be by training a pixel-classifier, such as *Ilastik* or *Cell Profiler Analyst*, to identify microtubules, while ignoring vesicular and other structures. Pixel-classifiers work by assigning labels to pixels depending on the user-chosen pixel features such as intensity, texture descriptors, and edge filters. Following training by identifying key features and addition of a number of images that contain those features, the pixel-classifier can robustly identify complex structures that general thresholding would not be able to (Berg et al., 2019). With stable cell lines generated, one would be able to accurately train a pixel-classifier with a high number of cell images to identify microtubular structures and consequently import them into a colocalization analysis pipeline.

4.3. High-throughput Assaying of KIF1A

Established assays for transport kinesins and dynein have been adapted to high-throughput screening formats including ATPase assays, FRET-based biochemical assays, and inducible-transport assays. So far, the only transport kinesin that has been probed for small-molecule modulators of its activity is the conventional kinesin, kinesin-1 (also termed KIF5). The first assay, an ELIPA ATPase assay along with an orthogonal ADP-Glo ATPase assay, identified seven hits in total, three activators and four inhibitors, from the 1280 compound Library of Pharmacologically Active Compounds (LOPAC) library (Figure 1.7; Kadakkuzha et al., 2014). Following secondary screening only two

inhibitors and one activator were confirmed, a weak ATPase activator and a cysteine site modifier. Of note was the Z' generated for this assay, 0.92, indicating this assay was quite robust in assaying kinesin-1 ATPase activity. The second assay was a novel FRET-based biochemical assay in which the authors exploited the interaction of a lysosomal cargo-adaptor, SKIP, with kinesin light-chain 2 (KLC2; Randall et al., 2017). The W-acidic-motif-peptide of SKIP relieves autoinhibition and allows for SKIP to bind to KLC2, thus inducing activation of the motor. As such, the authors wanted to find compounds that can induce relief of autoinhibition while simultaneously inhibiting SKIP binding thereby inducing activation in a SKIP-independent manner. Interestingly, the authors found a molecule from the Chemogenomic Library (Pfizer, New York, NY, USA) and Hit-2-Lead library (Chembridge, San Diego, CA, USA) which they named Kinesore that blocked the interaction between the W-acidic-motif-peptide of SKIP and KLC2, relieving autoinhibition and activating the motor. Notably, both these assays may be adapted to high-throughput assaying of small molecule compounds of KIF1A. For the ATPase assay mentioned above, the only difference would be one would need to purify the motor domain of KIF1A for use with commercially available ELIPA kits. The FRET-based assay, however, is also adaptable for screening compounds that affect autoinhibition of KIF1A. KIF1A has multiple domains that regulate autoinhibition, in particular, the CC3 and PH domains, the NC and CC1 domains, as well as the CC1 and FHA domains (Huo et al., 2012; Wu et al., 2013; Ren et al., 2018). KIF1A autoinhibition is relieved through a variety of compounds that interact with various domains of KIF1A. For example, calmodulin (CaM), a Ca^{2+}-binding protein, when bound to the CC3 domain in physiologically elevated Ca^{2+} conditions induces an increase in DCV binding and trafficking (Stucchi et al., 2018). In addition, ARL-8B, a GTPase, strongly activates KIF1A following binding of CC3 by relieving inhibition, presumably through relieving CC3-PH domain interactions (Niwa et al., 2016). As the FRET-based assay was dependent on seeing a reduction of FRET due to blockage of the SKIP-KLC2 interaction, one can develop an assay that applies the same concept to the KIF1A-binding regions of ARL-8B, and the ARL-8B-binding regions of the CC3 domain. Conversely, something similar may be done with CaM, applying the same concept as discussed above.

Another transport-based assay strategy that could be adapted for a KIF1A-based high-throughput screen is the inducible Golgi/peroxisome dispersion assay (Figure 1.10; Kapitein et al., 2010; Vincent et al., 2020). Ultimately, this assay may yield a more

70

physiologically relevant set of hits that affect transport as this assay would be done in a particular cellular environment depending on the cell line one chooses. This has its benefits and drawbacks. For example, if this assay was run in a non-neuronal cell line such as COS-7, benefits would include the absence of possible neuronal specific factors that may affect KIF1A activity, absence of endogenous KIF1A, or absence of neuron-enriched microtubule post-translational modifications (PTMs) which affect KIF1A function (Bai et al., 2008; Tischfield and Engle, 2010; Hawrylycz et al., 2012). This would yield more KIF1A-specific hits absent of any possible perturbations seen in a neuronal environment. However, the presence of neuronal specific factors may be a benefit. Perhaps one wants KIF1A to be perturbed via microtubules rich in neuron-enriched PTMs or neuron-specific factors to assess whether these affect the functionality of the hit, in which case a neuron-like cell line, such as SK-N-SH, can be used. These benefits also hold true for my microtubule-binding and peripheral accumulation assay which is why stable cell lines are being generated for both COS-7 and SK-N-SH cells. Notably, the Golgi/peroxisome dispersion assay has already been adapted to a high-throughput screening format including a robust analysis for discovery of small molecule modulator of dynein (Vincent et al., 2020). The concept behind the Golgi/peroxisome dispersion assay is the same for both dynein and kinesins, except that the dynein transports the peroxisomes retrogradely to perinuclear regions versus the kinesins which would distribute the peroxisomes or Golgi to the cell periphery. An interesting aspect of this high-throughput assay was that the authors used mean GFP spot size at the perinuclear region to assess the degree of activation or inhibition as opposed to the fluorescence intensity distribution of the puncta. This allowed the assay to assess the perinuclear aggregated puncta intensity and spot sizes and determine the extent of activation or inhibition without dealing with issues of segmentation of closely packed cells as I ran into in my analysis, instead dealing with the relatively straight forward segmentation of nuclei. This assay was deemed to be highly robust achieving a Z' of 0.56. Ultimately, using this as an orthogonal assay, or even developing this as a primary assay for high-throughput screening of KIF1A if my assay does not generate a suitable Z', would be a relatively low-cost and already proven way to confirm or generate hits.

Another transport assay that could be feasibly translated to a high-throughput assay for small molecule modulators of KIF1A would be the platform developed by the Hermann lab, which allows for high-content organelle trafficking profiling in induced

pluripotent stem cell (iPSC)-derived neurons (Pal et al., 2018). In essence, neuronal progenitor cells (NPCs) are derived from iPSC's in microfluidic chambers and subsequently matured into whatever neuronal type one desires and whose protocols are available for at the time. Following maturation, live cell imaging is conducted, and particles are tracked in the soma, proximal and distal axons or dendrites. The microfluidic chambers allow for identification and segmentation of neuronal regions such as the soma, as well as proximal and distal axons and dendrites. If one used a CRISPR-Cas9 system to knock-in a fluorescently-tagged KIF1A into the iPSC's, one could use this screen to identify, in a very physiologically relevant environment, modulators of wild-type KIF1A transport activity. Even more importantly, one can knock-in a disease-causing KIF1A mutant and differentiate the iPSC's into a disease-relevant neuronal subtype such as an upper motor neuron or a glutamatergic neuron in the case of HSP. One would then have a very robust disease model in which you could assay for hits that would possibly specifically target that mutant and its downstream effects.

4.4. Potential Therapeutics and Tool Compounds

Currently, therapeutics for transport kinesins do not exist and tool compounds that allow for study of kinesin function are scarce. Broadly, compounds could be found that affect one or more of the three main domains of transport kinesins; the motor domain, regulatory domains, or cargo binding domains. At the moment, compounds found from high-throughput screens involving transport kinesins have found molecules that namely act on the motor domain. Kinesore, a kinesin-1 regulatory domain modulator is the only known confirmed modulator of a domain outside that of the motor domain (Randall et al., 2017). As high-throughput screens of small molecule libraries that target transport kinesins become more common, more compounds are becoming available that purportedly target kinesins. For example, in the kinesin-1 ATPase-based screen mentioned previously, two inhibitors and one activator were found (Kadakkuzha et al., 2014). The activator, P1,P4 -Di(adenosine-50) tetraphosphate ammonium salt (Ap4A) is proposed to inhibit adenosine kinase activity *in vitro* and *in vivo* and affects numerous biological activities such as causing nitric oxide release and alterations in calcium levels. The authors, however, did not test whether this molecule is kinesin-1 specific, which would be unlikely due to the conservation of sequence of the ATPase domain across kinesins. If this holds true, this molecule may be useful as a tool compound for

increasing ATPase activity across kinesins thereby useful for modulation studies of various transport kinesins. Interestingly, Ap4A, when cleaved, produces ATP and ADP as a byproduct which may serve as a mechanism of action of this compound on the ATPase domain of kinesin-1 by increasing ATP pools locally around the motor (Guranowski and Blanquet., 1985). However, because Ap4a is a known modulator of Ca^{2+} levels *in vitro* and *in vivo,* such a compound would be rendered relatively useless for studies of KIF1A in neurons as KIF1A is heavily modulated by Ca^{2+}-binding proteins such as CaM (Kadakkuzha et al., 2014; Stucchi et al., 2018). Furthermore, neuronal environments are sensitive to local and global changes in Ca^{2+} levels, with a variety of deleterious phenomena documented when Ca^{2+} homeostasis is altered (Gleichmann and Mattson., 2011; Tong et al., 2018; Glaser et al., 2019). An inhibitor of interest that was found was 4-chloromercuribenzoic acid which acts as a cystine active site modifier due to its interaction with free sulfhydryl groups (Kadakkuzha et al., 2014). Currently, no biochemical studies have been done that assess the effects of compounds of this class on the kinesin superfamily of proteins.

The question, however, remains as to what compounds could be found that alter KIF1A activity in either an inhibitory or activating manner. Most likely a majority of hits would not be KIF1A or transport kinesin specific in general as many hits would most likely work on regulatory pathways that affect kinesins such as through kinase or phosphatase activity modulation. In addition, these hits may work on processes that affect transport such as microtubule destabilization and stabilization. It is also important to discuss how such compounds could alter activity downstream of KIF1A activity and consequently disease states.

One possibility would be compounds that bind KIF1A-specific regions of the motor domain and allosterically regulate ATPase activity or microtubule-binding such as is seen with Monastrol in Eg5 (Figure 4.1A; Kapoor et al., 2000; Maliga et al., 2002). Although the structure and function of the motor domain is conserved across kinesins, motors such as Eg5 and KIFC1 have specific sequences within these highly conserved regions (Maliga et al., 2002; Yang et al., 2014). As such, it is not unreasonable to believe that an ATPase assay would uncover novel regulators of ATPase activity in KIF1A through either allosteric regulation of the nucleotide-binding pocket, or mechanical actuator regions such as Switch I/II. In addition, it is possible that certain compounds exist that act similar to the compound adenylyl-imidodiphosphate (AMP-PNP), a non-

hydrolysable analogue of ATP used in various testing of kinesin function (Cai et al., 2007; Kaul et al., 2011). Ideally, such a compound would be cell-permeable as currently membranes must be permeabilized for AMP-PNP to enter cells. Furthermore, microtubule-binding assays or microtubule-gliding assays could identify allosteric regulators or direct modulators of domains involved in microtubule-binding such as the neck linker or K-loop of KIF1A. A second, more complex region to assess and target compounds for, is the regulatory regions of KIF1A, which include the NC, CC1, FHA, and CC2 domains. As the autoinhibition seen in KIF1A and mechanisms that regulate this process are not well understood, assays that would allow for targeting of this domain via a small-molecule library or biologics would be difficult. Ultimately, secondary assays that specifically assess the autoinhibitory process would be needed to screen hits for this region. A possible type of compound that could, in theory, act as an activator, could be dimeric macrocyclic peptides (Figure 4.1B; Ito et al., 2015; Vinogradov et al., 2019). These biologics could theoretically induce the dimerization of the KIF1A monomers through cross-linking of regulatory domains such as the CC1 domains of separate monomers. How these types of molecules would overcome the inherent autoinhibition in wildtype KIF1A is unknown. However, in mutant KIF1A, where either the motor is inefficient due to an inability to stay on the microtubule tracks, or due to a reduced efficiency in the ATPase, increasing the pool of activated motors via macrocyclic peptide-induced dimerization could alleviate downstream effects of cargo transport insufficiencies. Lastly, the cargo-binding domain, which also has a regulatory function via the CC3-PH domain interaction, can be targeted for both inhibitory and activating compounds. FRET-based assays, as mentioned above, can be devised to allow for assessment of changes in interaction between the CC3 and PH domains of KIF1A. As such, discovered compounds may act similarly to that of Kinesore, in which they bind specific regulatory motifs of the KIF1A tail such as ARL8B or CaM binding sites, activating the motor in the process independent of regulatory proteins. Conversely, inhibition can occur via molecules that bind to regions adjacent to that of known regulatory sites of the tail domain that either competitively inhibit or allosterically inhibit binding of regulatory molecules.
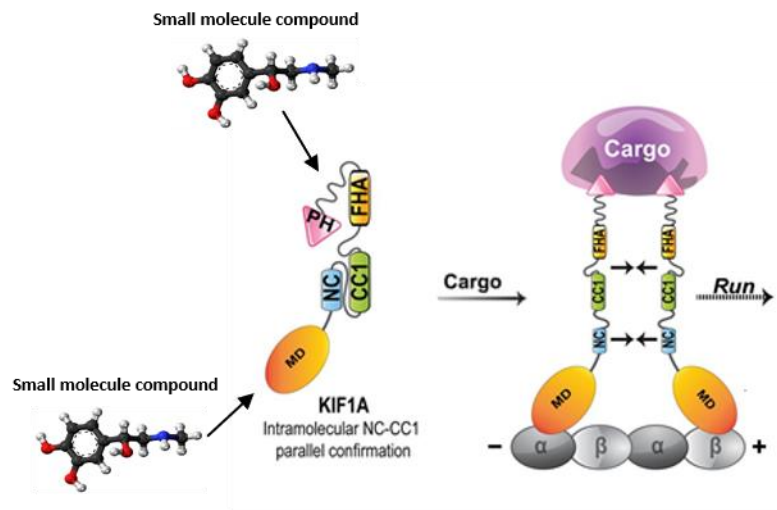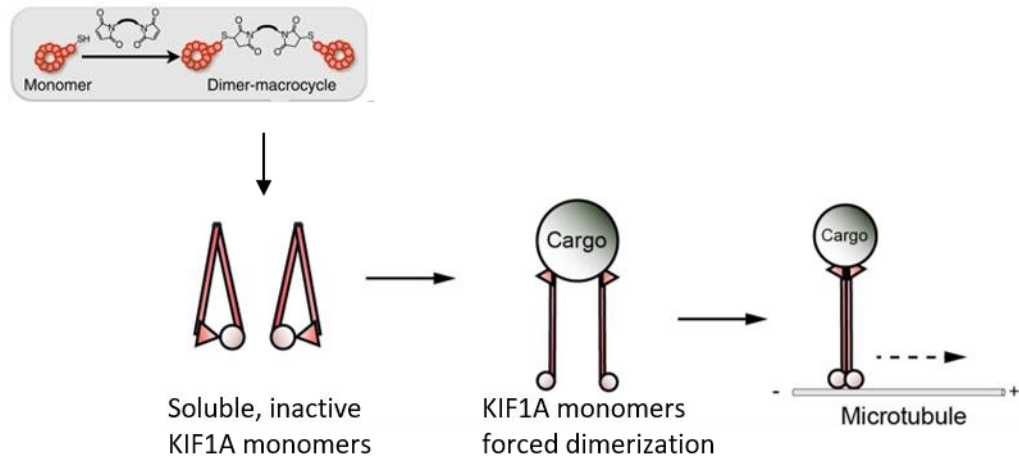
Figure 4.1. Potential KIF1A-specific hit compounds.
A) A schematic representing small molecule compounds working on various domains of KIF1A. Small molecule modulators of the domain may result in increased ATPase activity or increased microtubule on-rates resulting in activation of the motor. Conversely, they may inhibit the motor in similar ways. Small molecule modulators may also disrupt interactions between the CC3 and PH domains resulting in relief of autoinhibition and activation of motors (Gabrych et al., 2019). B) A schematic representing dimerized macrocycle peptides working to activate KIF1A monomers via forced dimerization (Ito et al., 2015; Gabrych et al., 2019).

Another consideration when screening for compounds using a cell-based, phenotypic screen, would be the likely probability of getting false positive hits. These hits could make it look as if KIF1A itself is being modulated but instead affects KIF1A regulatory molecules such as glycogen synthase kinase 3 beta (GSK3β) or calmodulin kinase II (CaMKII) (Stucchi et al., 2018; Gan et al., 2020). Conversely, false positive hits could work on the microtubule network via destabilization or stabilization of the tracks.

As such, robust secondary assays are needed to confirm KIF1A-specificity of the hits. The assay I developed took into account the latter consideration by co-expressing the KIF1A variants with a microtubule marker EB3-mKate2. If molecules were to destabilize microtubules, a phenotype similar to that seen in fenbendazole-treated cells would be seen (Dogra et al., 2018). Conversely, stabilization of the microtubules could mimic phenotypes seen through paclitaxel treatment although my assay would not detect this, but the change in dynamics could affect transport (Yang and Horwitz., 2017). Although compounds that affect regulatory molecules and microtubules directly are needed as tool compounds and experimental treatments, particularly for certain types of cancers and neuropathology's such as Alzheimer's disease in the case of GSK3β, ultimately I was looking for KIF1A-specific compounds as this would minimize off-target effects in the body due to the neuron-enriched expression of KIF1A.

Lastly, how would activators and inhibitors of KIF1A activity relieve pathological deficits seen in KAND? Previously, I reviewed an extensive list of possible pathological cargo-mediated processes that would result due to deficits in KIF1A function (Gabrych et al., 2019). A non-exhaustive list includes defects in synapse formation and maintenance, neuronal developmental, maintenance, and plasticity, autophagy disruptions, possible APP misprocessing and glial support of myelination (Figure 4.2). For example, in mutants that affect the ability of KIF1A to bind ATP, such as T99M, decreases motor activity (Nieh et al., 2015). Consequently, proper spatiotemporal delivery of important cargos such as the SVPs is impacted resulting in downstream consequences in the formation and maintenance of synapses. Indeed, SVP cargos such as synaptophysin, an adaptor critical for endocytic recycling and synaptic vesicle maturation, when knocked out, results in similar symptomology as complicated HSP patients including intellectual disability, epilepsy, and hypotonia (Becher et al., 1999; Schoch et al., 2001; Gordon and Cousin, 2013; Harper et al., 2017). Inability to deliver synaptophysin to maturing and matured synapses due to defects in motor activity may mimic knock-out phenotypes. In this case, activators that increase the availability of the binding pocket to ATP, or conversely, more strongly bind the microtubules via enhancements to K-loop function, would be ideal. If one found a regulatory region activating compound, such as a dimeric macrocyclic peptide that induced dimerization of a greater population of KIF1A motors, this could increase the available pool of active motors possibly compensating for the decrease in activity seen in a loss-of-function mutant. Conversely, in mutants that cause

hyperactivation of KIF1A, such as the V8M mutant, over-accumulation of cargo at synapses is often seen, suggesting excessive cargo accumulation may be pathogenic (Chiba et al., 2019). Conversely, due to the increased motility and on-rate of such mutants, KIF1A may not be able to stop at the proper synaptic site leading to mis-delivery of cargo to different regions of the neuron. The DCV cargo, nerve growth factor (NGF), may give insights into how a hyperactivating mutation can cause a degenerative phenotype in affected neuronal populations of HSP patients. NGF is critical for neuroprotection against excitotoxicity, regulates axon outgrowth, and modulates receptivity to myelination (Kume et al., 2000; Turney et al., 2016). Compartmentalization of NGF is integral to how an axon responds to such a signal. When NGF is compartmentalized to the soma and proximal axon, axonal pruning occurs, whilst when contained in the distal axon, apoptosis-induced soma and axonal degeneration is seen (Geden and Deshmukh, 2016; Geden et al., 2019). If the hyperactivating mutant results in compartmentalization of NGF to the distal axon, it may result in the degeneration of the neuron as is seen in the upper motor neurons of HSP patients. As such, inhibitors that either reduce the efficiency of the motor through reduction in force output, microtubule on-rate, or disruption of regulatory processes, may allow for changes in localizations of cargos thereby altering spatiotemporal effects seen in neurons.

KIF1A transport deficits and resulting cellular phenotype

Synaptic vesicle precursors (SVPs) — ↓ Synapse formation & maintenance

Dense core vesicles (DCVs) — ↓ Neuronal development, maintenance, & plasticity

TrkA vesicles — ↓ NGF signaling & neuronal survival

ATG-9 vesicles — ↓ Autophagy

BACE-1 vesicles — ↓ NRG processing & glial support of myelination

↑ APP misprocessing
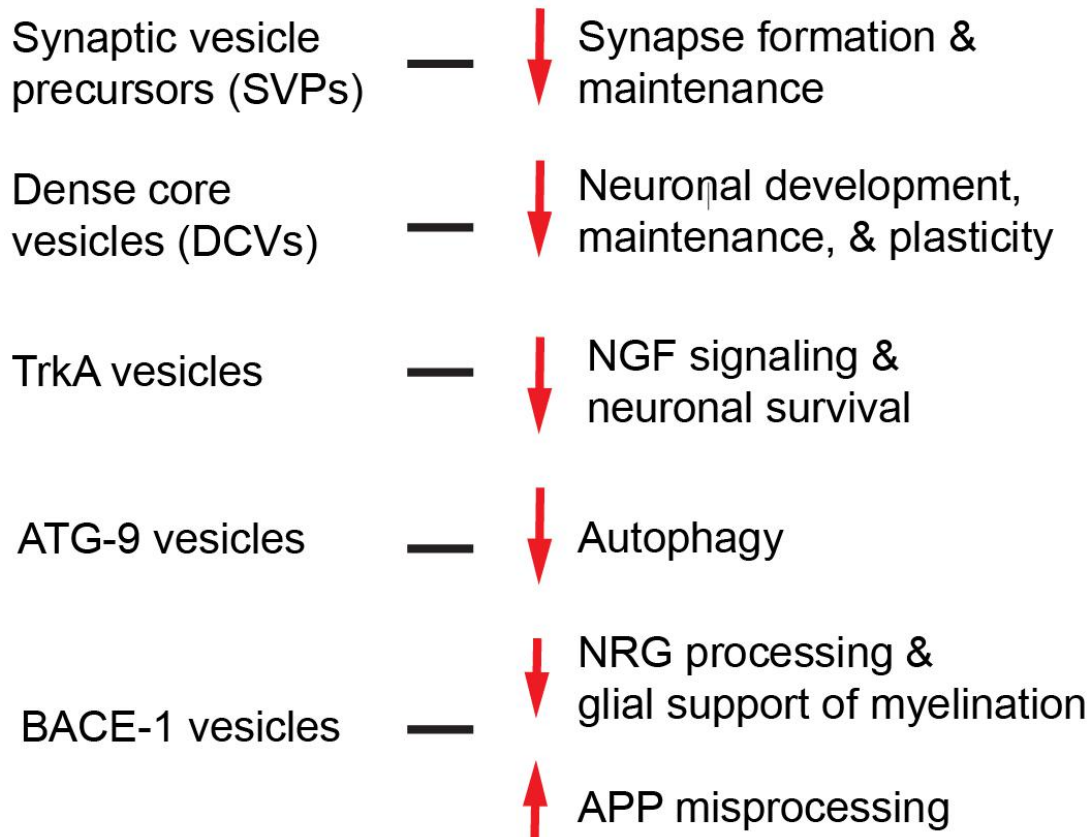
Figure 4.2. Summary of KIF1A cargos and potential cellular effects from trafficking defects.
A list of KIF1A-transported cargos and the potential downstream cellular effects when trafficking is compromised by KIF1A mutants in neurons.

4.5. Conclusion and Future Directions

I sought to design a high-throughput screen of small-molecule modulators of KIF1A. Namely, I focused on designing an assay that could robustly differentiate inactive, autoinhibited, monomeric motors from active, dimeric, microtubule-bound motors. I generated four plasmids that incorporate a GFP-tagged, full length KIF1A motor (Table 3.1). I characterized the phenotypes of all four plasmids when co-expressed with EB3-mKate2, a microtubule marker, and found that in the wild-type conditions, motors were soluble, and displayed a diffuse localisation in the cytoplasm. Conversely, in the V8M mutant, motors peripherally accumulated and colocalized with

EB3-mKate2. I further demonstrated this in two cell lines, one neuronal (SK-N-SH), and one non-neuronal (COS-7). I was able to generate two polyclonal COS-7 and SK-N-SH stably expressing EB3-mKate2, with monoclonal colony generation being currently underway. Lastly, I was able to construct a high-throughput analysis pipeline using *CellProfiler* software that allows for quantification of fluorescence intensity distribution across cells, as well as begin preliminary construction of a high-throughput analysis pipeline for colocalization and overlap between the microtubule marker EB3-mKate2, and the variants of KIF1A-GFP.

Ultimately, my work sets the stage for downstream optimization of a microtubule-binding and peripheral accumulation assay for a high-throughput screening format. However, a number of steps must be undertaken prior to using this assay in a high-throughput screen. Future work will involve three major steps to ensure the assays viability. The first step is to generate monoclonal stable cell lines that co-express EB3-mKate2 and one KIF1A-GFP variant per cell line, to reduce variability from cell to cell for analysis optimization. Secondly, fluorescence intensity distribution, colocalization, and overlap analysis optimization will need to be conducted on a large population of stable cell lines confirm proper segmentation and downstream analyses dependent on ideal segmentation. It is possible that segmentation will still be difficult to accomplish due to the varying intensities of signal in distal processes, therefore, a whole-cell stain will need to be chosen and validated for segmentation of whole cells. Lastly, once cells and analyses have been optimized, validation of the assay itself through generation of a Z' will need to be done prior to proceeding to a pilot screen.

My work is significant as it contributes another standardized transport-based kinesin assay optimized to a high-throughput screening format for either primary, orthogonal, or secondary screening. Secondly, the assay is relatively low-cost which allows labs with less resources to be able to conduct adjacent screens either with reagents I generated, or with alternate transport kinesins of interest. Thirdly, my assay may generate hits which affect multiple domains of KIF1A including the motor domain, regulatory domains, or cargo-binding domains. This is novel as currently, transport kinesin based high-throughput screens typically focus on the ATPase region within the motor domain.

Furthermore, the significance of potential hits extends to KIF1A-associated neurological disorders such as HSP and PEHO syndrome as there is currently no KIF1A-targeted therapeutics or tool compounds. Both loss-of-function and gain-of-function motor mutants may result in aberrant subcellular localizations of essential neuronal cargos. These cargos play a variety of roles in the development, maturation, and viability of the nervous system, and many are implicated in other neurodegenerative disorders. To further our understanding of kinesin-3 motors roles in these disorders, cellular characterization of disease-related mutants needs to be carried out. Hits that are able to alter motility, regulatory, or cargo-binding properties of KIF1A allow for tool compound probing of disease-associated mechanisms of action.

Overall, my work on developing an assay suitable for high-throughput screen of small molecule modulators of KIF1A sets the groundwork for potential discovery of KIF1A-specific hits and potential life-altering therapeutics for patients with KAND.

References

Bai, M., Papoudou-Bai, A., Karatzias, G., Doukas, M., Goussia, A., Stefanaki, K., et al. (2008). Immunohistochemical expression patterns of neural and neuroendocrine markers, the neural growth factor receptors and the β-tubulin II and IV isotypes in human thymus. *Anticancer Research*, *28*(1 A), 295–304.

Barkus, R. V, Klyachko, O., Horiuchi, D., Dickson, B. J., & Saxton, W. M. (2008). Identification of an axonal kinesin-3 motor for fast anterograde vesicle transport that facilitates retrograde transport of neuropeptides. *Molecular Biology of the Cell, 19*(1), 274–283. https://doi.org/10.1091/mbc.e07-03-0261

Becher, A., Drenckhahn, A., Pahner, I., Margittai, M., Jahn, R., & Ahnert-Hilger, G. (1999). The Synaptophysin–Synaptobrevin Complex: a Hallmark of Synaptic Vesicle Maturation. *The Journal of Neuroscience*, *19*(6), 1922–1931. https://doi.org/10.1523/jneurosci.19-06-01922.1999

Bellofatto, M., De Michele, G., Iovino, A., Filla, A., & Santorelli, F. M. (2019). Management of hereditary spastic paraplegia: A systematic review of the literature. *Frontiers in Neurology*, Vol. 10. https://doi.org/10.3389/fneur.2019.00003

Bentley, M., & Banker, G. (2016). The cellular mechanisms that maintain neuronal polarity. *Nature Reviews Neuroscience*, Vol. 17, pp. 611–622. https://doi.org/10.1038/nrn.2016.100

Berg, S., Kutra, D., Kroeger, T., Straehle, C. N., Kausler, B. X., Haubold, C., Schiegg, M., Ales, J., Beier, T., Rudy, M., Eren, K., Cervantes, J. I., Xu, B., Beuttenmueller, F., Wolny, A., Zhang, C., Koethe, U., Hamprecht, F. A., & Kreshuk, A. (2019). Ilastik: Interactive Machine Learning for (Bio)Image Analysis. Nature Methods, 16(12), 1226–1232. https://doi.org/10.1038/s41592-019-0582-9

Bergnes, G., Brejc, K., & Belmont, L. (2005). Mitotic Kinesins: Prospects for Antimitotic Drug Discovery. Current Topics in Medicinal Chemistry, 5(2), 127–145. https://doi.org/10.2174/1568026053507697

Blackstone, C. (2018). Converging cellular themes for the hereditary spastic paraplegias. *Current Opinion in Neurobiology*, Vol. 51, pp. 139–146. https://doi.org/10.1016/j.conb.2018.04.025

Brooks, A. R., Harkins, R. N., Wang, P., Qian, H. S., Liu, P., & Rubanyi, G. M. (2004). Transcriptional silencing is associated with extensive methylation of the CMV promoter following adenoviral gene delivery to muscle. Journal of Gene Medicine, 6(4), 395–404. https://doi.org/10.1002/jgm.516

Cai, D., Hoppe, A. D., Swanson, J. A., & Verhey, K. J. (2007). Kinesin-1 structural organization and conformational changes revealed by FRET stoichiometry in live cells. Journal of Cell Biology, 176(1), 51–63. https://doi.org/10.1083/jcb.200605097

Cawley, N. X., Li, Z., & Loh, Y. P. (2016). Biosynthesis, trafficking, and secretion of pro-opiomelanocortin-derived peptides. *Journal of Molecular Endocrinology*, Vol. 56, pp. T77–T97. https://doi.org/10.1530/JME-15-0323

Chen, C. W., Peng, Y. F., Yen, Y. C., Bhan, P., Muthaiyan Shanmugam, M., Klopfenstein, D. R., & Wagner, O. I. (2019). Insights on UNC-104-dynein/dynactin interactions and their implications on axonal transport in Caenorhabditis elegans. Journal of Neuroscience Research, 97(2), 185–201. https://doi.org/10.1002/jnr.24339

Cheon, C. K., Lim, S. H., Kim, Y. M., Kim, D., Lee, N. Y., Yoon, T. S., et al. (2017). Autosomal dominant transmission of complicated hereditary spastic paraplegia due to a dominant negative mutation of KIF1A, SPG30 gene. *Scientific Reports*, *7*(1). https://doi.org/10.1038/s41598-017-12999-9

Chiba, K., Takahashi, H., Chen, M., Obinata, H., Arai, S., Hashimoto, K., Oda, T., McKenney, R. J., & Niwa, S. (2019). Disease-associated mutations hyperactivate KIF1A motility and anterograde axonal transport of synaptic vesicle precursors. Proceedings of the National Academy of Sciences of the United States of America, 116(37), 18429–18434. https://doi.org/10.1073/pnas.1905690116

Chitre, M., Nahorski, M. S., Stouffer, K., Dunning-Davies, B., Houston, H., Wakeling, E. L., Brady, A. F., Zuberi, S. M., Suri, M., Parker, A. P. J., & Woods, C. G. (2018). PEHO syndrome: The endpoint of different genetic epilepsies. Journal of Medical Genetics, 55(12). https://doi.org/10.1136/jmedgenet-2018-105288

Dean, C., & Dresbach, T. (2006). Neuroligins and neurexins: Linking cell adhesion, synapse formation and cognitive function. *Trends in Neurosciences*, Vol. 29, pp. 21–29. https://doi.org/10.1016/j.tins.2005.11.003

Dieni, S., Matsumoto, T., Dekkers, M., Rauskolb, S., Ionescu, M. S., Deogracias, R.,et al. (2012). BDNF and its pro-peptide are stored in presynaptic dense core vesicles in brain neurons. *Journal of Cell Biology, 196*(6), 775–788. https://doi.org/10.1083/jcb.201201038

Dogra, N., Kumar, A., & Mukhopadhyay, T. (2018). Fenbendazole acts as a moderate microtubule destabilizing agent and causes cancer cell death by modulating multiple cellular pathways. Scientific Reports, 8(1). https://doi.org/10.1038/s41598-018-30158-6

Duarte-Neves, J., Gonçalves, N., Cunha-Santos, J., Simões, A. T., den Dunnen, W. F. A., Hirai, H., et al. (2015). Neuropeptide Y mitigates neuropathology and motor deficits in mouse models of Machado-Joseph disease. *Human Molecular Genetics*, *24*(19), 5451–5463. https://doi.org/10.1093/hmg/ddv271

Ebbing, B., Mann, K., Starosta, A., Jaud, J., Schöls, L., Schüle, R., & Woehlke, G. (2008). Effect of spastic paraplegia mutations in KIF5A kinesin on transport activity. *Human Molecular Genetics*, *17*(9), 1245–1252. https://doi.org/10.1093/hmg/ddn014

Endow, S. A., Kull, F. J., & Liu, H. (2010). Kinesins at a glance. In Journal of Cell Science (Vol. 123, Issue 20, pp. 3420–3424). J Cell Sci. https://doi.org/10.1242/jcs.064113

Erlich, Y., Edvardson, S., Hodges, E., Zenvirt, S., Thekkat, P., Shaag, A., et al. (2011). Exome sequencing and disease-network analysis of a single family implicate a mutation in KIF1A in hereditary spastic paraparesis. *Genome Research*, *21*(5), 658–664. https://doi.org/10.1101/gr.117143.110

Ermak, G., Cancasci, V. J., & Davies, K. J. A. (2003). Cytotoxic effect of doxycycline and its implications for tet-on gene expression systems. Analytical Biochemistry, 318(1), 152–154. https://doi.org/10.1016/S0003-2697(03)00166-0

Ernfors, P., Lee, K. F., & Jaenisch, R. (1994). Mice lacking brain-derived neurotrophic factor develop with sensory deficits. *Nature*, *368*(6467), 147–150. https://doi.org/10.1038/368147a0

Eschbach, J., Sinniger, J. Ô., Bouitbir, J., Fergani, A., Schlagowski, A. I., Zoll, J., Geny, B., René, F., Larmet, Y., Marion, V., Baloh, R. H., Harms, M. B., Shy, M. E., Messadeq, N., Weydt, P., Loeffler, J. P., Ludolph, A. C., & Dupuis, L. (2013). Dynein mutations associated with hereditary motor neuropathies impair mitochondrial morphology and function with age. Neurobiology of Disease, 58, 220–230. https://doi.org/10.1016/j.nbd.2013.05.015

Farías, G. G., Guardia, C. M., De Pace, R., Britt, D. J., & Bonifacino, J. S. (2017). BORC/kinesin-1 ensemble drives polarized transport of lysosomes into the axon. Proceedings of the National Academy of Sciences of the United States of America, 114(14), E2955–E2964. https://doi.org/10.1073/pnas.1616363114

Fink, J. K. (2013). Hereditary spastic paraplegia: Clinico-pathologic features and emerging molecular mechanisms. *Acta Neuropathologica*, Vol. 126, pp. 307–328. https://doi.org/10.1007/s00401-013-1115-8

Fleck, D., N. Garratt, A., Haass, C., & Willem, M. (2012). BACE1 Dependent Neuregulin Processing: Review. Current Alzheimer Research, 9(2), 178–183. https://doi.org/10.2174/156720512799361637

Gabrych, D. R., Lau, V. Z., Niwa, S., & Silverman, M. A. (2019). Going Too Far Is the Same as Falling Short†: Kinesin-3 Family Members in Hereditary Spastic Paraplegia. In Frontiers in Cellular Neuroscience (Vol. 13). Frontiers Media S.A. https://doi.org/10.3389/fncel.2019.00419

Gauthier, L. R., Charrin, B. C., Borrell-Pagès, M., Dompierre, J. P., Rangone, H., Cordelières, F. P., et al. (2004). Huntingtin controls neurotrophic support and survival of neurons by enhancing BDNF vesicular transport along microtubules. *Cell, 118*(1), 127–138. https://doi.org/10.1016/j.cell.2004.06.018

Geden, M. J., & Deshmukh, M. (2016). Axon degeneration: Context defines distinct pathways. *Current Opinion in Neurobiology*, Vol. 39, pp. 108–115. https://doi.org/10.1016/j.conb.2016.05.002

Geden, M. J., Romero, S. E., & Deshmukh, M. (2019). Apoptosis versus axon pruning: Molecular intersection of two distinct pathways for axon degeneration. *Neuroscience Research*, Vol. 139, pp. 3–8. https://doi.org/10.1016/j.neures.2018.11.007

Gennerich, A., & Vale, R. D. (2009). Walking the walk: how kinesin and dynein coordinate their steps. In Current Opinion in Cell Biology (Vol. 21, Issue 1, pp. 59–67). NIH Public Access. https://doi.org/10.1016/j.ceb.2008.12.002

Gjørlund, M. D., Nielsen, J., Pankratova, S., Li, S., Korshunova, I., Bock, E., & Berezin, V. (2012). Neuroligin-1 induces neurite outgrowth through interaction with neurexin-1β and activation of fibroblast growth factor receptor-1. FASEB Journal, 26(10), 4174–4186. https://doi.org/10.1096/fj.11-202242

Glaser, T., Arnaud Sampaio, V. F., Lameu, C., & Ulrich, H. (2019). Calcium signalling: A common target in neurological disorders and neurogenesis. In Seminars in Cell and Developmental Biology (Vol. 95, pp. 25–33). Elsevier Ltd. https://doi.org/10.1016/j.semcdb.2018.12.002

Gleichmann, M., & Mattson, M. P. (2011). Neuronal calcium homeostasis and dysregulation. In Antioxidants and Redox Signaling (Vol. 14, Issue 7, pp. 1261–1273). Antioxid Redox Signal. https://doi.org/10.1089/ars.2010.3386

Gokce, O., & Sudhof, T. C. (2013). Membrane-Tethered Monomeric Neurexin LNS-Domain Triggers Synapse Formation. *Journal of Neuroscience, 33*(36), 14617–14628. https://doi.org/10.1523/JNEUROSCI.1232-13.2013

Gordon, S. L., & Cousin, M. A. (2013). X-linked intellectual disability-associated mutations in synaptophysin disrupt synaptobrevin II retrieval. Journal of Neuroscience, 33(34), 13695–13700. https://doi.org/10.1523/JNEUROSCI.0636-13.2013

Gumy, L. F., & Hoogenraad, C. C. (2018). Local mechanisms regulating selective cargo entry and long-range trafficking in axons. *Current Opinion in Neurobiology*, Vol. 51, pp. 23–28. https://doi.org/10.1016/j.conb.2018.02.007

Guranowski, A., & Blanquet, S. (1985). Phosphorolytic cleavage of diadenosine 5',5-P1,P4-tetraphosphate. Properties of homogeneous diadenosine 5',5-P1,P4-tetraphosphate α,β-phosphorylase from Saccharomyces cerevisiae. Journal of Biological Chemistry, 260(6), 3542–3547.

Hammond, J. W., Cai, D., Blasius, T. L., Li, Z., Jiang, Y., Jih, G. T., et al. (2009). Mammalian Kinesin-3 motors are dimeric in vivo and move by processive motility upon release of autoinhibition. *PLoS Biology*, *7*(3), 0650–0663. https://doi.org/10.1371/journal.pbio.1000072

Harper, C. B., Mancini, G. M. S., van Slegtenhorst, M., & Cousin, M. A. (2017). Altered synaptobrevin-II trafficking in neurons expressing a synaptophysin mutation associated with a severe neurodevelopmental disorder. *Neurobiology of Disease*, *108*, 298–306. https://doi.org/10.1016/j.nbd.2017.08.021

Hawrylycz, M. J., et al. (2012). An anatomically comprehensive atlas of the adult human transcriptome. *Nature, 445*, 391-399. doi:10.1038/nature11405

Hayashi, K., Matsumoto, S., Miyamoto, M. G., & Niwa, S. (2019). Physical parameters describing neuronal cargo transport by kinesin UNC-104. In Biophysical Reviews (Vol. 11, Issue 3, pp. 471–482). Springer Verlag. https://doi.org/10.1007/s12551-019-00548-9

Hazan, J., Fonknechten, N., Mavel, D., Paternotte, C., Samson, D., Artiguenave, F., et al. (1999). Spastin, a new AAA protein, is altered in the most frequent form of autosomal dominant spastic paraplegia. *Nature Genetics, 23*(3), 296–303. https://doi.org/10.1038/15472

Hedera, P. (2018). Hereditary Spastic Paraplegia Overview. In *GeneReviews®.* Retrieved from http://www.ncbi.nlm.nih.gov/pubmed/20301682

Hertz, N. T., Berthet, A., Sos, M. L., Thorn, K. S., Burlingame, A. L., Nakamura, K., & Shokat, K. M. (2013). A neo-substrate that amplifies catalytic activity of parkinson's-disease- related kinase PINK1. Cell, 154(4), 737–747. https://doi.org/10.1016/j.cell.2013.07.030

Hilz, M. J. (2002). Assessment and evaluation of hereditary sensory and autonomic neuropathies with autonomic and neurophysiological examinations. Clinical Autonomic Research, 12(1 SUPPL.), I33–I43. https://doi.org/10.1007/s102860200017

Hinckelmann, M. V., Zala, D., & Saudou, F. (2013). Releasing the brake: Restoring fast axonal transport in neurodegenerative disorders. *Trends in Cell Biology*, Vol. 23, pp. 634–643. https://doi.org/10.1016/j.tcb.2013.08.007

Hirokawa, N., Nitta, R., & Okada, Y. (2009). The mechanisms of kinesin motor motility: Lessons from the monomeric motor KIF1A. *Nature Reviews Molecular Cell Biology*, Vol. 10, pp. 877–884. https://doi.org/10.1038/nrm2807

Hirokawa, N., Noda, Y., Tanaka, Y., & Niwa, S. (2009). Kinesin superfamily motor proteins and intracellular transport. *Nature Reviews Molecular Cell Biology*, Vol. 10, pp. 682–696. https://doi.org/10.1038/nrm2774

Hirokawa, N., Niwa, S., & Tanaka, Y. (2010). Molecular motors in neurons: Transport mechanisms and roles in brain function, development, and disease. In Neuron (Vol. 68, Issue 4, pp. 610–638). Neuron. https://doi.org/10.1016/j.neuron.2010.09.039

Hirokawa, N., & Tanaka, Y. (2015). Kinesin superfamily proteins (KIFs): Various functions and their relevance for important phenomena in life and diseases. *Experimental Cell Research*, Vol. 334, pp. 16–25. https://doi.org/10.1016/j.yexcr.2015.02.016

Hoang, H. T., Schlager, M. A., Carter, A. P., & Bullock, S. L. (2017). DYNC1H1 mutations associated with neurological diseases compromise processivity of dynein-dynactin-cargo adaptor complexes. Proceedings of the National Academy of Sciences of the United States of America, 114(9), E1597–E1606. https://doi.org/10.1073/pnas.1620141114

Hung, C. O. Y., & Coleman, M. P. (2016). KIF1A mediates axonal transport of BACE1 and identification of independently moving cargoes in living SCG neurons. *Traffic*, *17*(11), 1155–1167. https://doi.org/10.1111/tra.12428

Huo, L., Yue, Y., Ren, J., Yu, J., Liu, J., Yu, Y., Ye, F., Xu, T., Zhang, M., & Feng, W. (2012). The CC1-FHA tandem as a central hub for controlling the dimerization and activation of kinesin-3 KIF1A. Structure, 20(9), 1550–1561. https://doi.org/10.1016/j.str.2012.07.002

Inglese, J., Johnson, R. L., Simeonov, A., Xia, M., Zheng, W., Austin, C. P., & Auld, D. S. (2007). High-throughput screening assays for the identification of chemical probes. In Nature Chemical Biology (Vol. 3, Issue 8, pp. 466–479). Nature Publishing Group. https://doi.org/10.1038/nchembio.2007.17

Ishigami, S., Sandkvist, M., Tsui, F., Moore, E., Coleman, T. A., & Lawrence, D. A. (2007). Identification of a novel targeting sequence for regulated secretion in the serine protease inhibitor neuroserpin. *Biochemical Journal, 402*(1), 25–34. https://doi.org/10.1042/bj20061170

Ito, K., Sakai, K., Suzuki, Y., Ozawa, N., Hatta, T., Natsume, T., et al. (2015). Artificial human Met agonists based on macrocycle scaffolds. *Nature Communications*, *6*. https://doi.org/10.1038/ncomms7373

Ji, L., Wu, H.-T., Qin, X.-Y., & Lan, R. (2017). Dissecting carboxypeptidase E: properties, functions and pathophysiological roles in disease. *Endocrine Connections*, *6*(4), R18–R38. https://doi.org/10.1530/ec-17-0020

Kadakkuzha, B. M., Spicer, T. P., Chase, P., Richman, J. B., Hodder, P., & Puthanveettil, S. V. (2014). High-throughput screening for small molecule modulators of motor protein kinesin. Assay and Drug Development Technologies, 12(8), 470–480. https://doi.org/10.1089/adt.2014.579

Kaneko, T., Furuta, K., Oiwa, K., Shintaku, H., Kotera, H., & Yokokawa, R. (2020). Different motilities of microtubules driven by kinesin-1 and kinesin-14 motors patterned on nanopillars. Science Advances, 6(4). https://doi.org/10.1126/sciadv.aax7413

Kapitein, L. C., Schlager, M. A., Van Der Zwan, W. A., Wulf, P. S., Keijzer, N., & Hoogenraad, C. C. (2010). Probing intracellular motor protein activity using an inducible cargo trafficking assay. Biophysical Journal, 99(7), 2143–2152. https://doi.org/10.1016/j.bpj.2010.07.055

Kapoor, T. M., Mayer, T. U., Coughlin, M. L., & Mitchison, T. J. (2000). Probing spindle assembly mechanisms with monastrol, a small molecule inhibitor of the mitotic kinesin, Eg5. Journal of Cell Biology, 150(5), 975–988. https://doi.org/10.1083/jcb.150.5.975

Karcher, R. L., Deacon, S. W., & Gelfand, V. I. (2002). Motor -cargo interactions: The key to transport specificity. *Trends in Cell Biology*, Vol. 12, pp. 21–27. https://doi.org/10.1016/S0962-8924(01)02184-5

Kasem, E., Kurihara, T., & Tabuchi, K. (2018). Neurexins and neuropsychiatric disorders. *Neuroscience Research*, Vol. 127, pp. 53–60. https://doi.org/10.1016/j.neures.2017.10.012

Kaur, S., Van Bergen, N. J., Verhey, K. J., Nowell, C. J., Budaitis, B., Yue, Y., Ellaway, C., Brunetti-Pierri, N., Cappuccio, G., Bruno, I., Boyle, L., Nigro, V., Torella, A., Roscioli, T., Cowley, M. J., Massey, S., Sonawane, R., Burton, M. D., Schonewolf-Greulich, B., … Christodoulou, J. (2020). Expansion of the phenotypic spectrum of de novo missense variants in kinesin family member 1A (KIF1A). Human Mutation, 41(10), 1761–1774. https://doi.org/10.1002/humu.24079

Kawaguchi, K. (2013). Role of kinesin-1 in the pathogenesis of SPG10, a rare form of hereditary spastic paraplegia. *Neuroscientist*, *19*(4), 336–344. https://doi.org/10.1177/1073858412451655

Kelliher, M. T., Saunders, H. A., & Wildonger, J. (2019). Microtubule control of functional architecture in neurons. *Current Opinion in Neurobiology*, Vol. 57, pp. 39–45. https://doi.org/10.1016/j.conb.2019.01.003

Klebe, S., Lossos, A., Azzedine, H., Mundwiller, E., Sheffer, R., Gaussen, M., et al. (2012). KIF1A missense mutations in SPG30, an autosomal recessive spastic paraplegia: Distinct phenotypes according to the nature of the mutations. *European Journal of Human Genetics*, *20*(6), 645–649. https://doi.org/10.1038/ejhg.2011.261

Klopfenstein, D. R. (2004). The Lipid Binding Pleckstrin Homology Domain in UNC-104 Kinesin is Necessary for Synaptic Vesicle Transport in Caenorhabditis elegans. *Molecular Biology of the Cell*, *15*(8), 3729–3739. https://doi.org/10.1091/mbc.e04-04-0326

Kondo, M., Takei, Y., & Hirokawa, N. (2012). Motor Protein KIF1A Is Essential for Hippocampal Synaptogenesis and Learning Enhancement in an Enriched Environment. *Neuron*, *73*(4), 743–757. https://doi.org/10.1016/j.neuron.2011.12.020

Korten, T., & Diez, S. (2008). Setting up roadblocks for kinesin-1: Mechanism for the selective speed control of cargo carrying microtubules. Lab on a Chip, 8(9), 1441–1447. https://doi.org/10.1039/b803585g

Krueger, D. D., Tuffy, L. P., Papadopoulos, T., & Brose, N. (2012). The role of neurexins and neuroligins in the formation, maturation, and function of vertebrate synapses. *Current Opinion in Neurobiology*, Vol. 22, pp. 412–422. https://doi.org/10.1016/j.conb.2012.02.012

Kume, T., Nishikawa, H., Tomioka, H., Katsuki, H., Akaike, A., Kaneko, S., et al. (2000). p75-mediated neuroprotection by NGF against glutamate cytotoxicity in cortical cultures. *Brain Research*, *852*(2), 279–289. https://doi.org/10.1016/S0006-8993(99)02226-X

Kurth, I. (2010). Hereditary Sensory and Autonomic Neuropathy Type II. 1–11. https://www.ncbi.nlm.nih.gov/books/NBK49247/

Lee, J. R., Srour, M., Kim, D., Hamdan, F. F., Lim, S. H., Brunel-Guitton, C., et al. (2015). De novo mutations in the motor domain of KIF1A cause cognitive impairment, spastic paraparesis, axonal neuropathy, and cerebellar atrophy. *Human Mutation*, *36*(1), 69–78. https://doi.org/10.1002/humu.22709

Lim, A., Rechtsteiner, A., & Saxton, W. M. (2017). Two kinesins drive anterograde neuropeptide transport. *Molecular Biology of the Cell*, *28*(24), 3542–3553. https://doi.org/10.1091/mbc.e16-12-0820

Liu, Y. T., Laurá, M., Hersheson, J., Horga, A., Jaunmuktane, Z., Brandner, S., et al. (2014). Extended phenotypic spectrum of KIF5A mutations: From spastic paraplegia to axonal neuropathy. *Neurology*, *83*(7), 612–619. https://doi.org/10.1212/WNL.0000000000000691

Lo, K. Y., Kuzmin, A., Unger, S. M., Petersen, J. D., & Silverman, M. A. (2011). KIF1A is the primary anterograde motor protein required for the axonal transport of dense-core vesicles in cultured hippocampal neurons. *Neuroscience Letters*, *491*(3), 168–173. https://doi.org/10.1016/j.neulet.2011.01.018

Lochner, J. E., Kingma, M., Kuhn, S., Meliza, C. D., Cutler, B., & Scalettar, B. A. (1998). Real-time imaging of the axonal transport of granules containing a tissue plasminogen activator/green fluorescent protein hybrid. *Molecular Biology of the Cell*, *9*(9), 2463–2476. Retrieved from http://www.ncbi.nlm.nih.gov/pubmed/9725906

Lopes, J., Quint, D. A., Chapman, D. E., Xu, M., Gopinathan, A., & Hirst, L. S. (2019). Membrane mediated motor kinetics in microtubule gliding assays. Scientific Reports, 9(1). https://doi.org/10.1038/s41598-019-45847-z

Macarrón, R., & Hertzberg, R. P. (2009). Design and implementation of high-throughput screening assays. Methods in Molecular Biology (Clifton, N.J.), 565, 1–32. https://doi.org/10.1007/978-1-60327-258-2_1

Maday, S., Twelvetrees, A. E., Moughamian, A. J., & Holzbaur, E. L. F. (2014). Axonal transport: cargo-specific mechanisms of motility and regulation. *Neuron*, *84*(2), 292–309. https://doi.org/10.1016/j.neuron.2014.10.019

Maeder, C. I., Shen, K., & Hoogenraad, C. C. (2014). Axon and dendritic trafficking. *Current Opinion in Neurobiology*, Vol. 27, pp. 165–170. https://doi.org/10.1016/j.conb.2014.03.015

Maliga, Z., Kapoor, T. M., & Mitchison, T. J. (2002). Evidence that monastrol is an allosteric inhibitor of the mitotic kinesin Eg5. Chemistry and Biology, 9(9), 989–996. https://doi.org/10.1016/S1074-5521(02)00212-0

Marlin, M. C., & Li, G. (2015). Biogenesis and Function of the NGF/TrkA Signaling Endosome. In *International review of cell and molecular biology* (Vol. 314, pp. 239–257). https://doi.org/10.1016/bs.ircmb.2014.10.002

Marras, C., Lang, A., van de Warrenburg, B. P., Sue, C. M., Tabrizi, S. J., Bertram, L., et al. (2016). Nomenclature of genetic movement disorders: Recommendations of the international Parkinson and movement disorder society task force. *Movement Disorders*, Vol. 31, pp. 436–457. https://doi.org/10.1002/mds.26527

Mayer, T. U., Kapoor, T. M., Haggarty, S. J., King, R. W., Schreiber, S. L., & Mitchison, T. J. (1999). Smart molecule inhibitor of mitotic spindle bipolarity identified in a phenotype-based screen. Science, 286(5441), 971–974. https://doi.org/10.1126/science.286.5441.971

McQuin, C., Goodman, A., Chernyshev, V., Kamentsky, L., Cimini, B. A., Karhohs, K. W., Doan, M., Ding, L., Rafelski, S. M., Thirstrup, D., Wiegraebe, W., Singh, S., Becker, T., Caicedo, J. C., & Carpenter, A. E. (2018). CellProfiler 3.0: Next-generation image processing for biology. PLoS Biology, 16(7). https://doi.org/10.1371/journal.pbio.2005970

Meyer F. (1994). Topographic distance and watershed lines. Signal Process, 38, 113-125. https://doi.org/10.1016/0165-1684(94)90060-4

Millecamps, S., & Julien, J. P. (2013). Axonal transport deficits and neurodegenerative diseases. *Nature Reviews Neuroscience*, Vol. 14, pp. 161–176. https://doi.org/10.1038/nrn3380

Moughamian, A. J., & Holzbaur, E. L. F. (2012). Dynactin Is Required for Transport Initiation from the Distal Axon. Neuron, 74(2), 331–343. https://doi.org/10.1016/j.neuron.2012.02.025

Nieh, S., Madou, M. R. Z., Sirajuddin, M., Fregeau, B., Mcknight, D., Lexa, K., et al. (2015). De novo mutations in KIF1A cause progressive encephalopathy and brain atrophy. *Annals of Clinical and Translational Neurology*, *2*(6), 623–635. https://doi.org/10.1002/acn3.198

Nirenberg, M. J., Liu, Y., Peter, D., Edwards, R. H., & Pickel, V. M. (1995). The vesicular monoamine transporter 2 is present in small synaptic vesicles and preferentially localizes to large dense core vesicles in rat solitary tract nuclei. *Proceedings of the National Academy of Sciences*, *92*(19), 8773–8777. https://doi.org/10.1073/pnas.92.19.8773

Nirschl, J. J., Ghiretti, A. E., & Holzbaur, E. L. F. (2017). The impact of cytoskeletal organization on the local regulation of neuronal transport. *Nature Reviews Neuroscience*, Vol. 18, pp. 585–597. https://doi.org/10.1038/nrn.2017.100

Niwa, S., Tanaka, Y., & Hirokawa, N. (2008). KIF1Bβ- and KIF1A-mediated axonal transport of presynaptic regulator Rab3 occurs in a GTP-dependent manner through DENN/MADD. *Nature Cell Biology*, *10*(11), 1269–1279. https://doi.org/10.1038/ncb1785

Niwa, S., Lipton, D. M., Morikawa, M., Zhao, C., Hirokawa, N., Lu, H., & Shen, K. (2016). Autoinhibition of a Neuronal Kinesin UNC-104/KIF1A Regulates the Size and Density of Synapses. *Cell Reports*, *16*(8), 2129–2141. https://doi.org/10.1016/j.celrep.2016.07.043

Ohba, C., Haginoya, K., Osaka, H., Kubota, K., Ishiyama, A., Hiraide, T., et al. (2015). De novo KIF1A mutations cause intellectual deficit, cerebellar atrophy, lower limb spasticity and visual disturbance. *Journal of Human Genetics*, *60*(12), 739–742. https://doi.org/10.1038/jhg.2015.108

Okada, Y., Yamazaki, H., Sekine-Aizawa, Y., & Hirokawa, N. (1995). The neuron-specific kinesin superfamily protein KIF1A is a unique monomeric motor for anterograde axonal transport of synaptic vesicle precursors. *Cell*, *81*(5), 769–780. https://doi.org/10.1016/0092-8674(95)90538-3

Olenick, M. A., & Holzbaur, E. L. F. (2019). Dynein activators and adaptors at a glance. *Journal of Cell Science*, *132*(6), jcs227132. https://doi.org/10.1242/jcs.227132

Oteyza, A. C., Battaloğlu, E., Ocek, L., Lindig, T., Reichbauer, J., Rebelo, A. P., et al. (2014). Motor protein mutations cause a new form of hereditary spastic paraplegia. *Neurology*, *82*(22), 2007–2016. https://doi.org/10.1212/WNL.0000000000000479

Pal, A., Glaß, H., Naumann, M., Kreiter, N., Japtok, J., Sczech, R., & Hermann, A. (2018). High content organelle trafficking enables disease state profiling as powerful tool for disease modelling. Scientific Data, 5. https://doi.org/10.1038/sdata.2018.241

Park, J. J., Cawley, N. X., & Loh, Y. P. (2008). Carboxypeptidase e cytoplasmic tail-driven vesicle transport is key for activity-dependent secretion of peptide hormones. Molecular Endocrinology, 22(4), 989–1005. https://doi.org/10.1210/me.2007-0473

Pilling, A. D., Horiuchi, D., Lively, C. M., & Saxton, W. M. (2006). Kinesin-1 and dynein are the primary motors for fast transport of mitochondria in Drosophila motor axons. Molecular Biology of the Cell, 17(4), 2057–2068. https://doi.org/10.1091/mbc.E05-06-0526

Pollock, N., De Hostos, E. L., Turck, C. W., & Vale, R. D. (1999). Reconstitution of membrane transport powered by a novel dimeric kinesin motor of the Unc104/KIF1a family purified from Dictyostelium. Journal of Cell Biology, 147(3), 493–505. https://doi.org/10.1083/jcb.147.3.493

Puzzo, D., Privitera, L., Leznik, E., Fa, M., Staniszewski, A., Palmeri, A., & Arancio, O. (2008). Picomolar Amyloid- Positively Modulates Synaptic Plasticity and Memory in Hippocampus. *Journal of Neuroscience*, *28*(53), 14537–14545. https://doi.org/10.1523/JNEUROSCI.2692-08.2008

Ramser, E. M., Gan, K. J., Decker, H., Fan, E. Y., Suzuki, M. M., Ferreira, S. T., & Silverman, M. A. (2013). Amyloid-β oligomers induce tau-independent disruption of BDNF axonal transport via calcineurin activation in cultured hippocampal neurons. Molecular Biology of the Cell, 24(16), 2494–2505. https://doi.org/10.1091/mbc.E12-12-0858

Randall, T. S., Yip, Y. Y., Wallock-Richards, D. J., Pfisterer, K., Sanger, A., Ficek, W., Steiner, R. A., Beavil, A. J., Parsons, M., & Dodding, M. P. (2017). A small-molecule activator of kinesin-1 drives remodeling of the microtubule network. Proceedings of the National Academy of Sciences of the United States of America, 114(52), 13738–13743. https://doi.org/10.1073/pnas.1715115115

Reck-Peterson, S. L., Redwine, W. B., Vale, R. D., & Carter, A. P. (2018). The cytoplasmic dynein transport machinery and its many cargoes. In Nature Reviews Molecular Cell Biology (Vol. 19, Issue 6, pp. 382–398). Nature Publishing Group. https://doi.org/10.1038/s41580-018-0004-3

Ren, J., Wang, S., Chen, H., Wang, W., Huo, L., & Feng, W. (2018). Coiled-coil 1-mediated fastening of the neck and motor domains for kinesin-3 autoinhibition. Proceedings of the National Academy of Sciences of the United States of America, 115(51), E11933–E11942. https://doi.org/10.1073/pnas.1811209115

Roda, R. H., Schindler, A. B., & Blackstone, C. (2017). Multigeneration family with dominant SPG30 hereditary spastic paraplegia. *Annals of Clinical and Translational Neurology*, *4*(11), 821–824. https://doi.org/10.1002/acn3.452

Ross, J. L., Ali, M. Y., & Warshaw, D. M. (2008). Cargo transport: molecular motors navigate a complex cytoskeleton. *Current Opinion in Cell Biology*, Vol. 20, pp. 41–47. https://doi.org/10.1016/j.ceb.2007.11.006

Roy, S. (2014). Seeing the unseen: The hidden world of slow axonal transport. *Neuroscientist*, Vol. 20, pp. 71–81. https://doi.org/10.1177/1073858413498306

Russo, A. F. (2017). Overview of Neuropeptides: Awakening the Senses? *Headache*, *57 Suppl 2*(Suppl 2), 37–46. https://doi.org/10.1111/head.13084

Saha, A. R., Hill, J., Utton, M. A., Asuni, A. A., Ackerley, S., Grierson, A. J., Miller, C. C., Davies, A. M., Buchman, V. L., Anderton, B. H., & Hanger, D. P. (2004). Parkinson's disease α-synuclein mutations exhibit defective axonal transport in cultured neurons. In Journal of Cell Science (Vol. 117, Issue 7, pp. 1017–1024). J Cell Sci. https://doi.org/10.1242/jcs.00967

Samanta, D., & Gokden, M. (2019). PEHO syndrome: KIF1A mutation and decreased activity of mitochondrial respiratory chain complex. *Journal of Clinical Neuroscience*, *61*, 298–301. https://doi.org/10.1016/j.jocn.2018.10.091

Saxton, W. M., & Hollenbeck, P. J. (2012). The axonal transport of mitochondria. *Journal of Cell Science*, *125*(9), 2095–2104. https://doi.org/10.1242/jcs.053850

Schimert, K. I., Budaitis, B. G., Reinemann, D. N., Lang, M. J., & Verhey, K. J. (2019). Intracellular cargo transport by single-headed kinesin motors. Proceedings of the National Academy of Sciences of the United States of America, 116(13), 6152–6161. https://doi.org/10.1073/pnas.1817924116

Schnell, L., Schneider, R., Kolbeck, R., Barde, Y. A., & Schwab, M. E. (1994). Neurotrophin-3 enhances sprouting of corticospinal tract during development and after adult spinal cord lesion. *Nature*, *367*(6459), 170–173. https://doi.org/10.1038/367170a0

Schoch, S., Deák, F., Königstorfer, A., Mozhayeva, M., Sara, Y., Südhof, T. C., & Kavalali, E. T. (2001). SNARE Function Analyzed in Synaptobrevin/VAMP Knockout Mice. *Science*, *294*(5544), 1117–1122. https://doi.org/10.1126/science.1064335

Sgro, A. E., Bajjalieh, S. M., & Chiu, D. T. (2013). Single-axonal organelle analysis method reveals new protein-motor associations. *ACS Chemical Neuroscience*, *4*(2), 277–284. https://doi.org/10.1021/cn300136y

Shin, H., Wyszynski, M., Huh, K. H., Valtschanoff, J. G., Lee, J. R., Ko, J., et al. (2003). Association of the kinesin motor KIF1A with the multimodular protein liprin-α. *Journal of Biological Chemistry*, *278*(13), 11393–11401. https://doi.org/10.1074/jbc.M211874200

Shubeita, G. T., Tran, S. L., Xu, J., Vershinin, M., Cermelli, S., Cotton, S. L., Welte, M. A., & Gross, S. P. (2008). Consequences of Motor Copy Number on the Intracellular Transport of Kinesin-1-Driven Lipid Droplets. Cell, 135(6), 1098–1107. https://doi.org/10.1016/j.cell.2008.10.021

Siddiqui, N., & Straube, A. (2017). Intracellular cargo transport by kinesin-3 motors. *Biochemistry (Moscow)*, *82*(7), 803–815. https://doi.org/10.1134/s0006297917070057

Siddiqui, N., Zwetsloot, A. J., Bachmann, A., Roth, D., Hussain, H., Brandt, J., Kaverina, I., & Straube, A. (2019). PTPN21 and Hook3 relieve KIF1C autoinhibition and activate intracellular transport. Nature Communications, 10(1). https://doi.org/10.1038/s41467-019-10644-9

Sittampalam, G. S., Coussens, N. P., Editor, A. S., Arkin, M., Auld, D., Austin, C., Bejcek, B., Glicksman, M., Inglese, J., Iversen, P. W., Mcgee, J., Mcmanus, O., Minor, L., Napper, A., Peltier, J. M., Riss, T., Trask, O. J., & Weidner, J. (2004). Assay Guidance Manual. In Assay Guidance Manual (Issue Md). Eli Lilly & Company and the National Center for Advancing Translational Sciences. http://www.ncbi.nlm.nih.gov/pubmed/22553861

Song, Y. H., Marx, A., Müller, J., Woehlke, G., Schliwa, M., Krebs, A., Hoenger, A., & Mandelkow, E. (2001). Structure of a fast kinesin: Implications for ATPase mechanism and interactions with microtubules. EMBO Journal, 20(22), 6213–6225. https://doi.org/10.1093/emboj/20.22.6213

Soppina, V., & Verhey, K. J. (2014). The family-specific K-loop influences the microtubule on-rate but not the superprocessivity of kinesin-3 motors. *Molecular Biology of the Cell, 25*(14), 2161–2170. https://doi.org/10.1091/mbc.e14-01-0696

Soppina, V., Norris, S. R., Dizaji, A. S., Kortus, M., Veatch, S., Peckham, M., & Verhey, K. J. (2014). Dimerization of mammalian kinesin-3 motors results in superprocessive motion. *Proceedings of the National Academy of Sciences*, *111*(15), 5562–5567. https://doi.org/10.1073/pnas.1400759111

Stavoe, A. K. H., & Holzbaur, E. L. F. (2019). Axonal autophagy: Mini-review for autophagy in the CNS. *Neuroscience Letters*, Vol. 697, pp. 17–23. https://doi.org/10.1016/j.neulet.2018.03.025

Stavoe, A. K. H., Hill, S. E., Hall, D. H., & Colón-Ramos, D. A. (2016). KIF1A/UNC-104 Transports ATG-9 to Regulate Neurodevelopment and Autophagy at Synapses. *Developmental Cell*, *38*(2), 171–185. https://doi.org/10.1016/j.devcel.2016.06.012

Steinmetz, M. O., & Akhmanova, A. (2008). Capturing protein tails by CAP-Gly domains. In Trends in Biochemical Sciences (Vol. 33, Issue 11, pp. 535–545). Elsevier. https://doi.org/10.1016/j.tibs.2008.08.006

Stucchi, R., Plucińska, G., Hummel, J. J. A., Zahavi, E. E., Guerra San Juan, I., Klykov, O., et al. (2018). Regulation of KIF1A-Driven Dense Core Vesicle Transport: Ca2+/CaM Controls DCV Binding and Liprin-α/TANC2 Recruits DCVs to Postsynaptic Sites. *Cell Reports, 24*(3), 685–700. https://doi.org/10.1016/j.celrep.2018.06.071

Tanaka, Y., Niwa, S., Dong, M., Farkhondeh, A., Wang, L., Zhou, R., & Hirokawa, N. (2016). The Molecular Motor KIF1A Transports the TrkA Neurotrophin Receptor and Is Essential for Sensory Neuron Survival and Function. *Neuron, 90*(6), 1215–1229. https://doi.org/10.1016/j.neuron.2016.05.002

Tandon, N., Thakkar, K., LaGory, E., Liu, Y., & Giaccia, A. (2018). Generation of Stable Expression Mammalian Cell Lines Using Lentivirus. Bio-Protocol, 8(21). https://doi.org/10.21769/bioprotoc.3073

Tcherniuk, S., van Lis, R., Kozielski, F., & Skoufias, D. A. (2010). Mutations in the human kinesin Eg5 that confer resistance to monastrol and S-trityl-l-cysteine in tumor derived cell lines. Biochemical Pharmacology, 79(6), 864–872. https://doi.org/10.1016/j.bcp.2009.11.001

Teschendorf, C., Warrington, K. H., Siemann, D. W., & Muzyczka, N. (2002). Comparison of the EF-1α and the CMV promoter for engineering stable tumor cell lines using recombinant adeno-associated virus. Anticancer Research, 22(6 A), 3325–3330.

The Uniprot Consortium. (2019). UniProt; a worldwide hub of protein knowledge. *Nucleic Acids Res, 47*, D506-515. https://doi.org/10.1093/nar/gky1049

Tischfield, M. A., & Engle, E. C. (2010). Distinct α- and β-tubulin isotypes are required for the positioning, differentiation and survival of neurons: New support for the "multi-tubulin" hypothesis. In Bioscience Reports (Vol. 30, Issue 5, pp. 319–330). Biosci Rep. https://doi.org/10.1042/BSR20100025

Tomishige, M., Klopfenstein, D. R., & Vale, R. D. (2002). Conversion of Unc104/KIF1A kinesin into a processive motor after dimerization. Science, 297(5590), 2263–2267. https://doi.org/10.1126/science.1073386

Tong, B. C. K., Wu, A. J., Li, M., & Cheung, K. H. (2018). Calcium signaling in Alzheimer's disease & therapies. In Biochimica et Biophysica Acta - Molecular Cell Research (Vol. 1865, Issue 11, pp. 1745–1760). Elsevier B.V. https://doi.org/10.1016/j.bbamcr.2018.07.018

Travaglini, L., Aiello, C., Stregapede, F., D'Amico, A., Alesi, V., Ciolfi, A., et al. (2018). The impact of next-generation sequencing on the diagnosis of pediatric-onset hereditary spastic paraplegias: new genotype-phenotype correlations for rare HSP-related genes. *Neurogenetics*, *19*(2), 111–121. https://doi.org/10.1007/s10048-018-0545-9

Turney, S. G., Ahmed, M., Chandrasekar, I., Wysolmerski, R. B., Goeckeler, Z. M., Rioux, R. M., et al. (2016). Nerve growth factor stimulates axon outgrowth through negative regulation of growth cone actomyosin restraint of microtubule advance. *Molecular Biology of the Cell*, *27*(3), 500–517. https://doi.org/10.1091/mbc.e15-09-0636

Vale, R. D. (2003). The molecular motor toolbox for intracellular transport. *Cell*, *112*(4), 467–480. Retrieved from http://www.ncbi.nlm.nih.gov/pubmed/12600311

Van De Warrenburg, B. P., Schouten, M. I., De Bot, S. T., Vermeer, S., Meijer, R., Pennings, M., et al. (2016). Clinical exome sequencing for cerebellar ataxia and spastic paraplegia uncovers novel gene-disease associations and unanticipated rare disorders. *European Journal of Human Genetics*, *24*(10), 1460–1466. https://doi.org/10.1038/ejhg.2016.42

VanDelinder, V., Imam, Z. I., & Bachand, G. (2019). Kinesin motor density and dynamics in gliding microtubule motility. Scientific Reports, 9(1). https://doi.org/10.1038/s41598-019-43749-8

Verge, V., Merlio, J., Grondin, J., Ernfors, P., Persson, H., Riopelle, R., et al. (1992). Colocalization of NGF binding sites, trk mRNA, and low-affinity NGF receptor mRNA in primary sensory neurons: responses to injury and infusion of NGF. *The Journal of Neuroscience*, *12*(10), 4011–4022. https://doi.org/10.1523/jneurosci.12-10-04011.1992

Verhey, K. J., & Hammond, J. W. (2009). Traffic control: Regulation of kinesin motors. In Nature Reviews Molecular Cell Biology (Vol. 10, Issue 11, pp. 765–777). Nat Rev Mol Cell Biol. https://doi.org/10.1038/nrm2782

Vincent, J., Preston, M., Mouchet, E., Laugier, N., Corrigan, A., Boulanger, J., Brown, D. G., Clark, R., Wigglesworth, M., Carter, A. P., & Bullock, S. L. (2020). A High-Throughput Cellular Screening Assay for Small-Molecule Inhibitors and Activators of Cytoplasmic Dynein-1-Based Cargo Transport. SLAS Discovery, 25(9), 985–999. https://doi.org/10.1177/2472555220920581

Vinogradov, A. A., Yin, Y., & Suga, H. (2019). Macrocyclic Peptides as Drug Candidates: Recent Progress and Remaining Challenges. In Journal of the American Chemical Society (Vol. 141, Issue 10, pp. 4167–4181). American Chemical Society. https://doi.org/10.1021/jacs.8b13178

Wang, X., Xu, Z., Tian, Z., Zhang, X., Xu, D., Li, Q., Zhang, J., & Wang, T. (2017). The EF-1α promoter maintains high-level transgene expression from episomal vectors in transfected CHO-K1 cells. Journal of Cellular and Molecular Medicine, 21(11), 3044–3054. https://doi.org/10.1111/jcmm.13216

Webb, M. R. (1992). A continuous spectrophotometric assay for inorganic phosphate and for measuring phosphate release kinetics in biological systems. Proceedings of the National Academy of Sciences of the United States of America, 89(11), 4884–4887. https://doi.org/10.1073/pnas.89.11.4884

Willem, M. (2016). Proteolytic processing of Neuregulin-1. *Brain Research Bulletin*, Vol. 126, pp. 178–182. https://doi.org/10.1016/j.brainresbull.2016.07.003

Wong, M. Y., Zhou, C., Shakiryanova, D., Lloyd, T. E., Deitcher, D. L., & Levitan, E. S. (2012). Neuropeptide delivery to synapses by long-range vesicle circulation and sporadic capture. Cell, 148(5), 1029–1038. https://doi.org/10.1016/j.cell.2011.12.036

Wu, Y. E., Huo, L., Maeder, C. I., Feng, W., & Shen, K. (2013). The Balance between Capture and Dissociation of Presynaptic Proteins Controls the Spatial Distribution of Synapses. Neuron, 78(6), 994–1011. https://doi.org/10.1016/j.neuron.2013.04.035

Wüst, R. C. I., Houtkooper, R. H., & Auwerx, J. (2020). Confounding factors from inducible systems for spatiotemporal gene expression regulation. In Journal of Cell Biology (Vol. 219, Issue 7). Rockefeller University Press. https://doi.org/10.1083/JCB.202003031

Xue, X., Jaulin, F., Espenel, C., & Kreitzer, G. (2010). PH-domain-dependent selective transport of p75 by kinesin-3 family motors in non-polarized MDCK cells. Journal of Cell Science, 123(10), 1732–1741. https://doi.org/10.1242/jcs.056366

Yamaguchi, J., Suzuki, C., Nanao, T., Kakuta, S., Ozawa, K., Tanida, I., et al. (2018). Atg9a deficiency causes axon-specific lesions including neuronal circuit dysgenesis. *Autophagy*, *14*(5), 764–777. https://doi.org/10.1080/15548627.2017.1314897

Yan, R. (2017). Physiological Functions of the β-Site Amyloid Precursor Protein Cleaving Enzyme 1 and 2. *Frontiers in Molecular Neuroscience*, *10*. https://doi.org/10.3389/fnmol.2017.00097

Yang, B., Lamb, M. L., Zhang, T., Hennessy, E. J., Grewal, G., Sha, L., Zambrowski, M., Block, M. H., Dowling, J. E., Su, N., Wu, J., Deegan, T., Mikule, K., Wang, W., Kaspera, R., Chuaqui, C., & Chen, H. (2014). Discovery of potent KIFC1 inhibitors using a method of integrated high-throughput synthesis and screening. Journal of Medicinal Chemistry, 57(23), 9958–9970. https://doi.org/10.1021/jm501179r

Yang, C. P. H., & Horwitz, S. B. (2017). Taxol®: The first microtubule stabilizing agent. In International Journal of Molecular Sciences (Vol. 18, Issue 8). MDPI AG. https://doi.org/10.3390/ijms18081733

Yonekawa, V., Harada, A., Okada, Y., Funakoshi, T., Kanai, Y., Takei, Y., et al. (1998). Defect in synaptic vesicle precursor transport and neuronal cell death in KIF1A motor protein-deficient mice. *Journal of Cell Biology*, *141*(2), 431–441. https://doi.org/10.1083/jcb.141.2.431

Yuan, A., Rao, M. V., Veeranna, & Nixon, R. A. (2017). Neurofilaments and neurofilament proteins in health and disease. *Cold Spring Harbor Perspectives in Biology*, *9*(4). https://doi.org/10.1101/cshperspect.a018309

Zahn, T. R., Angleson, J. K., MacMorris, M. A., Domke, E., Hutton, J. F., Schwartz, C., & Hutton, J. C. (2004). Dense core vesicle dynamics in Caenorhabditis elegans neurons and the role of kinesin UNC-104. *Traffic*, *5*(7), 544–559. https://doi.org/10.1111/j.1600-0854.2004.00195.x

Zegzouti, H., Zdanovskaia, M., Hsiao, K., & Goueli, S. A. (2009). ADP-Glo: A bioluminescent and homogeneous adp monitoring assay for Kinases. Assay and Drug Development Technologies, 7(6), 560–572. https://doi.org/10.1089/adt.2009.0222

Zhang, J. H., Chung, T. D. Y., & Oldenburg, K. R. (1999). A simple statistical parameter for use in evaluation and validation of high throuput screening assays. Journal of Biomolecular Screening, 4(2), 67–73. https://doi.org/10.1177/108705719900400206

Zúñiga, R. A., Gutiérrez-González, M., Collazo, N., Sotelo, P. H., Ribeiro, C. H., Altamirano, C., Lorenzo, C., Aguillón, J. C., & Molina, M. C. (2019). Development of a new promoter to avoid the silencing of genes in the production of recombinant antibodies in chinese hamster ovary cells. Journal of Biological Engineering, 13(1). https://doi.org/10.1186/s13036-019-0187-y

Appendix
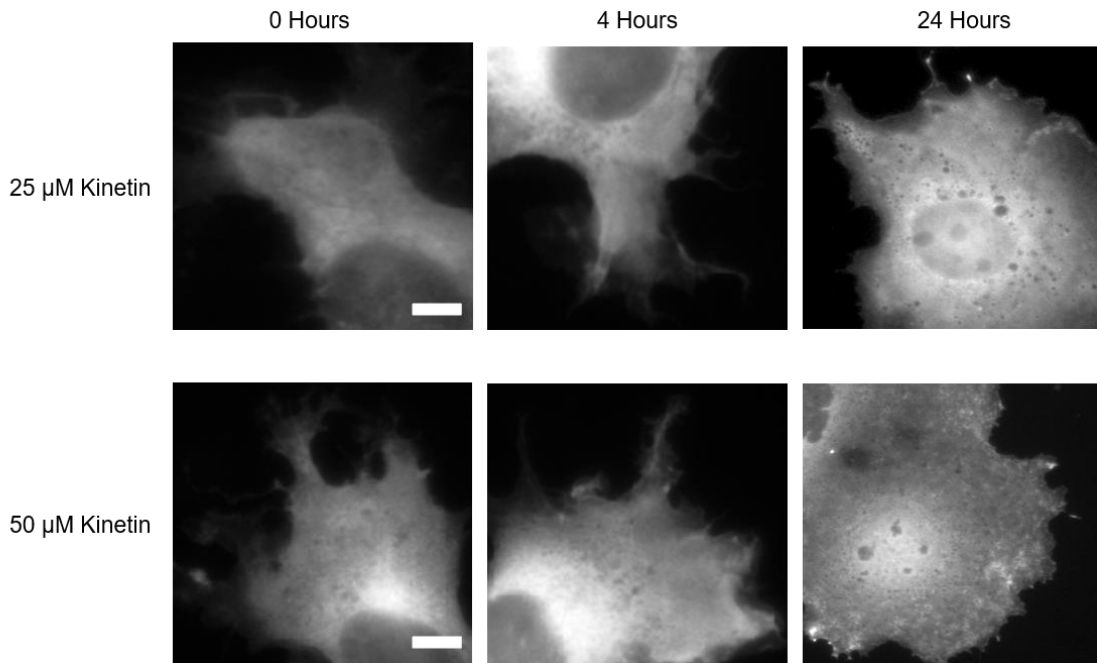
Figure A.1. Testing of a potential positive control, kinetin.
Kinetin, a cytokine, was tested as a potential positive control. Kinetin is a cell-permeable cytokine that is converted to kinetin triphosphate (KTP), an ATP analogue, in cells (Hertz et al., 2013). I wanted to see whether KTP would stimulate an increase in activated KIF1A through microtubule-binding and peripheral distribution. COS-7 cells were transfected with KIF1A-GFP and allowed to express for 24 hours. Kinetin was added at 25µM or 50µM concentrations and subsequently fixed, mounted and imaged at varying time points. Numbers above images represent time post-kinetin addition when cells were fixed. No peripheral accumulation or microtubular phenotype was seen at any time point or concentration. Scale bar:10µm.
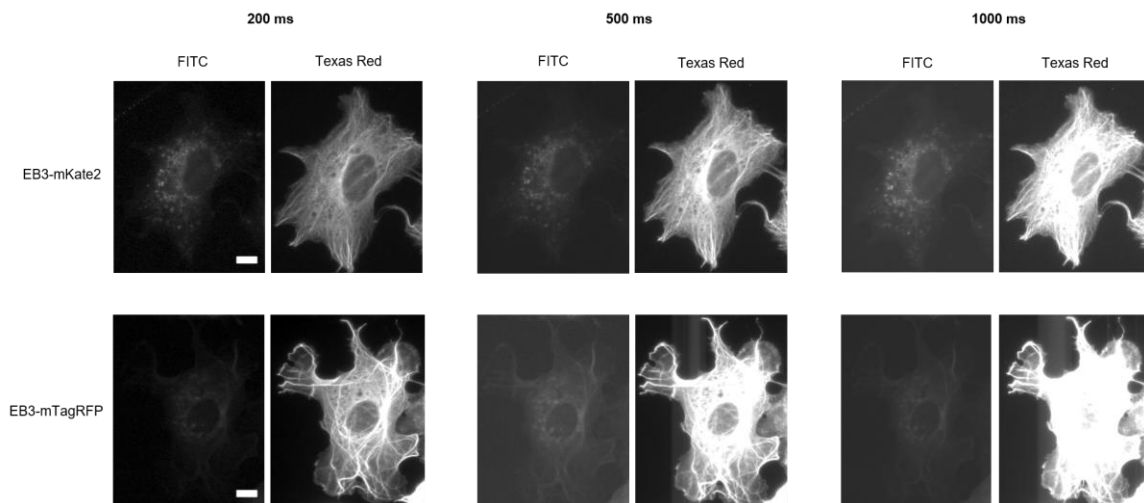
Figure A.2. Bleed-through testing of EB3 fusion constructs.
Colocalization and overlap analyses require robust identification of cellular features such as microtubules. Bleed-through of fluorescence between fluorescent channels can mimic colocalization and overlap. I tested two fluorophores, mKate2 and mTagRFP, to see whether there is bleed-through from one channel to the next by imaging COS-7 cells transfected with either EB3-mKate2 or EB3-mTagRFP. No bleed through was seen at any exposure for EB3-mKate2. EB3-mTagRFP did show bleed through at all three exposures tested. Scale bar:10μm.